University of Arizona

Southern California Tree-Ring Study

31 December 2017

David M. Meko, Connie A. Woodhouse, and Erica R. Bigio

Final Report to California Department of Water Resources

Agreement 4600011071

Table of Contents

List of Tables

List of Figures

Executive Summary

The goal of this project was to develop tree-ring based reconstructions of streamflow and precipitation for southern California. These reconstructions, along with existing reconstructions for northern and central California and an updated reconstruction of the Colorado River, provide information about statewide and regional drought for the past millennium.

For this project, six southern California records were reconstructed: four for total water year precipitation (Ojai, Lake Arrowhead, San Gabriel Dam, and Cuyamaca) and two for water year streamflow (Arroyo Seco and Santa Ana River), along with a reconstruction of Kern River streamflow in the southern Sierra Nevada. In addition, a reconstruction for Colorado River flow at Lees Ferry was updated. Two versions of the eight reconstructions were developed. One set emphasizes the best match with the observed records, called the most skillful set. This set of the reconstructions extends back to the early 1400s. The second set of reconstructions emphasizes length, and starts in the 1100s. The most skillful California reconstructions end in 2016, while the most skillful Colorado River reconstruction ends in 2015. The updated Colorado River reconstruction, most skillful version, is very similar to the reconstructions developed and published in 2006 and 2007 by the authors.

The reconstructions provide a way to evaluate the characteristics of instrumental period streamflow and precipitation in the context of past centuries. Metrics such as average flow and variance for different intervals of time were used make this evaluation. One of the most notable findings in this assessment is that, over the 20th and 21st centuries, southern California precipitation and streamflow, along with Kern River streamflow, have been more variable with correspondingly less year-to-year persistence, than over the past six centuries. In contrast, average flow and precipitation are not markedly different over the instrumental period, compared to the past six-centuries, although there is a tendency for the instrumental period to be wetter than average compared to similar length periods in the past.

The longer records also allow an assessment of the cyclic behavior that may not be detectable in the shorter instrumental records. A cycle of moisture variability at a periodicity of about 13 years is present in recent decades in both southern California and the Upper Colorado River basin, but is not a consistent feature over the multi-century time frame of the reconstructions. A cycle with an average period of about 23 years is present in the most skill streamflow reconstructions. In the longest reconstructions, a cycle slightly longer than 100 years is evident in the southern California and the Kern River but not in the Colorado River.

This set of reconstructions shows that the instrumental period contains a subset of the droughts that have occurred over past centuries. In all of the reconstructions, longer droughts (consecutive years below the instrumental record average) have occurred over the past centuries. In some cases, these droughts are just a year or two longer, while in other cases, droughts are more than double the length of the longest instrumental period drought. In the precipitation reconstructions, droughts that persist for four years are not uncommon, but these extended records document droughts lasting up to 13 years, with even longer droughts in some of the streamflow reconstructions. However, some shorter periods of drought during the instrumental period match or exceed the average annual drought intensity in reconstructions over their full length. In particular, in southern California, a number of the reconstructions indicate that the 2012-2016 drought was the worst 5-year drought in the past six centuries, as measured by the percent of average annual precipitation or streamflow.

When southern California (represented by the San Gabriel Dam precipitation reconstruction) is compared with the Sacramento River and the Colorado River at Lees Ferry, the reconstructions document concurrence of drought events across the three regions. Periods of widespread drought are evident throughout the past six centuries, but most events are limited to three or four years. These concurrent

droughts have occurred approximately twice a century, but range from four events in the 18th century to one event in the 20th century. While the majority of these widespread drought events persist for only a few years, two events, 1452-1460 and 1775-1783, persist for nine years. Concurrent droughts do not impact each basin in exactly the same way. These dry periods tend to overlap, with variable duration and overall magnitude from region to region. For example, the 11-year period from 1451-1461 included nine years of consecutively below average flow in the upper Colorado River basin, while it was broken by one above average year in the Sacramento basin and by four separate above average years in southern California.

From a west-wide perspective, periods of dryness in southern California do not occur in geographic isolation, but are typically part of larger patterns of drought across the western US. However, these patterns vary, indicating that different large-scale circulation patterns influence regionally persistent dry conditions. Some patterns suggest the influence of ENSO, with dry conditions extending across the Southwest into Arizona, New Mexico, and Texas, similar to the 1950s. In other cases, drought also extends north across the state, and through the intermountain West, suggesting persistent blocking of moisture flow, with the jet stream directed far to the north.

This study provides a long-term perspective for evaluating southern California precipitation and streamflow variability over the past centuries. The reconstructions document the range of drought conditions that have occurred in Southern California, and could occur in the future. These extended records show that the relatively short instrumental records represent a subset of the conditions that are possible, and should be useful for guiding expectations for future drought, under natural climate variability alone.

1.Introduction

This study addresses variability of precipitation and river discharge in six Southern California basins, the Kern River Basin and the Upper Colorado River Basin over the past 1000 years. The study includes development of new and updated tree-ring chronologies, reconstruction of specified hydroclimatic records, and analysis of time series properties of the reconstructions, as well as the magnitude and duration of drought events. An additional product of the study is a guidebook for water managers covering the use of tree-ring data to better understand drought duration. The guidebook, not discussed in this report, can be obtained from the California Department of Water Resources (CADWR). Work on the study began in the fall of 2015 and was completed in the fall of 2017.

Project tasks included field collections, laboratory work (preparation, dating and measurement of samples), statistical chronology development, reconstruction, and analysis of reconstructions. The analysis of the reconstructions has six components: 1) Quantify droughts and wet periods, 2) Identify cycles and quasi-cycles, 3) Check consistency of reconstructions with other paleoclimatic data, 4) Place statistics for the instrumental period in a long-term context, 5) Identify cyclical patterns in covariation of drought in Southern California, Northern California/Central Valley, and the Upper Colorado River Basin (UCRB) and 6) Identify spatial modes of drought patterns over western North America during episodes of most severe Southern California drought.

Field collections, development of tree-ring chronologies, reconstruction modeling, and methods of analyzing reconstructions are described in the Data and Methods section. Findings and interpretation for selected key reconstructions are described in the Results section. Annual reconstructed time series, additional basic data (e.g., the tree-ring chronologies), along with a comprehensive set of results are included as in appendices and/or digital spreadsheets.

2. Data and Methods

Tree-ring samples were collected in several trips to Southern California, the Sierra Nevada, and the Upper Colorado River Basin. Samples were combined with tree-ring measurements from previous collections to create updated tree-ring site chronologies, which were then converted statistically into reconstructions of natural flow or precipitation for the water year (October-September). Finally, reconstructions were analyzed to address project objectives. This section on Data and Methods is subdivided into four topics: 1) Tree-Ring Data, 2) Reconstruction Targets, 3) Reconstructions and 4) Analysis of Reconstructions.

2.1 Tree-Ring Data

Field Collections. Twenty-five sites were updated and five new tree-ring sites were collected during trips to Southern California, the Sierra Nevada and the Upper Colorado River Basin between October 2015 and November 2016. Sites to be updated were identified by high correlation of existing tree-ring data with flow or precipitation records to be reconstructed. For the Upper Colorado River Basin, site selection was based on key chronologies used in the Colorado River reconstruction of Woodhouse et al. (2006). One new collection was made in the UCRB and combined with existing data to strengthen the signal at a site in eastern Utah. Archive wood samples at the University of Arizona's Laboratory of Tree-Ring Research (LTRR) were also used to identify California sites with old trees or remnant wood. Site information for the chronologies collected and developed, including information on tree-species, number of samples, and time coverage of the final chronology is listed in Table 1, and site locations are shown on the maps in Figure1.

Chronology Development. These main steps were followed for chronology development: 1) cross-dating by skeleton plot (Stokes and Smiley 1968), 2) ring measurement using a Velmex sliding stage, 3) initial quality control on dating using **COFECHA** (Holmes 1983), 4) final quality check with **Lockdown** program (MATLAB) including re-measurement of wood as necessary, and 5) computation of

site chronology by **ARSTAN** (Cook et al., 2007). After chronologies were developed, the wood samples were catalogued and boxed for archiving at the LTRR.

For the update chronologies, identified by 'Update' in the site name in Table 1, samples from previous collections were merged with the new samples collected. In two cases (MWC and BFB sites), data from nearby sites were combined into one chronology because sites were close geographically and the climate response of the chronologies was similar. During this process, the quality of the older collections was reviewed and short or poor-quality series were discarded. For the final chronology, an Expressed Population Signal (EPS) of at least 0.85 (Wigley et al. 1984) was used to judge whether there were enough samples in the early portion to summarize the common signal among the individual samples.

To create each final site chronology, measured tree-ring series were detrended by a 100%N spline, defined as a cubic spline with a frequency response of 0.5 for a wavelength equal to the length of the series (Cook and Peters 1981). The detrended tree-ring series, or index, is defined as the ratio of the measured ring-width to the fitted curve. Tukey's biweight robust mean was used to average the detrended ring-width from individual cores or cross-sections into a "standard" site chronology. This step included variance stabilization to account for effects of time-varying sample size and to remove any variance trends over the length of the site chronology (Osborn et al., 1997). A "residual" chronology was also generated by removing low-order autocorrelation, or persistence, from the detrended series before averaging into a site chronology. Autocorrelation, described as the dependence of growth in one year on growth in the previous few years, was removed by fitting the series with an autoregressive (AR) model with order selected by the minimum Akaike Information Criterion (AIC) (Akaike 1974, Box et al. 1994). The residual index is the residual from the AR model. Development of chronologies, including EPS testing and autoregressive modeling, was done with Program **ARSTAN** (Cook et al., 2007).

Tree-ring Dataset for this Study. A network of 46 tree-ring chronologies was assembled for this study. Tree-ring chronology site locations are marked on the map in Figure 1, and metadata for each chronology is listed in Appendix B. Besides the new or updated chronologies, a few existing tree-ring chronologies were added based on exploratory correlation analysis and knowledge of the quality of chronologies for hydroclimatic reconstruction from previous studies. The 46 tree-ring sites can be divided into two groups: 9 for Colorado River reconstruction and 37 for reconstructions in southern California. All chronologies used in the reconstructions were standardized uniformly in the same way, described above, as the chronologies from new collections and updates.

The set of chronologies has start years ranging from -350 to 1710, and end years ranging from 1992 to 2016. After truncation to eliminate early parts of the chronologies with insufficient sample depth (number of trees), the start year of usable site chronologies in the 46-site network ranges from 585 to 1775.

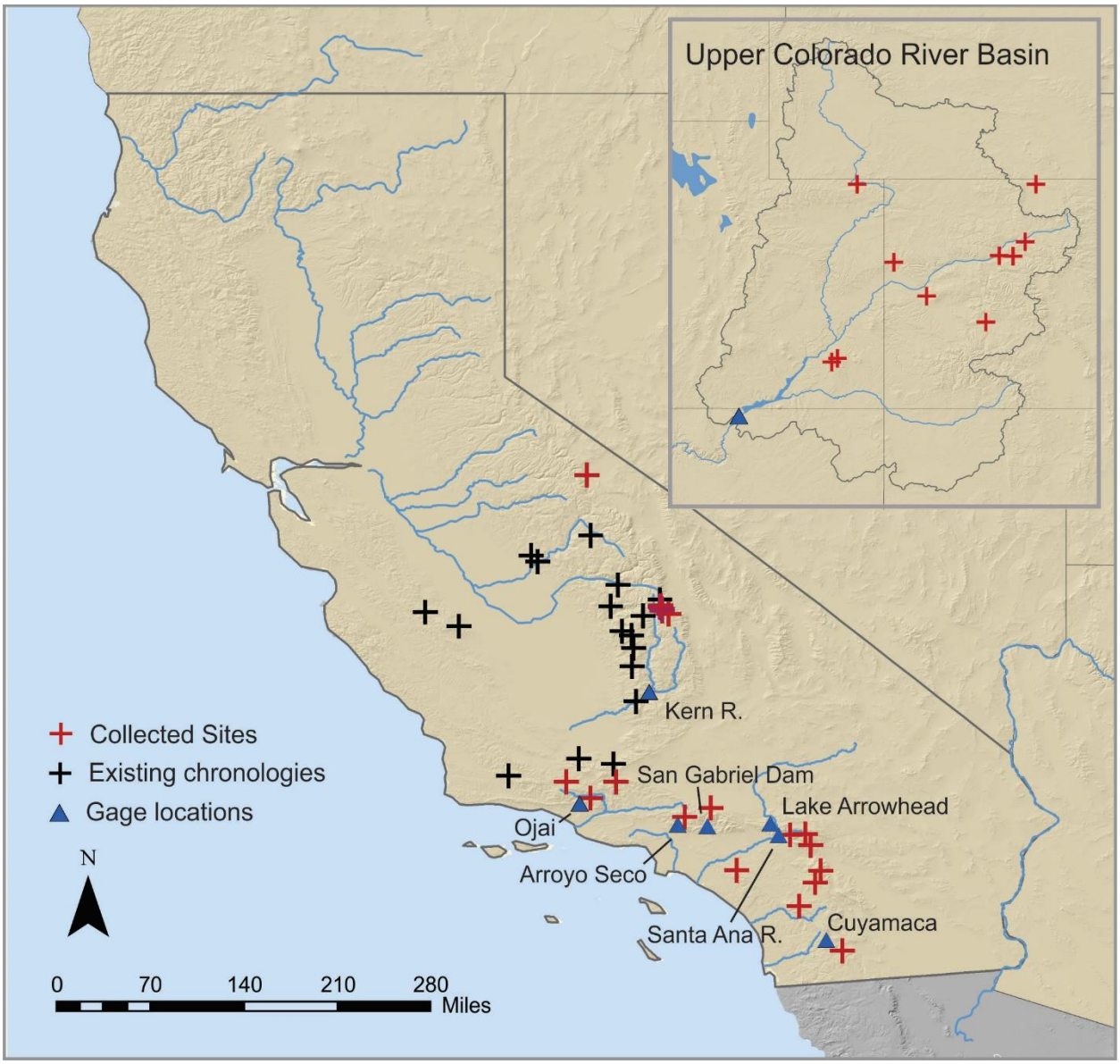

Figure 1. Map of collected chronologies (updated and new sites) and existing chronologies that contribute to the network of 46 sites.

Table 1. Site collections of tree-ring data for development of reconstruction models.

	Southern California										
No	**Code**	**Site Name**	**Latitude**	**Longitude**	**Elevation (ft)**	**Species**	**# samples**	**# dated**	**# measured**	**First year***	**Last year**
1	PMN	Pine Mountain North Update	34.67	-119.37	4428	PSMA	31	26	26	1333	2015
2	MWC	Mount Wilson Live/Ladybug	34.25	-118.10	4854	PSMA	45	45	34	1190	2015
3	MPS	Maple Spring Update	33.73	-117.55	4225	PSMA	22	17	17	1657	2015
4	KSU	Keen Camp Summit Update	33.68	-116.69	4835	PSMA	24	22	22	1458	2015
5	LCU	Lion Canyon Update	33.63	-116.71	4851	PSMA	24	24	24	1494	2015
6	FCU	Fry Creek Update	33.35	-116.88	5028	PSMA	38	38	34	1617	2015
7	539	539 Peterson Update [PT9]	34.00	-116.76	4631	PSMA	24	24	24	1692	2015
8	552	552 Peterson Update [PT2]	34.11	-116.98	4631	PSMA	26	24	24	1628	2015
9	LGU	Mt. Laguna Update	32.87	-116.42	5947	PIJE	28	28	28	1648	2015
10	RRT	Red Reef Trail	34.50	-119.12	5196	PSMA	26	26	26	1411	2015
11	HLC	Hard Luck Campground	34.67	-118.84	2919	PSMA	47	42	42	1645	2015
12	BIG	Bigrock Campground	34.40	-117.83	4858	PSMA	47	45	45	1393	2015
13	LPK	Lake Peak Update	34.12	-116.81	9896	PIFL	32	26	26	340	2015
	Southern Sierras										
No	**Code**	**Site Name**	**Latitude**	**Longitude**	**Elevation (ft)**	**Species**	**# samples**	**# dated**	**# measured**	**First year***	**Last year**
14	SBT	Siberian Pass Trail Update	36.47	-118.27	10929	PIBA	24	22	22	783	2015
15	GFS	Guyot Flat South Update	36.50	-118.35	10358	PIBA	30	28	28	931	2015
16	GFE	Guyot Flat East Update	36.52	-118.35	10913	PIBA	24	20	20	890	2015
17	GFN	Guyot Flat North Update	36.53	-118.36	10686	PIBA	24	14	14	1080	2015
18	CTS	Crabtree South Update	36.54	-118.37	10673	PIBA	24	20	20	1150	2015
19	CTN	Crabtree North Update	36.56	-118.36	10775	PIBA	24	23	23	941	2015
20	LCM	Log Cabin Mine Update	37.96	-119.16	8197	PIJE	26	26	26	1420	2016
	Upper Colorado River Basin										
No	**Code**	**Site Name**	**Latitude**	**Longitude**	**Elevation (ft)**	**Species**	**# samples**	**# dated**	**# measured**	**First year***	**Last year**
21	BFB	Beef Basin Update	37.93	-109.79	7446	PSME	25	20	14	350	2015
	SAH	Sweet Alice Hills	37.86	-109.90	8000	PSME	63	55	45	combined with BFB	
22	PUM	Pumphouse Update	39.96	-106.52	7823	PIED	22	20	20	1175	2015
23	RED	Red Canyon Update	39.70	-106.73	7141	PIED	20	20	20	1336	2015
24	TRG	Trail Gulch Update	39.71	-106.98	7252	PIED	22	17	12	996	2015
25	DOU	Douglas Pass Update	39.60	-108.81	8397	PSME	22	22	20	1382	2015
26	WIL	Wild Rose Update	39.01	-108.24	8203	PIED	20	20	20	1000	2015
27	RCK	Red Creek Update	38.56	-107.21	9397	PSME	22	22	20	1270	2015
28	DJU	Dutch John Update	40.95	-109.45	6783	PIED	22	19	19	1365	2015
29	NPC	North Park Update	40.96	-106.34	8105	PSME	22	22	22	1486	2015
							* final chronology, merged with prior collections				

2.2 Reconstruction targets

Reconstruction models were developed for the 8 river discharge and precipitation series listed in Table 2. Locations of the precipitation or streamflow gages are shown on the map in Figure 1. The river discharge records are adjusted records, and represent full natural flows. Reconstructed series are totals of volume discharge or precipitation for the October-September water year. The annual time series of observed data are listed in Appendix A. Arroyo Seco, a tributary of the Los Angeles River, drains a portion of the southern and western side of the San Gabriel Mountains. The gage, at elevation 1475 feet, is located near where the river meets the urban area of Pasadena. The Arroyo Seco watershed is small – the contributing area above the gage encompasses about 30 square miles. The headwaters are at around 5,000 feet, on the western side of Mt. Wilson. The gage records were obtained from the California Department of Water Resources for the years 1911-2015. San Gabriel Dam precipitation generally reflects the upper portion of the San Gabriel River basin. The San Gabriel Dam impounds the San Gabriel River, which has its headwaters in the San Gabriel Mountains, with peaks up to 10,000 feet. The precipitation data, 1938-2015, were obtained from the Los Angeles County Department of Public Works. The Santa Ana River drains the eastern portion of the Transverse Ranges, including the eastern San Gabriel Mountains, the San Bernadino Mountains and the San Jacinto Mountains. We reconstructed the gage at Mentone (1,965 ft) at the base of the San Bernardino Mountains. This flow at this gage is fed by snowmelt from San Gorgonio Peak, including Dry and Dollar Lakes, and by precipitation on the forested

upland area in the center of the range. Elevation drops sharply from the mountains to the San Bernardino Valley. The river is joined by tributaries from other ranges as it flows to the coast. The gage record was obtained from the California Department of Water Resources for the years 1901-2015. Lake Arrowhead precipitation reflects the northern and more arid side of the Transverse ranges, which contribute runoff to the Mojave River basin. The Lake Arrowhead precipitation gage is located on the northern side of the San Bernadino Mountains at 5,200 ft. The gage is part of the National Weather Service (NWS) Cooperative Network, and the record covers 1942-2015 (missing data were filled in using two nearby NWS Cooperative Network stations, Squirrel Inn 2 and Big Bear). Ojai precipitation generally represents the South-Central coast. The gage is 12 miles from the coast at an elevation of 745 feet. Precipitation at the gage is influenced by orographic lifting of Nordhoff Ridge and surrounding mountains with peaks rising to more than 6,000 feet. The precipitation data were obtained from the U.S. Historical Climatology Network for the years 1901-2014. Cuyamaca precipitation is broadly representative of the San Diego River Basin. This project's southernmost gage is located roughly 15 miles east of San Diego at an elevation of 4,600 feet, and is situated below Cuyamaca Peak, in the Laguna Mountains. Records were obtained from the Historical Climate Data Network for the years 1888-2014. The Kern River, with headwaters above 13,000 feet, is fed by snowmelt from Mt. Whitney, drains the southern portion of the Sierra Mountains near Bakersfield, CA, and eventually drains into California's Central Valley. The stream flow gage used in this analysis is located just downstream from Lake Isabella Dam. Records were obtained for the years 1930-2015 from the California Department of Water Resources. The Upper Colorado River is the source of about 90% of the water in the Colorado River system. The Lees Ferry (AZ) gage, which measures the upper basin flow, has been the subject of at least seven different tree-ring studies (e.g., Schulman 1945; Stockton and Jacoby 1976; Woodhouse et al. 2006; Meko et al. 2007), and was updated for this project. Estimated natural flow data were obtained from the US Bureau of Reclamation.

Table 2. Reconstruction targets. Columns are 1) river basin of study, 2) gage name of record used to represent the basin. 3) type of series (full natural flow (Q) or precipitation (P), 4) recording period (also the calibration period of reconstruction model), and 5) source of data[a].

River Basins	Record	Type	Years	Source
Los Angeles	Arroyo Seco, Pasadena	Q	1917-2014	CADWR
San Gabriel	San Gabriel Dam	P	1938-2015	LA County
Santa Ana	Santa Ana R. nr Mentone	Q	1917-2014	CADWR
Mohave	Lake Arrowhead	P	1942-2015	NWS Coop
South-Central Coast	Ojai	P	1893-2014	HCN
San Diego	Cuyamaca	P	1893-2014	HCN
Kern	Kern R. below Isabella	Q	1930-2015	CADWR
Upper Colorado	Colorado R., Lees Ferry	Q	1906-2015	BRec

[a]source of data: CADWR=California Dept. of Water Resources, NWS=National Weather Service Cooperative Network, HCN=Historical Climate Network, BRec =United States Bureau of Reclamation

2.3 Reconstruction

The series reconstructed (called the predictand), is either water year (October-September) precipitation or water year total river discharge, depending on the basin. The predictand was reconstructed using a two-stage statistical modeling process, and the same procedure was used for each of the eight target basins. The method, modified from Meko (1997), is summarized briefly here and described in more detail in Appendix D. In the first stage, tree-growth at each site is converted into an estimate of the flow or precipitation by stepwise regression (Myers 1990) of the predictand in year *t* on the tree-ring index in years *t*-1, *t* and *t*+1. Squared terms on the tree-ring predictors are included in the pool of potential predictors to allow for the possibility that the relationship between and the predictand is not linear. The outputs from this first stage of reconstruction are individual single-site reconstructions, one for each tree-ring site.

In the second stage of reconstruction, the individual single-site reconstructions are combined into a final reconstruction. For each gage, the arithmetic average of a subset of individual single-site reconstructions with a statistically significant and stable relationship with the predictand is computed. The final reconstruction values are interpolated by scatterplot smoothing (Cleveland 1979, Martinez and Martinez 2005). By this approach, the reconstructed predictand is linearly interpolated from a smoothed scatter plot of the observed predictand against the average of the single-site reconstructions. While the scatterplot-smoothing method of reconstruction method does not yield an "R^2 of regression", an ad hoc explained variance statistic, R^2=1-(SSE/SST), was computed as a measure of calibration accuracy. Here, SSE is the sum of squares of departures of observed minus reconstructed predictand, and SST is the sum of squares of departures of the observed predictand from its calibration period mean. R^2 multiplied by 100 can be interpreted as "percentage of variance explained" by the model.

The procedure was repeated for subsets of tree-ring chronologies with different periods of common time coverage to build a "most skillful" version of reconstruction, starting in the early 1400s or late 1300s, and a "longest" version of reconstruction, starting in the early 1100s. The longest reconstruction sacrifices some accuracy, as it necessarily relies on a reduced network of tree-ring sites. But this long view provides reconstructions for Southern California that overlap the latter part of medieval period, when tree-ring records documents extremely persistent drought in other parts of the western United States (e.g., Stine 1994, Meko et al. 2007). The most skillful reconstruction makes use of many of the most climate-sensitive tree-ring chronologies in Southern California.

The longest and most skillful versions of reconstruction were built by splicing together segments of nested, or sub-period, reconstructions (Meko 1997), each of which relies on a constant set of tree-ring chronologies for its full length. Exploratory analysis suggested using four nested reconstructions:

1. Rec1: starts in early 1100s; relies on only the longest available chronologies; least accurate of the nested reconstructions
2. Rec2: starts in the late 1390s to early 1400s; tree-ring network generally large enough to give close to maximum accuracy of reconstruction while still providing long time coverage
3. Rec3: starts in early 1700s: makes use of a dense tree-ring network; the most accurate reconstruction, but generally only marginally more accurate than Rec2
4. Rec4; highly variable start year, but extends as close as possible to present (2015 for Colorado River, 2016 for other basins); tree-ring network much smaller than for Rec2 and Rec3; generally lower reconstruction accuracy than Rec2 or Rec3; sole purpose is to provide the last reconstructed year

The longest reconstruction is the same as and Rec1, as it uses Rec1 for all reconstructed years. The most skillful reconstruction uses Rec4 for its last year, and a combination of Rec2 and Rec3 for all other years. Confidence intervals for the reconstruction were estimated by method of upper and lower smooths (Martinez and Martinez 2005). By this method, a 50% confidence bands are interpolated from separate smoothed scatterplots fit to the positive and negative cross-validation residuals of the reconstruction. The

width of resulting confidence bands varies with magnitude of reconstructed predictand, and can reflect the amplified uncertainty in wet years typical of many dendrohydrologic reconstructions (Meko and Woodhouse 2011).

2.4 Analysis of Reconstructions

The reconstructions were analyzed in order to: 1) quantify droughts and wet periods, 2) identify cycles and quasi-cycles, 3) check consistency of reconstructions with other paleoclimatic data, 4) place statistics for the instrumental period in a long-term context, 5) identify cyclical patterns in covariation of drought in Southern California, Northern California/Central Valley and the Upper Colorado River Basin (UCRB) and 6) identify spatial modes of drought patterns over western North America during episodes of most severe Southern California drought. The methods used in these analyses are described below.

Droughts and wet periods are summarized by two approaches. The first approach employed is runs analysis, as described by Salas et al. (1980). A run is defined by a sequence of two or more years below a threshold. The run-length is a measure of drought duration, or the number of years in the run sequence. The threshold used in this project was the mean of the instrumental record. Drought runs were tabulated for all reconstructions, then the average annual value (as percent of the mean) for each run event was determined. Scatterplots of drought duration and average annual intensity (cumulative departure/number of years in the run) for each event were generated. Events that occurred in the 20th and 21st centuries were highlighted. The second approach for identifying drought episodes was to calculate moving averages of each time series. The moving average windows were 5- , 10- , and 20-years in length. To identify the driest/lowest periods of each window length, the moving averages for the three window lengths were ranked, and the 10 lowest non-overlapping periods were identified for the 5-year and 10-year periods, and the lowest five intervals for the 20-year periods. The process was repeated for the wettest periods. The start and end years, along with the percent of the mean averaged for the years in the period were tabulated. In order to evaluate the distribution of these lowest ranking periods over time, time series plots were generated to show their occurrence in both the most skillful and longest reconstructions. In addition, a separate set of graphics shows the distribution of the wettest and driest 5- and 10-year average periods. The main body of this report shows results for San Gabriel Dam precipitation, including its longest most skillful reconstructions, while graphics for all basins are included in Appendix E.

Cycles in the reconstructions are summarized in this report by spectral analysis, wavelet analysis and smoothed time plots. These methods are described briefly below and in more detail in Appendix D. We use the term "cycles" loosely here to include variations that are rhythmic in some sense, but do not necessarily have a regular wavelength or period, and may be present in some parts of the time series and not in others. An example might be droughts that tend to recur at 20-year intervals. Sometimes the interval may be longer or shorter than 20 years, and the intensity – as magnitude of flow anomaly – may be larger or smaller.

Spectral analysis summarizes cycles by displaying the variance of the time series as a function of frequency, or its inverse – wavelength. The variance of a time series can be mathematically split up into contributions from different wavelengths. Rapid changes from year to year are high-frequency, or short-wavelength fluctuations. Gradual changes over decades or centuries are low-frequency, or long-wavelength fluctuations. The spectrum of a time series is a plot of the variance as function of wavelength or frequency. Usually a spectrum is plotted along with a line called the null continuum, which is the theoretical spectrum of a time series with the same total variance, but with variance distributed either evenly over all wavelengths (white noise), or with more variance at low frequencies than at high frequencies (red noise). Confidence bands can be computed and plotted around the spectrum to identify whether any given peak in the spectrum is statistically significant. This is a test of whether the spectrum at some wavelength differs significantly (e.g., α=0.05) from the null continuum. Spectra are estimated in this study by the smoothed-periodogram method (Bloomfield 2000).

Wavelet analysis (Torrence and Compo, 1998; Grinsted et al. 2004) is used to investigate the temporal evolution of wavelike or cyclical features in the instrumental and reconstructed precipitation and streamflow series. This contrasts with spectral analysis, which summarizes the cycle over the whole length of the series. Wavelet differs from spectral analysis by being applicable to nonstationary as well as to stationary series, in not relying on the assumption that cyclic variations be sinusoidal in form, and in being specifically intended to study cyclical variations that may "come and go" over the length of the time series. Wavelet analysis thus is useful for investigating wavelike features that may be localized to parts of a long times series. For example, wavelet analysis can directly address whether some multi-decadal rhythm in wet and dry periods occurs in a long reconstructed streamflow series, and can identify when that rhythm is absent or present, and when the rhythm is weaker or stronger. The continuous wavelet transform (CWT) is a color map that gives variance of a time series as a function time (x-axis) and wavelength or frequency (y-axis).

Wavelet analysis can be extended to multiple series to address whether cyclic variations in one series are related in some sense temporally with those in another series. The variations in two series may be in-phase (peaks occurring simultaneously, troughs occurring simultaneously), or out-of-phase (e.g., some time lag between peaks in the two series), or unrelated. Covariation of cyclic features in pairs of series can be summarized with the wavelet transform coherency, or WTC (Grinsted et al., 2004). We apply the WTC, which is analogous to correlation as a function of time and frequency, to study the covariation of hydrologic series in Southern California, the Sacramento River Basin and the Colorado River Basin.

Smoothed time series plots are used to display oscillations in the time series as a function of time. For these plots, annual time series were smoothed using a Gaussian filter with specified frequency response (Mitchell et al. 1966). Specifically, for all plots related to the cycle analysis, the filter is a 9-weight Gaussian filter that emphasizes variations at decadal and longer time scales and smooths out more rapid fluctuation. Additional information on this filter, including a listing of the filter weights, can be found in Appendix D.

Consistency of the new or updated reconstructions with previous versions was evaluated for the Kern and Colorado River reconstructions. A Kern River flow reconstruction was generated by Adams et al. (2015), and the reconstruction time series was downloaded from the supplemental data accompanying the 2015 paper for this assessment. The Colorado River at Lees Ferry reconstructions from Woodhouse et al. (2006; versions A and B) and Meko et al. (2007) were targeted for comparison with the Colorado River reconstructions from this project. In both sets of comparisons, correlation analysis and a visual analysis of the smoothed time series were used to assess the degree of similarity. In the Adams et al. (2015) Kern River reconstruction, the gage record was appended onto the reconstruction at 1893, so it was not possible to statistically evaluate the reconstruction skill, but a comparison of the lowest ranking single, 10-year, and 20-year average periods was made between the most skillful Kern reconstruction from this project and the Adams et al. (2015) reconstruction. For the Colorado River reconstructions, correlations of the reconstructions with the observed (natural flow) gage record were assessed. An evaluation of the statistical properties of the set of reconstructions, compared to the natural flow for 1906-1997 was made for the mean, median, maximum, minimum, upper and lower quartiles, standard deviation, and autocorrelation.

Statistical characteristics of the reconstructed precipitation or river discharge for the instrumental period are placed in a long-term context by two methods. First is comparison of the statistical measure for the full-length reconstruction with the same statistic computed for the instrumental period. Second is comparison of the statistic for the *m*-year instrumental period with the same statistic computed for many other *m*-year periods provided by the full-length reconstruction. Five statistics are examined: mean, median, standard deviation, skew, and lag-1 autocorrelation. The mean is the arithmetic average of the time series (e.g., annual flow or precipitation) for some designated period. The median is the middle value of the data distribution: half of the values are higher than the median and half are lower. The standard deviation is a measure of the variability or spread of the data, and is defined as the square root of the

averaged squared departure from the mean. Standard deviation has the same units as the time series itself. The variance is the square of the standard deviation, and so yields similar information about the spread of the data as the standard deviation.

Skew measures the symmetry of a time series. Some data distributions, such as the normal distribution, are symmetric about the mean, such that large positive departures from the mean are no more likely than large negative departures. Annual precipitation and annual river flow are often positively skewed because the distribution is limited by 0 on the low end (precipitation cannot be negative) but can have occasional very large positive departures. Lag-1 autocorrelation measures the persistence of a time series, or the correlation the series with itself shifted by one year. A positive lag-1 autocorrelation means a positive departure from the mean in year t tends to be followed by a positive departure in year t+1, and a negative departure in year t tends to be followed by a negative departure in year t+1. Various factors, including natural surface and underground storage of water, could lead to positive lag-1 autocorrelation in river discharge. Various carryover processes in tree-growth (e.g., photosynthate storage) can lead to positive autocorrelation in tree-ring series. Lag-1 autocorrelation in tree-ring series can affect the assessment of drought duration from tree rings.

The five statistics described above are summarized in tables. Tests are applied for the statistical significance of means and standard deviations in the instrumental period and long-term reconstructions. A *t*-test for difference of means (Mitchell et al. 1966) is applied to test the statistical significance of reconstruction means for the full-length reconstruction and for the shorter segment overlapping the gaged record. A variance-ratio test (Benjamin and Cornell, 1970) is applied to test for a difference of variance for the same subsets of data. Bar charts are used to summarize the tests on means and standard deviations.

A time-windowed analysis of statistics is applied to check whether the time series of reconstructed flow or precipitation in the *m*-year period covered by the gaged record is wetter or drier than other same-length periods over the tree-ring record. Dot plots are used to summarize the standing of the gaged period among the wettest and driest (for the mean) and most-variable and least variable (for the standard deviation) non-overlapping *m*-year periods of the full reconstructions.

Patterns in covariation of drought in Southern California, Northern California/Central Valley, and the upper Colorado River basin are analyzed by several methods, including the use of three ranked and summed drought metrics to assess droughts, and cross-wavelet analysis, which is described above. Droughts in the three regions were ranked by duration of runs, cumulative deficit, and intensity (cumulative deficit/years in drought run), and then an overall score was calculated for each drought based on the three rankings (Biondi et al. 2002). In this analysis, runs were defined by consecutive years below the median. Events of three or more years in duration were considered. The distribution of drought as defined by the three metrics, and the overall score, was assess over past centuries and across the three regions.For these analyses, the Meko et al. (2014) reconstruction of the Sacramento River Index (Sacramento, Feather, American, and Yuba Rivers) was selected to represent northern California/Central Valley and the San Gabriel precipitation reconstruction from this project to represent southern California. The updated Colorado River reconstruction at Lees Ferry from this project was selected to represent the UCRB. The common period of analysis was 1416-2012.

Spatial modes of drought over western North America are summarized by developing composite maps of western US drought conditions for intervals during which droughts were severe in southern California. The rankings of driest 10-year periods across Southern California were used to select six decades for comparison. Composite maps were generated using gridded drought (quantified by the Palmer Drought Severity Index which integrates moisture and temperature to estimate dryness) reconstructions from Cook et al. (2010). For these six periods, composite maps of reconstructed drought patterns were calculated by averaging reconstructed drought values at each gridpoint over the 10-year period. The maps were constructed by interpolating drought values between each gridpoint value to represent the spatial pattern of drought for each 10-year period across the western US.

3. Results

3.1 Reconstructions

The individual sub-period reconstructions, relying on between 2 and 16 tree-ring chronologies, explain 40-80% of the variance of the flow or precipitation (Figure 2). Whether a particular chronology is used by a reconstruction model depends on the time coverage of the chronology as well as its correlation with the target hydrologic series. Chronologies with exceptionally strong climatic signal may be shared by several reconstructions, although the weighting of importance of that chronology will differ from basin to basin. Tree-ring chronologies contributing to each of the time-nested models in the 8 target basins can be identified by referring to the cross-reference matrix table in Appendix C and the chronology metadata in Appendix B. The two middle groups of bar charts in Figure 2 show that little accuracy is sacrificed in dropping out some chronologies with late start dates and shifting back the start year of reconstruction from 1706 to the early 1400s.

Summary statistics of reconstruction models are listed in Table 3. The most skillful reconstructions explain 54%-79% of the variance of the predictand, while longest reconstructions explain 42%-67% of the variance. The most accurate reconstructions by the R^2 statistic are those for the Colorado River and Kern River (most skillful versions). The most accurate of the precipitation reconstructions is San Gabriel Dam (R^2=0.77). The exceptionally strong tracking of observed precipitation by the San Gabriel Dam reconstruction is illustrated in time series plots for the overlap period of observed and reconstructed precipitation (Figure 3a). Persistent drought sequences, such as 1948-51 and 2012-15 are well reconstructed, as are rapid switches between wet and dry conditions, such as 1983-84 and 1993-94. Largest errors occur in wet years (e.g., 1943, 1952, and 2005). Time plots of the full length of most skillful and longest reconstructions for San Gabriel Dam are shown in Figures 3b and 3c. Corresponding time plots of observed and reconstruction precipitation or discharge for all 8 basins are included in Appendix E. All reconstructions are also provided in the list of digital data products (see Appendix I).

Sharing of predictor tree-ring chronologies by reconstruction models for the various basins (except the Colorado River) forces a higher inter-basin correlation in the reconstructions than in the instrumental data. This bias in spatial correlation is evident in correlation matrices for the common period of 1942-2014 for the observed and reconstructed series. With the exception of the Colorado River, which shares no predictors with the other reconstructions, inter-basin correlations are lower for the observations (Table 4) than for the reconstructions (Table 5). If the Colorado River is omitted, the median inter-basin correlation over 1942-2014 is 0.85 for the observations and 0.95 for the reconstructions. A correlation matrix (not shown) for the full reconstructions (most skillful version), 1426-2015, indicates the inter-basin correlations for the instrumental period are representative of the correlations for full reconstruction period. The largest difference (long-term minus instrumental) in correlation is -0.08, and the median difference in correlation is -0.02.

Sharing of predictors by reconstruction models does not complicate interpretation of correlation of the Colorado River reconstruction with other reconstructions. Independence of tree-ring networks allows the reconstructions to be applied to assess changes in spatial correlation of hydroclimate from Colorado to California over time. The observed flows of the Colorado, 1942-2014, are most highly correlated with flows of the Kern (r=0.56; Figure 4). This correlation is underestimated in the reconstructions for the same period (r=0.48), likely because tree-rings are imperfect recorders of discharge. The reconstructions suggest that the coherence between Colorado River and Kern River flows has been a bit higher in over 1942-2014 than over the full period of most skill reconstruction, 1426-2015 (r=0.42). Overall, considering the Colorado and other basins, spatial coherence or inter-basin correlation of hydrologic series is similar over the full tree-ring record as over the shorter instrumental period, with just slightly lower correlation over the longer record.

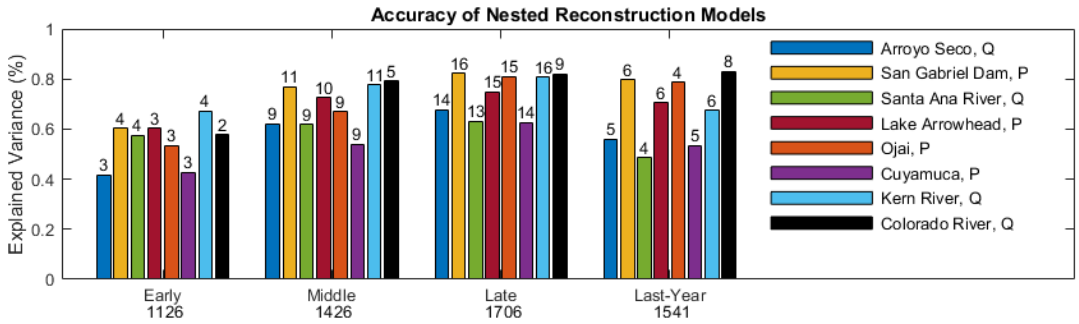

Basin	Early	Middle	Late	Last-Year
Arroyo Seco, Q	1125 2015	1404 2015	1706 2015	1461 2016
San Gabriel Dam, P	1126 2015	1405 2015	1706 2015	1468 2016
Santa Ana River, Q	1125 2015	1404 2015	1706 2015	1455 2016
Lake Arrowhead, P	1126 2015	1426 2015	1706 2015	1468 2016
Ojai, P	1126 2015	1391 2015	1706 2015	1456 2016
Cuyamuca, P	1126 2015	1404 2015	1696 2015	1461 2016
Kern River, Q	1125 2015	1404 2015	1535 2015	1467 2016
Colorado River, Q	1116 2014	1416 2014	1541 2014	1541 2015

Figure 2. Accuracy and time coverage of sub-period reconstructions. Top: accuracy as measured by decimal proportion of precipitation (P) or river discharge (Q) explained by reconstruction model. Number of tree-ring chronologies in model annotated at top of bar. Latest start date of reconstruction in any of the 8 basins annotated at bottom of group of bars. Bottom: time coverage of sub-period reconstructions. The models "Early", "Middle", "Late", and "Last-Year" correspond to sub-period reconstructions Rec1, Rec2, Rec3 and Rec4, as defined in Section 2.3. Chronologies used by each sub-period reconstruction can be identified by referring to the cross-reference table in Appendix C and tree-ring metadata in Appendix B.

Table 3. Summary statistics[a] of reconstruction models

	Most Skillful			Longest Model		
Reconstruction	**Start Year**	**End Year**	**Explained Variance (R^2)**	**Start Year**	**End Year**	**Explained Variance (R^2)**
Arroyo Seco	1404	2016	0.62	1125	2015	0.42
San Gabriel Dam	1405	2016	0.77	1126	2015	0.60
Santa Ana R.	1405	2016	0.62	1125	2015	0.58
Lake Arrowhead	1426	2016	0.73	1126	2015	0.60
Ojai	1391	2016	0.67	1126	2015	0.53
Cuyamaca	1404	2016	0.54	1126	2015	0.43
Kern R. below Isabella	1404	2016	0.78	1125	2015	0.67
Colorado R.	1416	2015	0.79	1116	2014	0.58

[a]Time coverage of reconstructions, defined by the first and last year; and the percentage of variance explained by the reconstruction model in its calibration period.

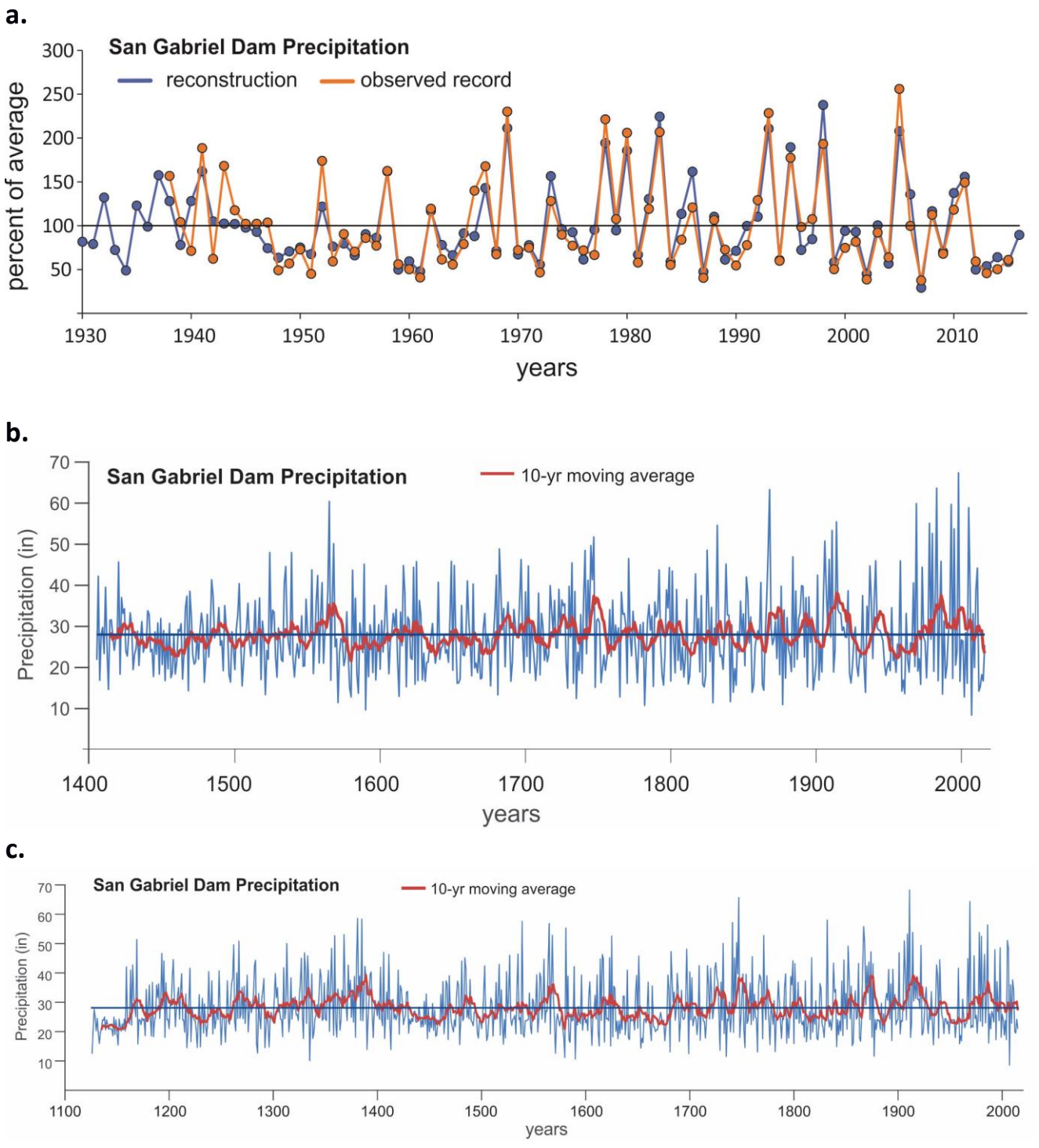

Figure 3. Time plots of observed and reconstructed precipitation for San Gabriel Dam. a) Comparison of reconstructed and observed precipitation for the calibration period. b) Annual values of most skillful reconstruction with 10-yr moving average (1405 – 2016). c) Annual values of longest reconstruction with 10-yr moving average (1126 – 2015). Precipitation is expressed as percent of instrumental mean (inches). The calibration period for the reconstructed and observed precipitation is the 1938-2015.

Table 4. Correlation matrix of observed precipitation and discharge series, 1942-2014.

	SECO	GABE	ANA	ARROW	OJAI	CUYA	KERN	COLO
SECO	1.00	0.93	0.90	0.87	0.87	0.77	0.76	0.35
GABE	0.93	1.00	0.89	0.93	0.93	0.85	0.80	0.43
ANA	0.90	0.89	1.00	0.86	0.84	0.84	0.82	0.42
ARROW	0.87	0.93	0.86	1.00	0.89	0.85	0.74	0.43
OJAI	0.87	0.93	0.84	0.89	1.00	0.82	0.79	0.42
CUYA	0.77	0.85	0.84	0.85	0.82	1.00	0.74	0.53
KERN	0.76	0.80	0.82	0.74	0.79	0.74	1.00	0.56
COLO	0.35	0.43	0.42	0.43	0.42	0.53	0.56	1.00

Table 5. Correlation matrix of most skillful reconstructions of precipitation and discharge series, 1426 - 2015.

	SECO	GABE	ANA	ARROW	OJAI	CUYA	KERN	COLO
SECO	1.00	0.95	0.94	0.94	0.97	0.92	0.95	0.42
GABE	0.95	1.00	0.95	0.99	0.99	0.97	0.94	0.43
ANA	0.94	0.95	1.00	0.92	0.95	0.95	0.97	0.45
ARROW	0.94	0.99	0.92	1.00	0.98	0.96	0.91	0.41
OJAI	0.97	0.99	0.95	0.98	1.00	0.97	0.96	0.44
CUYA	0.92	0.97	0.95	0.96	0.97	1.00	0.93	0.47
KERN	0.95	0.94	0.97	0.91	0.96	0.93	1.00	0.48
COLO	0.42	0.43	0.45	0.41	0.44	0.47	0.48	1.00

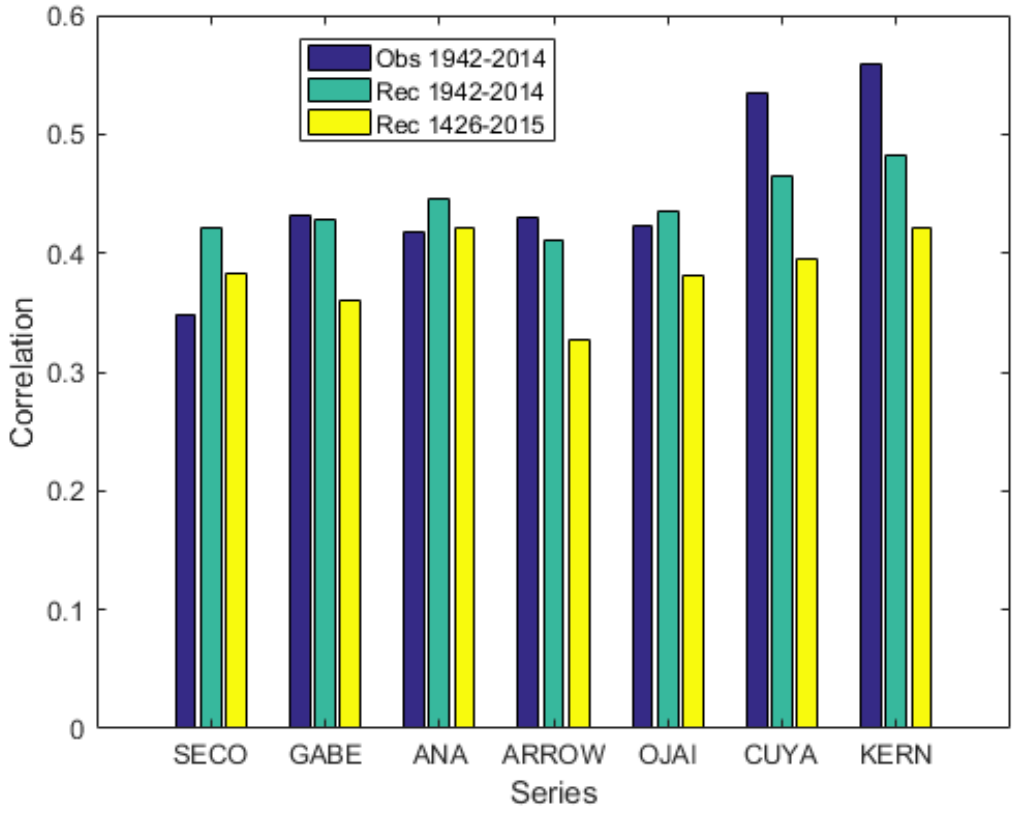

Figure 4. Correlation of Colorado River discharge with observed and reconstructed hydrologic series in other basins. Series along x-axis are either annual precipitation or annual total natural flow of rivers (see text). Instrumental period 1942-2014 is the period in common to all the observed time series and reconstructions. Reconstruction period 1426 is the common period of all most skillful reconstructions.

3.2 Droughts and Wet Periods

The magnitude and duration of droughts prior to the start of the instrumental records can be compared with those of instrumental period to place instrumental period events in a long-term context. Here, we use the San Gabriel Dam precipitation reconstructions as an example (results are available for the other reconstructions in Appendix G). Figure 5 shows drought events as consecutive years below the instrumental mean based on the runs analysis. As expected, this analysis shows that shorter droughts, lasting from 2 – 3 years, are more frequent than longer droughts. The annual average drought intensity typically decreases as drought duration increases because the hydroclimate deficits are averaged over a longer period of time. In some cases, the recent droughts are the most intense, on an average annual basis for a duration category, yet the full reconstruction highlights droughts of longer duration than the observed period.

For the most skillful reconstruction of the San Gabriel Dam precipitation, the longest drought lasted 8 years from 1569 – 1576 (Figure 5), but several other notable consecutive-year droughts occurred in the 20th and 21st centuries. For example, the driest 3-year period occurred from 1959 to 1961 and driest five-year period occurred from 2012 to 2016. The period from 1945 – 1951 nearly matched a mid-1600s event (1629 – 1635) as the driest seven-year drought of the record. The San Gabriel dam record highlights the mid-1600s as period of intense drought, including the most intense 4-, 6- and 7-year droughts of the reconstruction (i.e., 1652 – 1655, 1665 – 1670, and 1629 – 1635). The longest San Gabriel Dam

precipitation reconstruction exhibits many of the same droughts as the most skillful reconstruction, but highlights the remarkably long drought of the mid-1100s. Based on runs analysis, the longest drought in the San Gabriel Dam lasted 33 years, and occurred from 1126 – 1158 (Figure 6). Among shorter, yet relatively severe droughts in the 20th and 21st centuries, the periods from 1959 – 1961 and 1999 – 2004 are the driest 3- and 6-year droughts of this record. For additional plots for all gages in southern California, northern California and the Colorado River, see Appendix F.

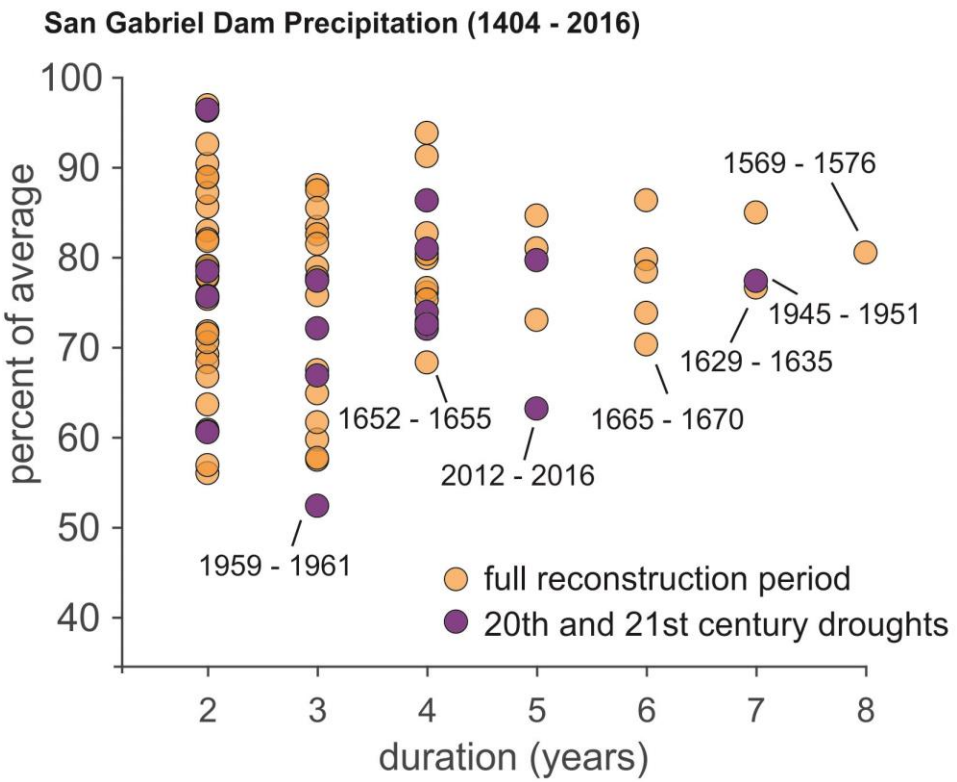

Figure 5. Scatterplot of San Gabriel Dam drought duration and average severity for each drought event based on runs analysis. Drought duration defined by the number of consecutive years below the instrumental mean. Orange dots indicate droughts during the tree-ring period (1404 – 1899), and purple dots indicate droughts during the instrumental period (1900 – 2016) of the reconstruction.

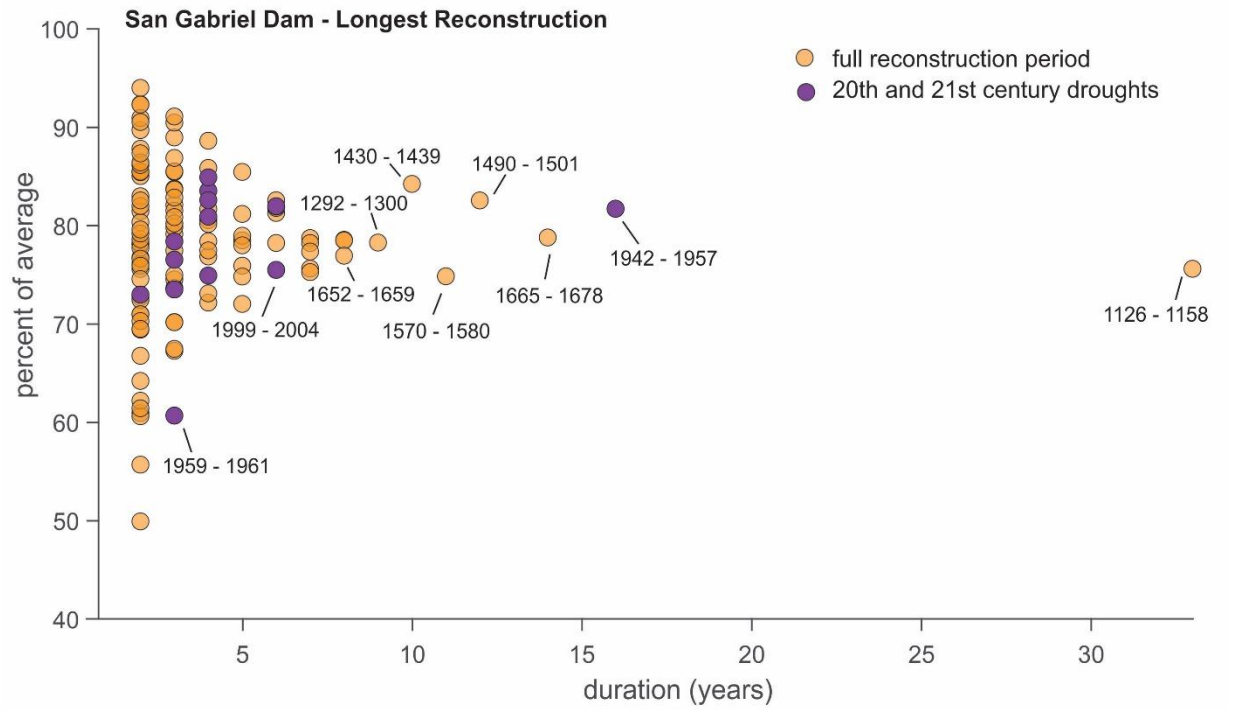

Figure 6. Scatterplot of San Gabriel Dam drought duration and annual average severity for each drought event. Drought duration defined by the number of consecutive years below the instrumental mean. Orange dots indicate droughts during the tree-ring period (1126 – 1899), and purple dots indicate droughts during the instrumental period (1900 – 2015) of the reconstruction.

Ranked moving averages identify the driest periods of a defined 5-, 10-, 20-year window length. In this case, a long dry period could contain one or more years above the mean value. For example, the mid-1400s drought ranks as one of the driest 10-year periods of the past 600 years for the San Gabriel Dam (Figure 7, bottom; results for the other reconstructions are available in Appendix G), yet it is composed of shorter multi-year droughts separated by one or two years above the mean. Based on runs analysis, this relatively long dry period would have been missed, but is visible in ranked moving averages shown in Figure 7 (bottom panel) and Table 6a. Tables 6a and 6b list the driest 5-, 10-, and 20-year periods in most skillful reconstructions in the 8 basins. Corresponding listings for wet periods can be found in tables 7a and 7b.

The moving averages for San Gabriel Dam precipitation show many examples of overlapping 5-, 10-, 20-year dry periods, where extreme shorter dry periods fall within longer dry periods. For example, the mid-1950s ranks as the one of the lowest 5-, 10- and 20-yr drought periods in the most skillful reconstruction. Other examples of overlapping shorter and longer droughts in the most skillful reconstructions are in the mid-1400s and mid-1600s, while the long San Gabriel Dam reconstructions highlights the clustering of dry periods in the 1100s (Figure 7, top panel). Figure 8 shows the timing of wet and dry periods by plotting the lowest and highest 5- and 10-yr moving averages together for the most skillful reconstruction of San Gabriel Dam precipitation. The dry periods tend to be fairly evenly distributed throughout the records, with a few gaps centered on 1500 and in the late 1800s. However, the wet periods tend to cluster towards the end of the record, from the mid-1800s to the end of the 20th century. During this interval of time, a number of wet periods (5 or 10-yr) occur in sequence, with no extreme droughts in between. There are also rapid shifts between extreme wet and dry conditions, such as the 1560s wet period that is followed by one of the driest periods on record (1570s – 1580s). Another example is shift from wet to dry in the first half of the 18th century.

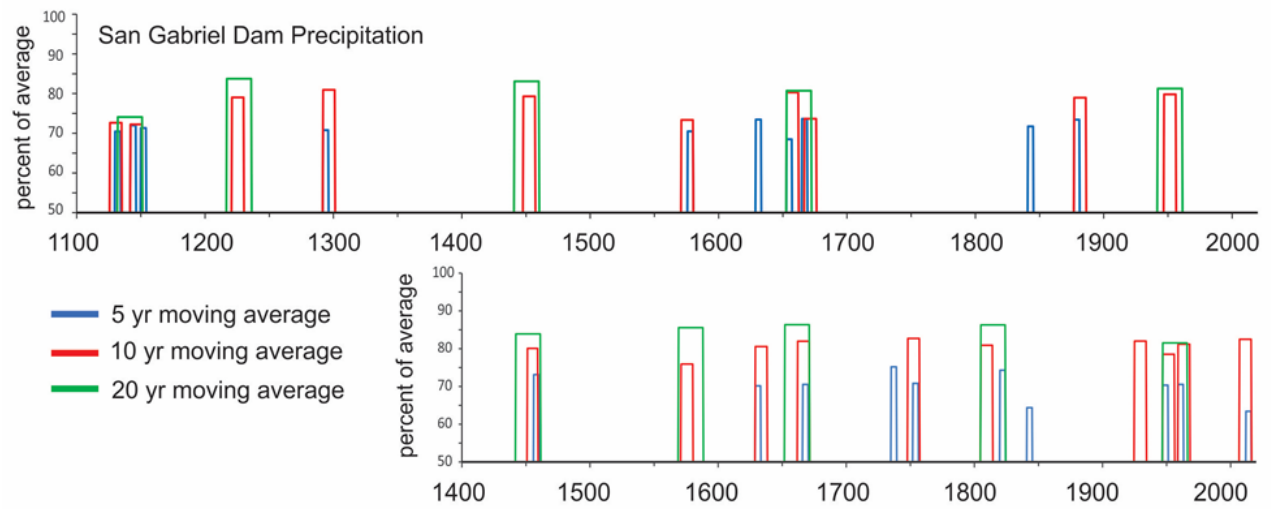

Figure 7. The lowest 5-, 10-, 20-year drought periods based on ranked moving averages for the most skillful and longest San Gabriel precipitation reconstructions. The results for the 5- and 10-yr droughts include the lowest 10 rankings, while the 20-yr droughts include the lowest 5 rankings.

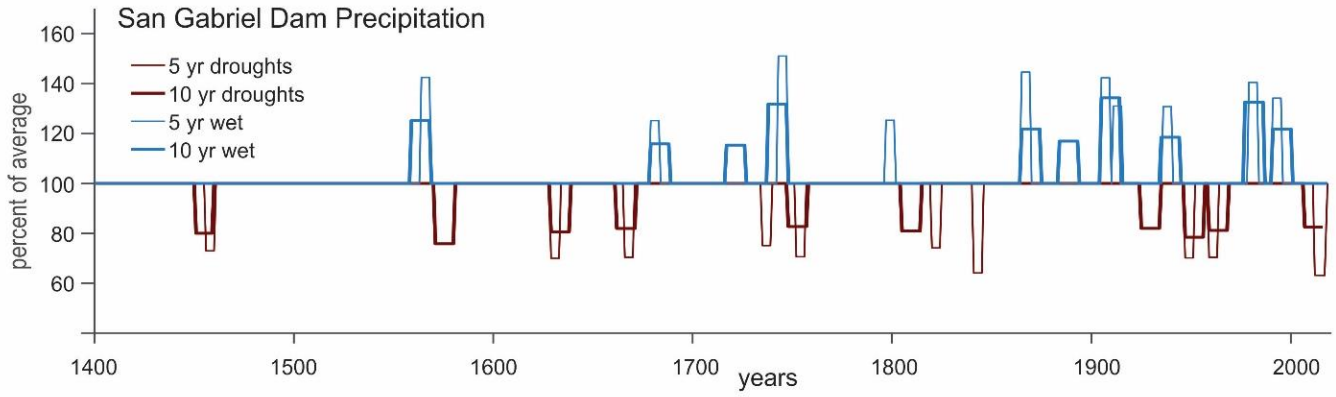

Figure 8. The 10 lowest 5- and 10-yr droughts and wet periods, based on ranked moving averages for the San Gabriel Dam Precipitation (most skillful reconstruction). Units are in percent of instrumental mean.

Table 6a. The 10 lowest ranking 5-, 10-, 20-yr drought periods of most skillful reconstructions for gages Arroyo Seco, San Gabriel Dam, Santa Ana River, and Lake Arrowhead. Moving averages expressed as percentage of instrumental mean.

5 yr moving average		5 yr moving average		5 yr moving average		5 yr moving average	
Arroyo Seco R	**% of mean**	**San Gabriel**	**% of mean**	**Santa Ana R**	**% of mean**	**L. Arrowhead**	**% of mean**
1841 - 1845	24.0	2012-2016	63.2	1841 - 1845	33.8	1841-1845	57.6
2012 - 2016	24.9	1841-1845	64.2	1666 - 1670	35.5	2012-2016	62.2
1947 - 1951	29.1	1628-1633	70.0	1628 - 1633	37.4	1576-1580	62.8
1629 - 1633	32.3	1947-1951	70.2	1958 - 1963	37.9	1456-1460	63.7
1752 - 1756	33.0	1959-1963	70.4	2012 - 2016	39.7	1628-1633	65.1
1666 - 1670	33.7	1666-1670	70.4	1947 - 1951	41.2	1666-1670	65.2
1456 - 1460	35.0	1752-1756	70.7	1456 - 1460	43.7	1947-1951	65.6
1927 - 1931	36.0	1456-1460	73.0	1753 - 1757	44.9	1752-1756	69.2
1735 - 1739	36.6	1820-1824	74.2	1571 - 1575	45.2	1953-1657	70.3
1806 - 1810	37.8	1735-1739	75.1	1496 - 1500	46.4	1735-1739	70.3
10 yr moving average		**10 yr moving average**		**10 yr moving average**		**10 yr moving average**	
Arroyo Seco R	**% of mean**	**San Gabriel**	**% of mean**	**Santa Ana R**	**% of mean**	**L. Arrowhead**	**% of mean**
1923 - 1934	42.6	1571-1580	75.8	1571 - 1580	46.6	1571-1580	68.1
1571 - 1580	43.3	1947-1956	78.5	1948 - 1957	47.2	1452-1461	73.3
1452 - 1461	44.8	1450-1459	80.0	1452 - 1461	49.9	1946-1955	75.5
1805 - 1814	45.6	1629-1638	80.5	1629 - 1638	49.9	1925-1934	76.3
1947 - 1956	46.1	1805-1814	80.9	1959 - 1968	53.2	1629-1638	78.1
1748 - 1757	48.7	1959-1968	81.2	1665 - 1674	53.5	1662-1671	78.5
1629 - 1638	50.2	1662-1671	82.0	1806 - 1815	54.0	1841-1850	78.5
1775 - 1784	51.2	1925-1934	82.0	1775 - 1784	57.0	1590-1599	78.6
1856 - 1865	51.4	2007-2016	82.5	1841 - 1850	57.4	2007-2016	79.4
1841 - 1850	52.1	1748-1757	82.7	1925 - 1934	57.6	1856-1865	79.6
20 yr moving average		**20 yr moving average**		**20 yr moving average**		**20 yr moving average**	
Arroyo Seco R	**% of mean**	**San Gabriel**	**% of mean**	**Santa Ana R**	**% of mean**	**L. Arrowhead**	**% of mean**
1442 - 1461	51.8	1947-1966	81.5	1947 - 1966	51.8	1442-1461	78.1
1947 - 1966	52.2	1442-1461	83.9	1442 - 1461	56.1	1571-1590	79.1
1569 - 1588	58.2	1569-1588	85.6	1629 - 1648	58.4	1947-1966	79.8
1629 - 1648	58.4	1805-1824	86.3	1571 - 1590	63.7	1652-1671	82.9
1917 - 1936	59.7	1652-1671	86.4	1652 - 1671	65.4	1841-1860	83.9

Table 6b. The 10 lowest ranking 5-, 10-, 20-yr drought periods of most skillful reconstructions for gages Ojai, Cuyamaca, Kern River, and Colorado River Moving averages expressed as percentage of instrumental mean

5 yr moving average		5 yr moving average		5 yr moving average		5 yr moving average	
Ojai	% of mean	Cuyamaca	% of mean	Kern River	% of mean	Colorado	% of mean
2012-2016	69.3	1841-1845	62.7	1841 - 1845	40.3	1581-1585	62.7
1841-1845	69.3	2012-2016	67.7	1666 - 1670	46.1	1457-1461	63.6
1959-1963	76.1	1666-1670	68.1	2012 - 2016	48.1	1844-1848	64.0
1628-1633	76.3	1959-1963	69.8	1628 - 1633	49.5	1499-1503	65.0
1735-1739	77.4	1628-1633	70.2	1456 - 1460	52.1	1778-1782	66.0
1665-1669	77.9	1576-1580	70.6	1947 - 1951	53.0	1684-1688	68.5
1947-1951	78.0	1653 - 1657	73.0	1653 - 1657	54.3	1542-1546	69.2
1752-1756	78.4	1752-1756	73.6	1752 - 1756	55.4	2000-2004	69.5
1820-1824	78.9	1456-1460	75.6	1576 - 1580	55.9	1664-1668	69.8
1456-1460	79.1	1947-1951	75.6	1960 - 1964	57.1	1755-1759	69.9
10 yr moving average		10 yr moving average		10 yr moving average		10 yr moving average	
Ojai	% of mean	Cuyamaca	% of mean	Kern River	% of mean	Colorado	% of mean
1571-1580	79.9	1571-1580	73.9	1571 - 1580	57.4	1452-1461	66.1
2007-2016	82.9	1629-1638	79.1	1629 - 1638	61.6	1499-1508	66.2
1450-1459	83.8	1662-1671	80.1	1452 - 1461	61.9	1583-1592	68.3
1629-1638	83.8	1959-1968	80.9	1925 - 1934	63.4	1773-1782	70.3
1946-1955	84.6	1452-1461	81.6	1947 - 1956	64.3	1623-1632	77.4
1925-1934	84.7	1840-1849	82.4	1841 - 1850	67.3	1706-1715	78.0
1805-1814	85.1	1860-1865	83.0	1668 - 1676	67.7	1874-1883	79.4
1748-1757	85.2	1947-1956	83.3	1806 - 1815	67.9	1896-1905	79.6
1860-1865	85.8	2007-2016	83.7	1775 - 1784	68.3	1662-1671	79.8
1959-1968	85.9	1748-1757	84.6	1856 - 1865	69.5	1728 1737	82.2
20 yr moving average		20 yr moving average		20 yr moving average		20 yr moving average	
Ojai	% of mean	Cuyamaca	% of mean	Kern River	% of mean	Colorado	% of mean
1442-1461	86.3	1571-1590	83.5	1947 - 1966	68.1	1442-1461	74.5
1947-1966	87.1	1947-1966	83.6	1442 - 1461	70.9	1579-1598	76.1
1569-1588	88.5	1652-1671	84.3	1571 - 1590	71.3	1493-1512	80.8
1628-1647	88.6	1629-1648	85.4	1653 - 1672	74.9	1886-1905	81.9
1805-1824	89.3	1442-1461	86.1	1629 - 1648	75.4	1622-1641	83.1

Table 7a. The 10 highest ranking 5-, 10-, 20-yr wet periods of most skillful reconstructions for gages Arroyo Seco, San Gabriel Dam, Santa Ana River, and Lake Arrowhead. Moving averages expressed as percentage of instrumental mean.

5 yr moving average		5 yr moving average		5 yr moving average		5 yr moving average	
Arroyo Seco R	**% of mean**	**San Gabriel**	**% of mean**	**Santa Ana R**	**% of mean**	**L. Arrowhead**	**% of mean**
1743 - 1747	212.6	1743-1747	151.1	1743 - 1747	195.8	1743-1747	140.3
1866 - 1870	206.2	1865-1869	144.6	1907 - 1911	188.8	1865-1869	139.1
1991 - 1995	199.6	1564-1568	142.5	1562 - 1568	172.2	1979-1983	134.5
1979 - 1983	197.7	1905-1909	142.3	1866 - 1870	170.9	1991-1995	133.7
1564 - 1568	193.2	1979-1983	140.4	1914 - 1918	167.5	1564-1568	132.9
1907 - 1911	187.8	1991-1995	134.2	1978 - 1983	166.4	1905-1909	131.5
1937 - 1941	164.4	1911-1915	131.0	1937 - 1941	157.1	1911-1915	127.4
1679 - 1683	152.3	1937-1941	130.8	1991 - 1996	147.0	1937-1941	124.5
1789 - 1793	140.9	1679-1683	125.1	1878 - 1893	142.9	1965-1969	123.4
1696 - 1700	140.6	1723-1727	122.8	1535 - 1539	138.8	1797-1801	121.2
10 yr moving average		**10 yr moving average**		**10 yr moving average**		**10 yr moving average**	
Arroyo Seco R	**% of mean**	**San Gabriel**	**% of mean**	**Santa Ana R**	**% of mean**	**L. Arrowhead**	**% of mean**
1906 - 1915	174.5	1905-1914	134.3	1906 - 1915	171.2	1977-1986	128.1
1977 - 1986	172.3	1977-1986	132.6	1740 - 1749	155.5	1905-1914	127.7
1992 - 2001	168.6	1738-1747	131.8	1977 - 1986	150.7	1738-1747	125.3
1738 - 1747	166.7	1559-1568	125.2	1560 - 1569	138.9	1991-2000	120.9
1559 - 1568	147.9	1865-1874	121.8	1937 - 1946	135.9	1559-1568	118.4
1867 - 1876	141.6	1991-2000	121.8	1991 - 2000	129.6	1865-1874	117.7
1935 - 1944	128.7	1935-1944	118.5	1865 - 1874	125.6	1935-1944	114.5
1679 - 1688	125.0	1884-1893	116.9	1883 - 1727	118.4	1884-1893	112.5
1693 - 1702	123.5	1679-1688	115.8	1679 - 1688	118.1	1679-1688	111.2
1723 - 1732	120.5	1717-1726	115.3	1883 - 1892	117.3	1723-1732	110.1
20 yr moving average		**20 yr moving average**		**20 yr moving average**		**20 yr moving average**	
Arroyo Seco R	**% of mean**	**San Gabriel**	**% of mean**	**Santa Ana R**	**% of mean**	**L. Arrowhead**	**% of mean**
1979 - 1998	154.0	1979-1998	119.6	1903 - 1922	139.8	1979-1998	117.2
1903 - 1922	131.0	1903-1922	119.5	1979 - 1998	129.2	1903-1922	114.6
1730 - 1749	123.1	1549-1568	116.9	1550 - 1569	123.2	1549-1568	111.0
1549 - 1568	122.3	1730-1749	113.3	1730 - 1749	118.5	1730-1749	109.4
1679 - 1698	113.2	1679-1698	110.1	1850 - 1869	106.1	1678-1697	106.6

Table 7b. The 10 highest ranking 5-, 10-, 20-yr wet periods of most skillful reconstructions for gages Ojai, Cuyamaca, Kern River, and Colorado River Moving averages expressed as percentage of instrumental mean.

5 yr moving average		5 yr moving average		5 yr moving average		5 yr moving average	
Ojai	% of mean	Cuyamaca	% of mean	Kern River	% of mean	Colorado	% of mean
1743-1747	148.0	1743-1747	134.6	1743 - 1747	193.4	1983-1987	152.0
1865-1869	144.7	1905-1909	131.4	1907 - 1911	187.0	1837-1841	147.2
1905-1909	141.5	1979-1983	129.8	1866 - 1870	186.9	1866-1870	141.1
1979-1983	141.3	1564-1568	129.3	1982 - 1986	182.2	1482-1486	138.6
1564-1568	141.3	1937-1941	127.8	1564 - 1568	177.9	1614-1618	137.6
1991-1995	135.8	1991-1995	127.6	1995 - 1999	149.9	1523-1527	132.0
1937-1941	130.5	1865-1869	127.5	1723 - 1727	148.6	1676-1680	129.7
1911-1915	129.1	1913-1917	120.3	1680 - 1684	140.9	1490-1494	126.3
1556-1560	122.7	1789-1793	119.8	1797 - 1801	139.6	1602-1606	125.9
1679-1683	122.5	1889-1893	119.6	1889 - 1893	139.2	1790-1794	124.8
10 yr moving average		10 yr moving average		10 yr moving average		10 yr moving average	
Ojai	% of mean	Cuyamaca	% of mean	Kern River	% of mean	Colorado	% of mean
1906-1915	133.3	1905-1914	122.2	1906 - 1915	164.6	1482-1491	134.5
1977-1986	132.4	1740-1749	121.6	1977 - 1986	162.7	1612-1621	131.9
1738-1747	128.5	1977-1986	120.5	1741 - 1750	157.5	1979-1988	126.5
1991-2000	125.0	1559-1568	119.1	1867 - 1876	146.3	1835-1844	125.4
1559-1568	124.9	1935-1944	118.2	1559 - 1568	144.5	1672-1681	124.2
1865-1874	120.8	1991-2000	116.5	1718 - 1727	132.1	1521-1530	120.2
1935-1944	115.6	1884-1893	115.3	1992 - 2001	131.5	1914-1923	117.4
1884-1893	115.0	1867-1876	112.0	1860 - 1869	129.9	1862-1871	117.4
1679-1688	114.9	1717-1726	111.3	1678 - 1687	123.0	1426-1435	113.8
1717-1726	112.2	1679-1688	111.0	1936 - 1945	121.9	1718-1727	113.0
20 yr moving average		20 yr moving average		20 yr moving average		20 yr moving average	
Ojai	% of mean	Cuyamaca	% of mean	Kern River	% of mean	Colorado	% of mean
1979-1998	119.3	1549-1568	114.2	1549 - 1568	129.1	1602-1621	123.2
1903-1922	117.1	1903-1922	113.9	1679 - 1698	118.7	1476-1495	118.5
1549-1568	115.4	1979-1998	113.9	1732 - 1751	122.9	1911-1930	114.8
1730-1749	110.1	1730-1749	108.2	1903 - 1922	136.3	1969-1988	113.1
1679-1698	107.6	1680-1699	106.2	1967 - 1986	135.8	1825-1844	110.4

3.3 Cyclical and Quasi-Periodic Behavior

This section summarizes results of spectral analysis and wavelet analysis to identify possible cycles or quasi-cycles in observed and reconstructed precipitation or river discharge in the 8 study basins. Spectra of observed and reconstructed series for their overlap period are first compared with pairs of spectra plotted on the same axes to assess how effectively the reconstruction mirrors cycles in the observed data. Spectra with confidence bands and continuous wavelet transforms (CWTs) from wavelet analysis are then applied to check for significant cycles in the observed series and full-length reconstructions.

Ability to detect cycles. Spectra for observed and reconstructed series computed for their overlapping, or common, period show that the main spectral peaks in the observed series are generally mirrored by spectral peaks in the reconstructions. This ability to track spectral features is illustrated for San Gabriel Dam precipitation, using the observed series and the most skillful reconstruction (Figure 9). Spectral peaks in the reconstruction occur at approximately the same wavelengths as peaks in the observed series. The major, or highest peaks for the observed series are near 2.5 years and 13 years. The highest peak for reconstructed and observed precipitation is at about 2.5 years. The reconstructed peak near 13 years is much suppressed compared with the observed peak near 13 years, suggesting that this particular reconstruction may not fully capture decadal or multi-decadal cycles. Such comparative spectra (observations vs reconstructions) for the most skillful reconstructions in the other 7 basins similarly support the ability of reconstructions to track cycles at various wavelengths (Appendix H). Tracking of multi-decadal features, such as those near 13 years, is much better for some basins than others. Variations in the range 13-15 years are especially well tracked by reconstructions for the Colorado and Kern Basins (Appendix H. Figure 1a).

Comparative spectra such as those plotted in Figure 9 also serve to illustrate the loss of variance in reconstruction due to the limitations of tree-ring data as proxies for precipitation and streamflow. Because the total area under the spectrum is proportional to total variance of the series and because a reconstruction explains only part of the variance of the instrumental series, the total area under the spectrum of the reconstruction is less than the total area under the spectrum of the instrumental series. The less accurate the reconstruction, the greater the difference in areas under reconstructed and observed spectra. The difference of areas is most easily seen in the offsets of the null-continuum lines (dashed red and blue lines) in the spectral plots. The small vertical offsets for the San Gabriel, Kern and Colorado series reflect the relatively high accuracy of those reconstructions (Appendix H, Figure 1a).

The vertical offsets of reconstructed and observed spectra are larger for the longest reconstructions than for the most skillful reconstructions (Appendix H: Figure 1a and Figure 1b). This observation is consistent with the weaker hydrologic signal in the longest reconstructions due to the sparser network of tree-ring sites. Even so, the comparative spectra still support the ability of the longest reconstructions to capture spectral features in observed hydroclimate. With few exceptions, spectral peaks in the reconstructions occur near the wavelengths of spectral peaks in the observations (Appendix H, Figure 1b). For some basins, ability to identify wavelengths of important cyclic behavior deteriorates noticeably from the most skillful to the longest reconstructions. For example, the observed spectral peak near 13 years is exceptionally well-recorded in the most skillful reconstruction for the Colorado River, but barely evident as a minor spectral bump in the corresponding longest reconstruction (lower right plots in Figures 1a, 1b of Appendix H).

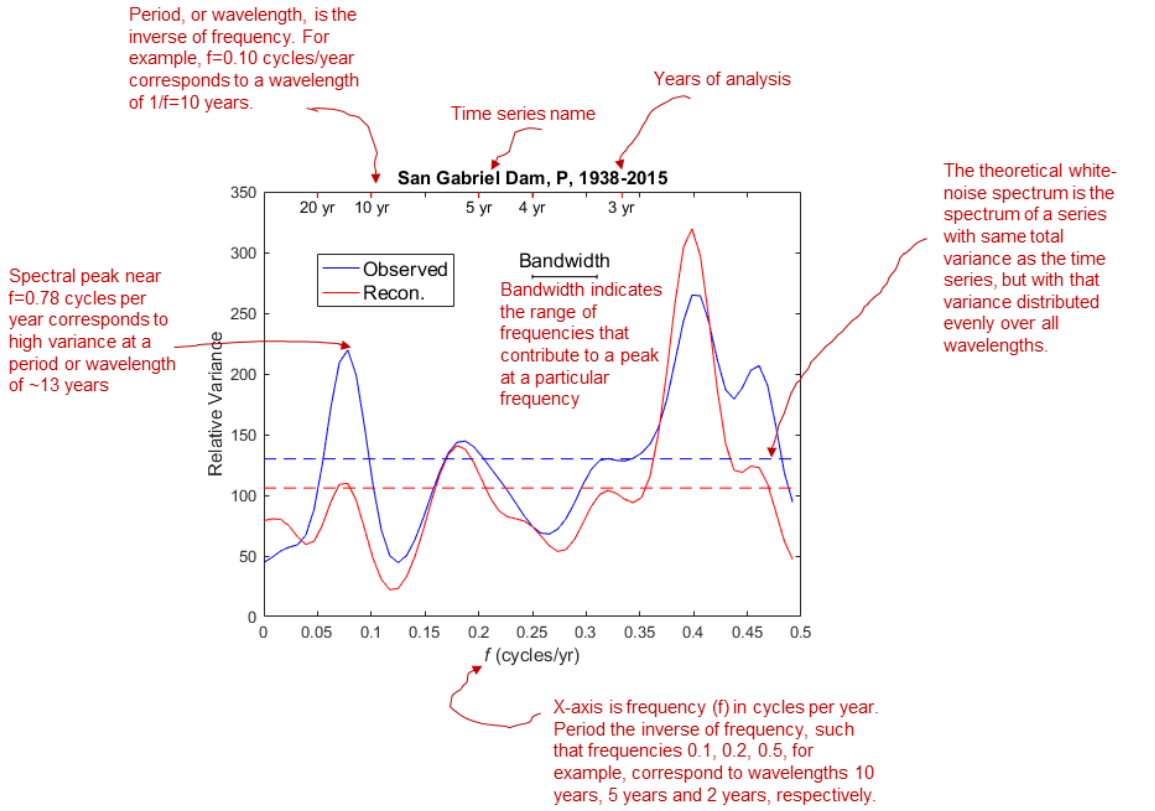

Figure 9: Comparative spectra of observed and reconstructed (most skillful) San Gabriel Dam precipitation. The x-axis is frequency, and ranges from 0 to 0.5 cycles per year. The corresponding range of wavelength, the inverse of frequency, is infinity to 2 years. (The x-axis is labeled along the top of the figure in period or wavelength.) The y-axis is proportional to variance contributed by a particular band of frequencies. Solid lines are the spectra, which give the distribution of variance as a function of frequency or wavelength. Dashed lines are the white noise null continua corresponding to the spectra of the same color. White noise is a series with the same variance as the time series analyzed but with that variance evenly distributed over frequencies. For example, the total area under the dashed blue line (area proportional to variance), is equal to the total area under the solid blue line. A cycle at some wavelength or frequency is reflected by a high spectral peak. Main spectral peaks in this series are near f=0.78 (wavelength 13 years) and f=0.4 (wavelength 2.5 years. Red annotation explains more about the elements of the spectral plot. Corresponding plots for all 8 basins and for the longest as well as the most skillful reconstructions, are in Appendix H.

Cycles in the Instrumental Series. San Gabriel Dam precipitation, 1938-2015, has a major spectral peak near 2.5 years, and a secondary peak near 13 years (Figure 10). The confidence bands around the spectrum allow an assessment of statistical significance of the spectral peak: for significance, the confidence band should not include the baseline spectrum used as the null continuum, which for San Gabriel Dam precipitation is white noise. For this particular series neither of the peaks is statistically significant (e.g., α=0.05), although the 2.5 year peak approaches significance (Figure 10). Analogous plots for other series indicate that peaks near 13 and 2.5 years are characteristic of all observed series in this study (Appendix H, Figure 2). All 8 of the observed series have one of their three major spectral peaks near 13 years. The 13-year peak reaches significance for the Kern, while the peak near 2.5 years is significant for precipitation the Lake Arrowhead and Cuyamaca precipitation reconstructions.

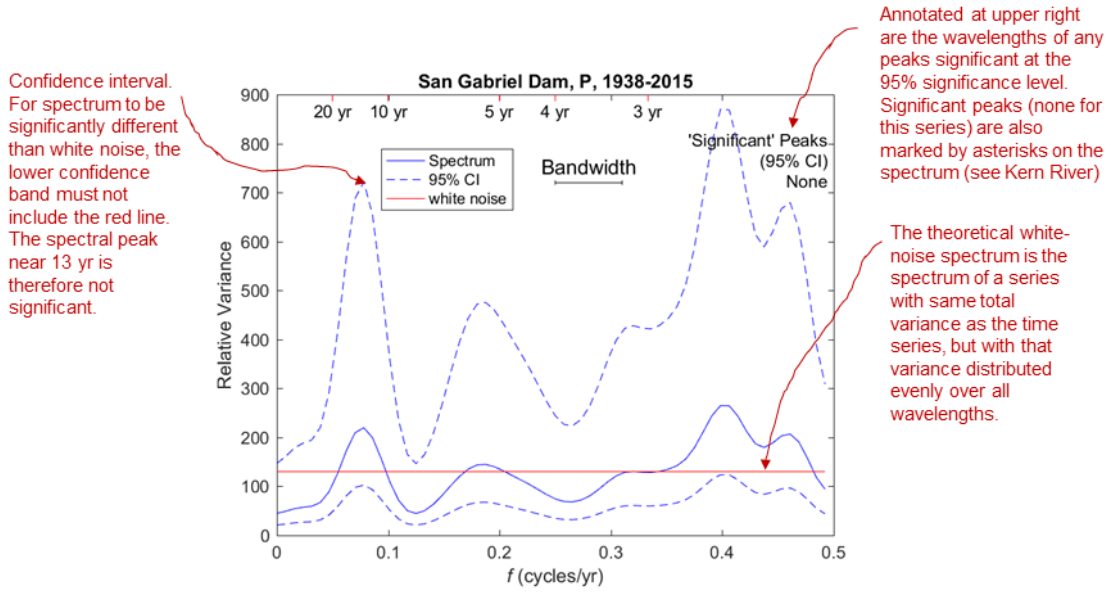

Figure 10. Spectrum with confidence interval of observed San Gabriel Dam precipitation. Spectrum is identical to that plotted as the solid blue line in Figure 9, although the y-axis here has a greater range to accommodate the plotting of the confidence interval. A peak is judged as significant if the 5% confidence interval of the spectrum does not include the null continuum. Here, neither the peak near f=0.78 (wavelength 13 years) nor the peak near f=0.4 (wavelength 2.5 years) are statistically significant. Refer to caption of Figure 9 for explanation of axes and general features of the spectrum. Corresponding plots for all 8 basins are in Appendix H.

The continuous wavelet transform (CWT) of observed San Gabriel Dam precipitation shows that the near-13-year cycle is fairly robust over 1938-2015, with strongest expression from the mid-1950s to about 2005 (Figure 11). A smoothed time series plot confirms that this rhythm is characterized mainly by wet periods in the late 1960s, near 1980 and mid-1990s alternating with dry periods bottoming out in the mid-1970s, late 1980s and early 2000s (Figure 11, bottom).

The spectral peak near 2.5 years in the observed San Gabriel Dam precipitation (Figure 10) and other series (Appendix H) would be interpreted as wet years tending to be followed by wet years 2 or 3 years later, or dry years to be followed by dry years 2 or 3 years later. Thus, the pattern is one of not quite alternating wet and dry years. For San Gabriel Dam and the other California series for which the 2.5 year spectral peak is relatively strong, the CWTs show that significant variance at high frequencies is confined to the period after about 1980.

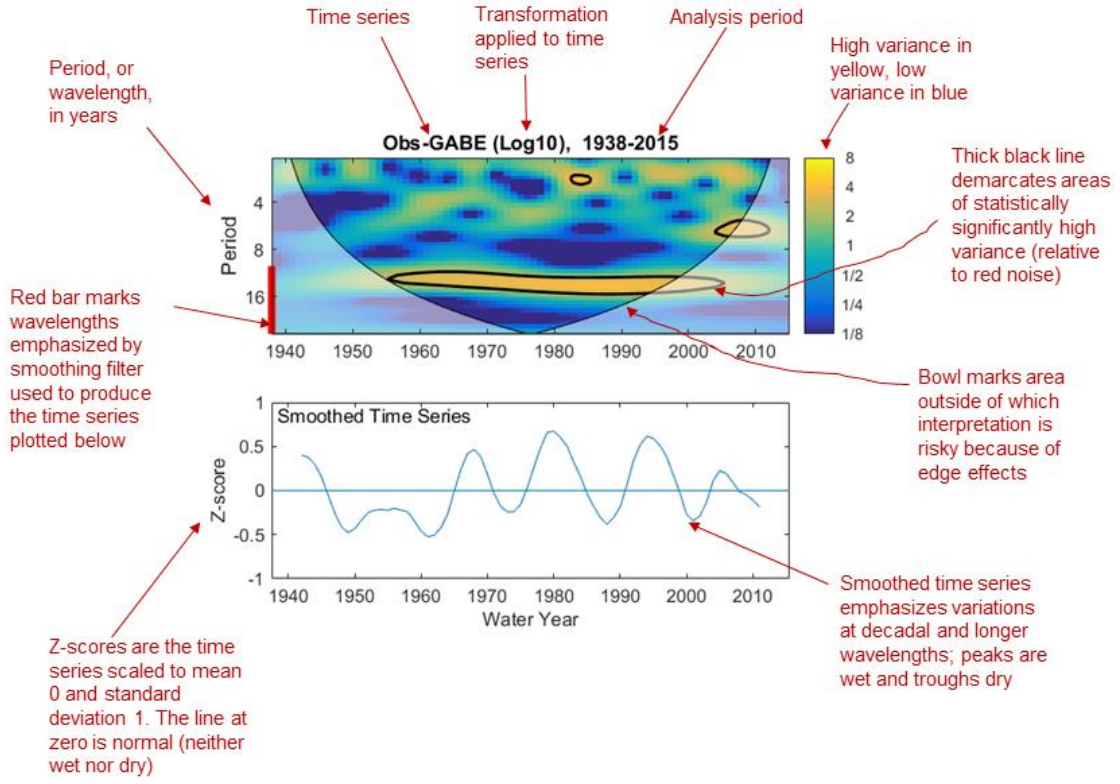

Figure 11: Continuous wavelet transform (CWT) of observed San Gabriel Dam precipitation. The CWT shows the temporal evolution of cycles or rhythmic variations in a time series in time-frequency space. The smoothed time plot shows the low-frequency variations in the series. For example, a narrow horizontal band of significantly high variance at wavelengths 12-16 year stretches from the mid-1950s to early 2000s (yellow disk bounded by thick black line). The time plot below shows that this rhythm is characterized by high flows centered in the late 1960s, near 1980 and early 1990s, alternating with low flows centered in the mid-1970s, late 1980s, and near 2000. This cyclic feature does not exist prior to the late 1960s or after the early 2000s. The early part of the series is dominated by a large fluctuation with a wet peak in the early 1940s and generally dry conditions through the 1950s and early 1960s. Corresponding plots for all 8 basins are in Appendix H.

Cycles in the Most Skillful Reconstructions. The most skillful reconstructions cover about six centuries and provide a sixfold to eightfold increase in length of time series over the instrumental records for which to check for cycles. Spectra of the full-length most skillful reconstructions show high frequencies dominating precipitation and low frequencies dominating discharge (Figure 12a). For example, the San Gabriel Dam precipitation series has a significant (α=0.05) major peak at wavelength of 2.6 years and a white-noise null continuum, while the Kern River series has a major peak at 22.3 years and a red-noise null continuum. Significant spectral peaks at wavelengths of 2-3 years appear in all basins except the Colorado.

Unlike the observed series, these reconstructions do not have spectral peaks near 13 years. The reconstructed streamflow series, however, do have considerable variance at longer wavelengths. The four flow reconstructions have spectral peaks at 22-24 years that reach significance (α=0.05) for Arroyo Seco, the Santa Ana River and the Kern River. The Colorado has a significant peak at 48.8 years, but also a secondary peak, not quite significant, at 23.4 years (Figure 12a).

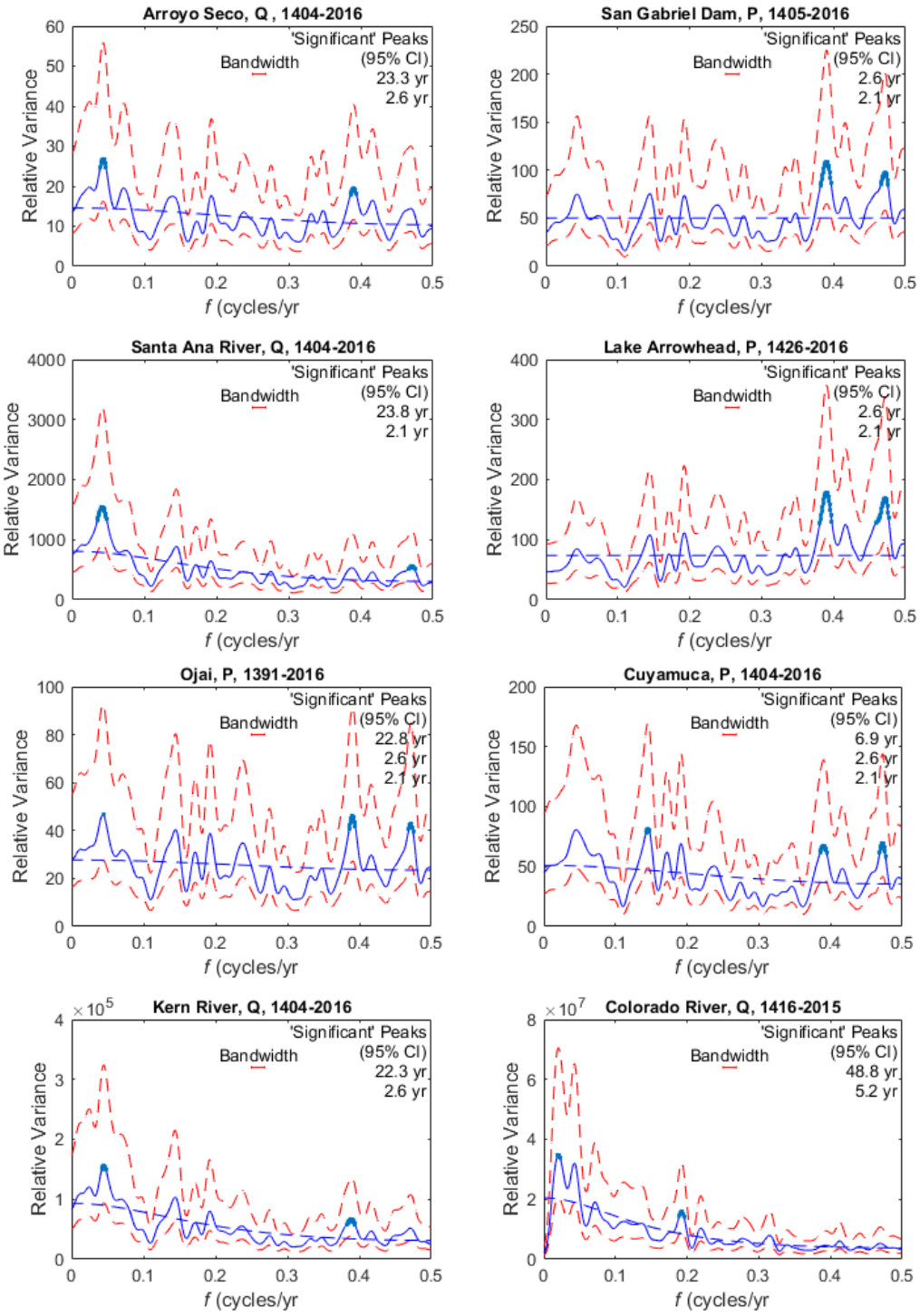

Figure 12a. Spectra with confidence intervals for most skillful reconstructions in 8 basins. Series and analysis period identified above each plot. Time series are either annual (water-year) precipitation (P) or full natural flow (Q). See Figures 9 - 10 for explanation of spectral plot.

CWTs for the most skill reconstructions show that high variance in the 20-30 year wavelength range for the California series is most prominent between 1700 and the mid-1900s (Figures 12b, 12c). For example, the Kern has a significant patch of variance at those wavelengths over the time segments 1710-1770 and 1840-1950. The central wavelength of the latter significant band increases gradually from about 16 years to 32 years over its time span (Figure 12c). The time series plots below the CWTs support the periodicity at about two decades, with waves having about 5 peaks and troughs per century in the interval of time for which the CWTs show high variance at wavelengths near 20 years. Some of these most skillful reconstructions also hint at high variance at very low frequencies, corresponding to wavelengths longer than 128 years. The CWT for the Kern, for example, has a broad band of yellow extending from about 1500 to 1900. This band does not reach significance. Spectral power near the longest wavelengths does reach significance from the early 1600s to late 1700s for the Cuyamaca series (Figure 12c).

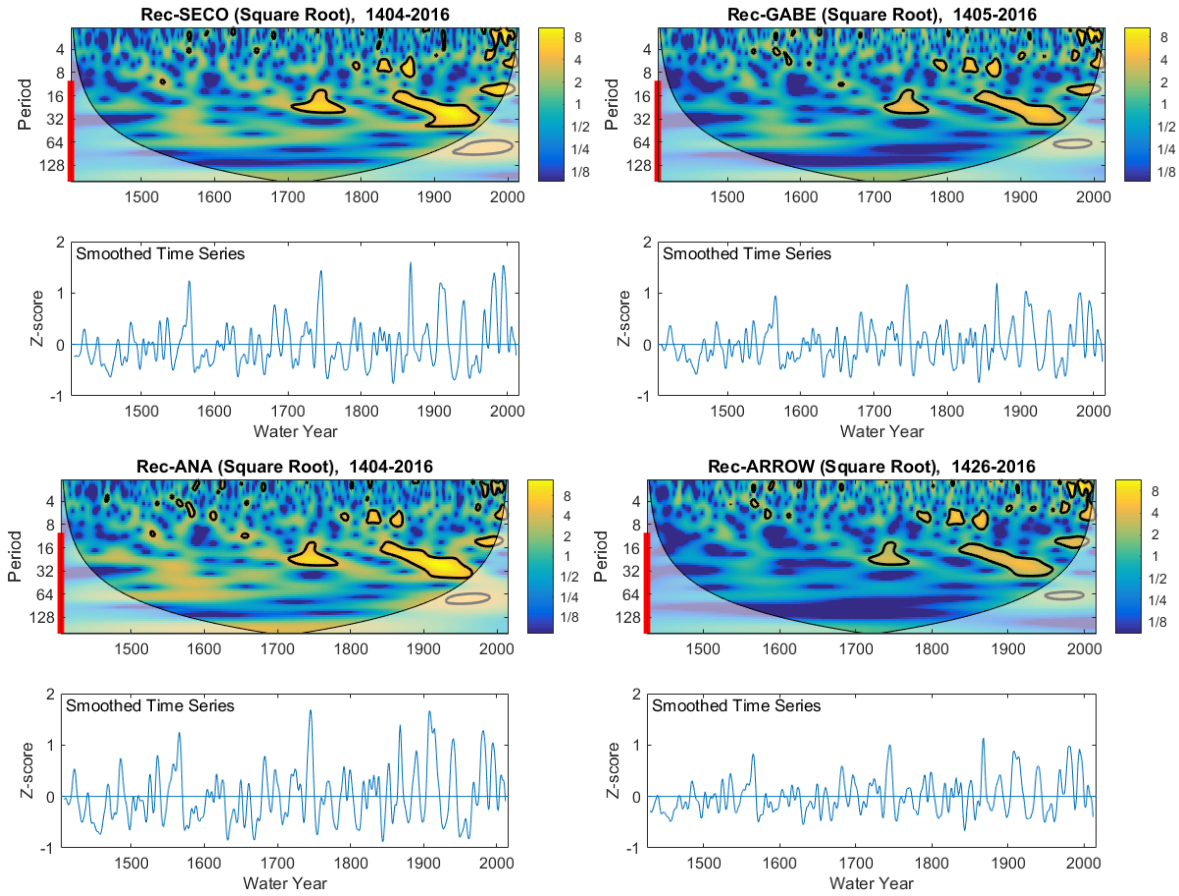

Figure 12b. Continuous wavelet transforms (CWT) of most skillful reconstructions for first 4 of 8 basins. Series and analysis period identified above each plot. Time series are either annual (water-year) precipitation (P) or full natural flow (Q). Refer to the annotated CWT in Figure 11 for interpretation of components of the plots.

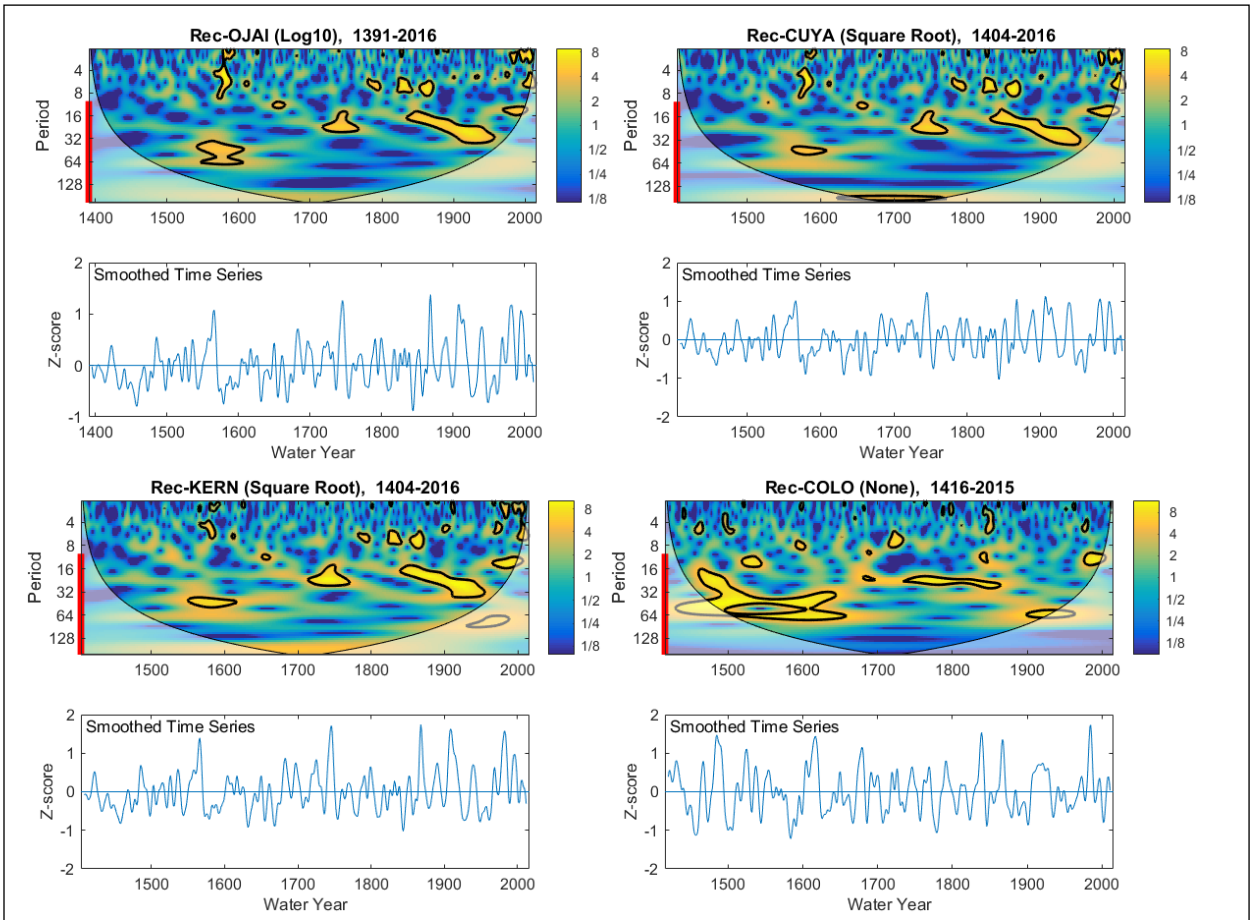

Figure 12c. Continuous wavelet transforms (CWT) of most skillful reconstructions for second 4 of 8 basins. Series and analysis period identified above each plot. Remainder of caption as in Figure 12b.

Cycles in the Longest Reconstructions. Spectra of all the longest California reconstructions except Lake Arrowhead and Cuyamaca have significant spectral peaks at wavelengths of about a century or longer (Figure 13a). These peaks occur at wavelengths ranging from 85 years for Arroyo Seco to 205 years for the Santa Ana River. The spectrum at very low frequencies is significantly higher than the red noise null continuum for Cuyamaca, but reaches its maximum at the infinite wavelength (frequency = 0). This means that any existing cycle at very low frequencies for Cuyamaca cannot be distinguished from trend with this length of time series and bandwidth of spectral estimate. The Colorado reconstruction does not have any significant peaks at the century wavelength or longer, buts does have a major and significant peak at 25.6 years and high variance at longer multi-decadal wavelengths.

Unlike the most skillful reconstructions, none of the longest California reconstructions have statistically significant spectral peaks near 23 years. But all except San Gabriel Dam and Lake Arrowhead have their highest secondary spectral peak (non-significant) at 22-23 years. In the CWTs for these longest reconstructions (Figures 13b, 13c) significant variance near 23 years is confined to the period after about 1400. This explains why the spectra peaks near 23 years lose significance in going from the most skillful to the longest reconstructions. The oscillations at wavelengths longer than a century appear to be robust over long segments of some reconstructions. For example, the CWT for San Gabriel Dam has a long narrow band of significant variance at wavelengths longer than 128 year that extends from ~1190 to 1910 (Figure 13b). The corresponding spectral peak for San Gabriel Dam is at 146 years (Figure 13a). The

smoothed time series plot for San Gabriel Dam (Figure 13b) shows a signature for this oscillation in the form of very long waves: the peaks near 1261, 1382, 1566, 1745, and 1868 have an average between-peak interval of 152 years.

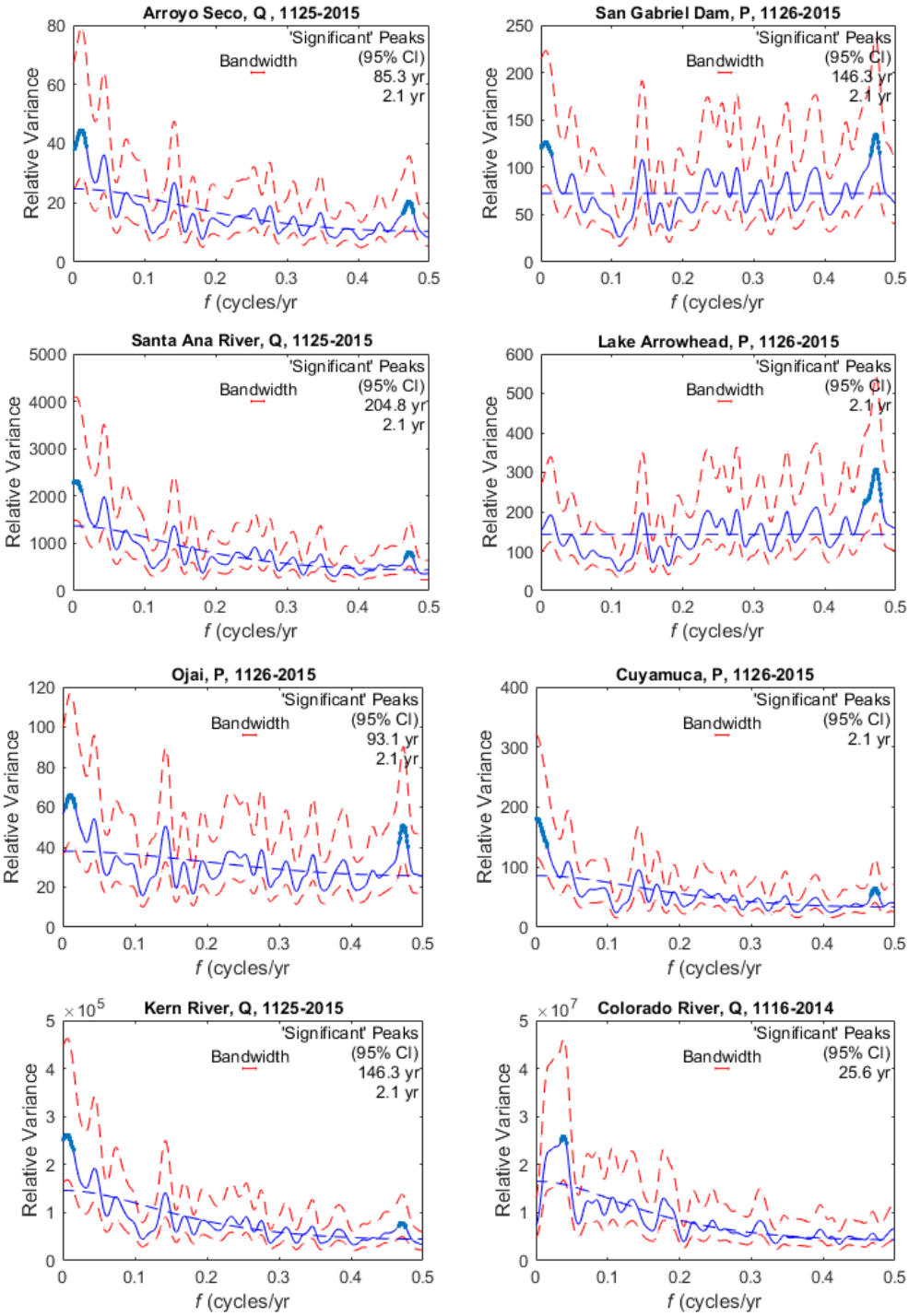

Figure 13a. Spectra with confidence intervals for longest reconstructions in 8 basins. Series and analysis period identified above each plot. Time series are either annual (water-year) precipitation (P) or full natural flow (Q). See Figures 9 - 10 for explanation of spectral plot.

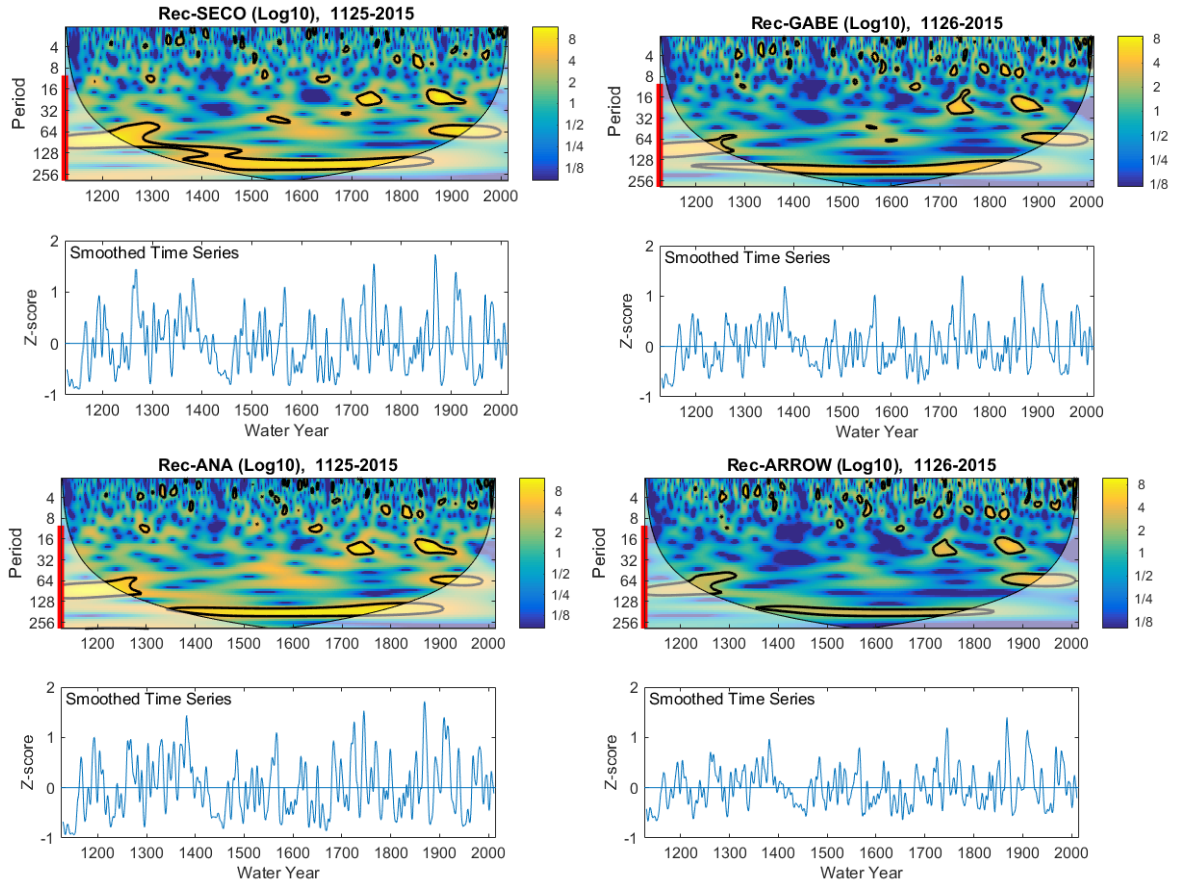

Figure 13b. Continuous wavelet transforms (CWT) of longest reconstructions for first 4 of 8 basins. Series and analysis period identified above each plot. Time series are either annual (water-year) precipitation (P) or full natural flow (Q). Refer to the annotated CWT in Figure 11 for interpretation of components of the plots.

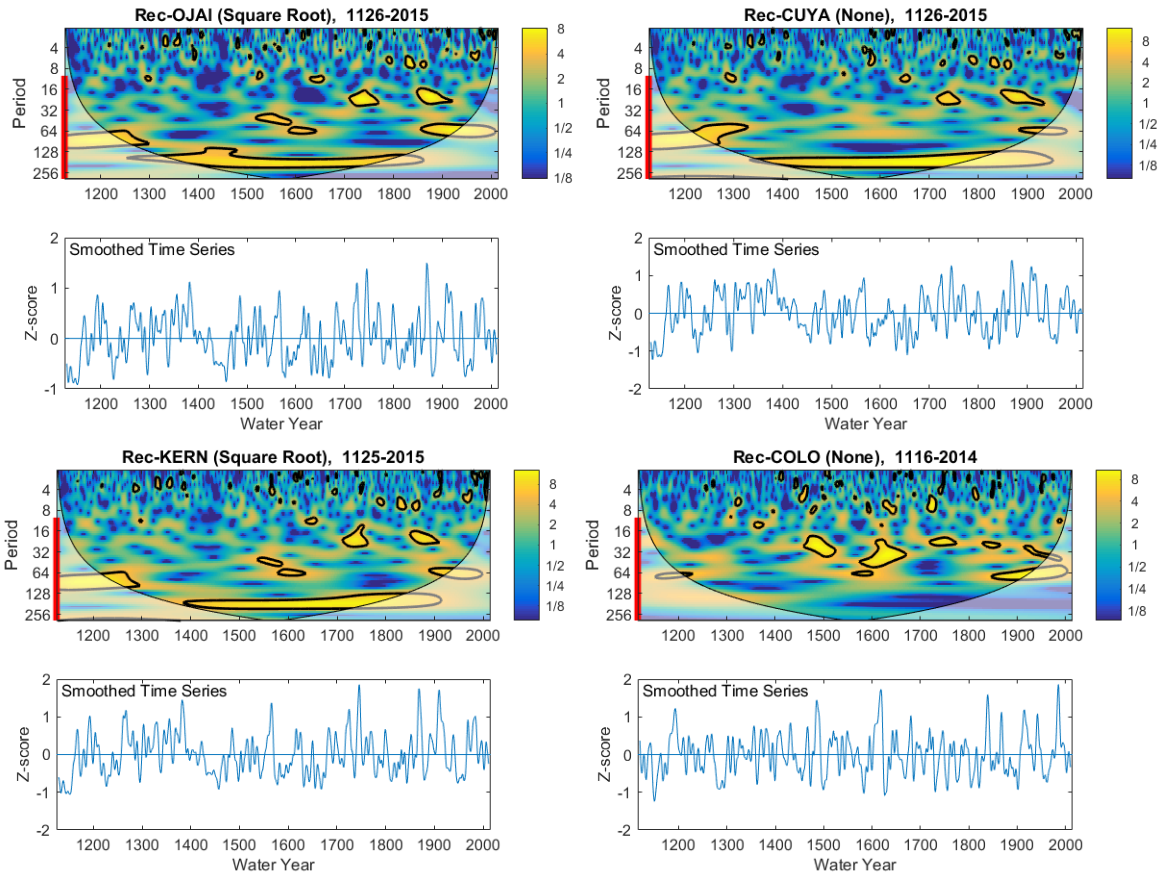

Figure 13c. Continuous wavelet transforms (CWT) of longest reconstructions for second 4 of 8 basins. Series and analysis period identified above each plot. Remainder of caption as in Figure 13b.

In summary, the longest reconstructions, while less accurate than the most skillful reconstructions, give some information on very low frequency fluctuations, as well as providing information on climate oscillations before 1400. In general, those plots show that for some gages significantly high variance occurs at wavelengths longer than a century. Also, the spectral peak near 23 years that is significant in the most skillful reconstructions generally becomes insignificant in the longest reconstructions. Any existing bi-decadal fluctuation apparently becomes less prominent before the start of the most skillful reconstructions.

3.4 Consistency with other Paleoclimatic Evidence

Kern River Comparisons. There is one existing reconstruction of the Kern River (Adams et al. 2015), although it is not clear what gage was used for the reconstruction. Since the record used in the calibration was reportedly obtained from CADWR, and it starts in 1894, we are guessing it must be from the Bakersfield gage, although the average flow volume appears to more closely reflect the Isabella gage used in this project. The reconstruction was calibrated using drought grid points from Cook et al. (2010) and extends back to 1 BC. Adams et al. (2015) do not provide calibration statistics and for the final reconstruction, they use instrumental data for 1894-2015, so a statistical comparison of the skill of this reconstruction compared to our most skillful and longest Kern River reconstructions is not possible.

It is likely that many of the same chronologies were used for both of the reconstructions, since the network of available tree-ring chronologies used to reconstruct the drought grid points is similar to what was used for this project (which also included some updated and several new chronologies). Given this, we expect the reconstructions to be similar. Correlation analysis indicates that our most skillful Kern River reconstruction is well correlated with the Adams Kern reconstruction (r = 0.75, 1404-1893), but the relationships is less strong with our longest Kern reconstruction (r = 0.53, 1126-1893). A comparison of the lowest flow single, 10-year, and 20-year averages shows some similarities and differences (Table 8). Specifically, more dry years and periods of 20th and 21st century rank as the most severe in the Adams reconstruction than in ours, particularly for single years. This may be due to the fact that the instrumental data are used for this period. When the most skillful Kern reconstruction is ranked over the instrumental period, nine of the ten lowest flows in the instrumental record rank in the lowest 15 years in the reconstruction, but in the full reconstruction ranking, only one of these years (1961, 2nd lowest in the instrumental record) is in the lowest ranking ten years. For 10-year periods, there is more similarity, with both reconstructions showing the severity of drought in the 1930s and 1940s-50s, as well as the 1570s, 1630s, and 1450s. For 20-year periods, both indicate severe dry conditions in the mid-1940 to mid-1960s, mid-1440 to mid-1460, and the last decades of the 1500s.

Table 8. Lowest flow single years, 10-year and 20-year averages (last year listed) for the most skillful (SK) Kern River reconstruction for this project and the Adams et al. 2015 Kern River reconstruction, 1404-2015.

Single Year			10-yr			20-yr	
Kern SK	Kern Adams		Kern SK	Kern Adams		Kern SK	Kern Adams
1580	2015		1580	1933		1966	1936
1585	1961		1638	1580		1461	1966
1571	2014		1461	1966		1590	1465
1782	1931		1934	1579		1672	1637
1961	1977		1956	1638		1648	1585
1613	1924		1850	1757			
1829	1990		1676	1994			
1654	2013		1815	1465			
1864	1841		1784	1505			
1765	1580		1865	1452			

Smoothed time series comparing the two Kern reconstructions from this study and the Adams reconstruction show similarities over some intervals (mid 1300s, early 1500s, 1700s), but many differences as well (Figure 14). Our reconstructions benefit from additional and updated tree-ring chronologies, and because the models were calibrated directly with the tree-ring data, instead of with drought reconstruction grid points, it is likely that the reconstructions generated for this project, and in particular, the most skillful reconstruction, are more reliable than the one based on PDSI grid points from Adams et al. (2015).

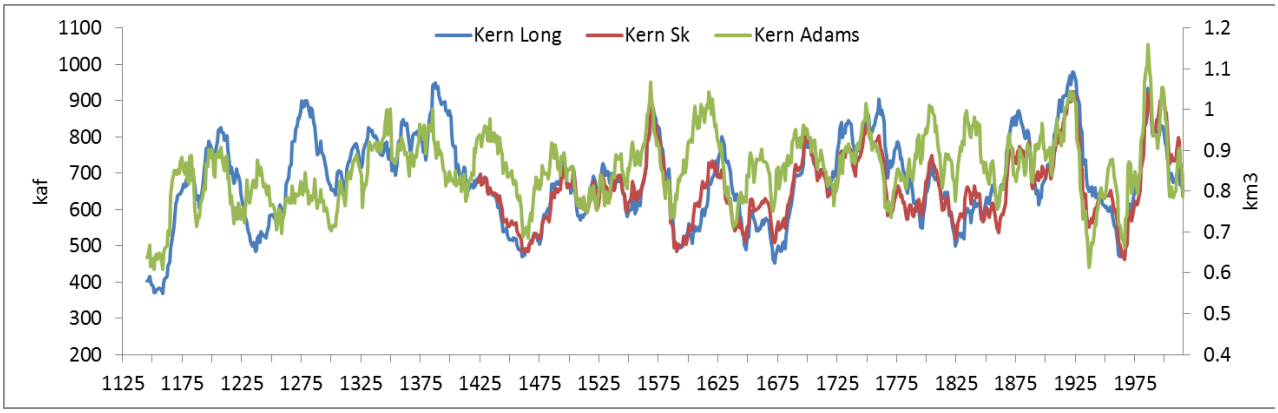

Figure 14. Kern River reconstructions from this project, Kern Long, Kern Sk (most skillful), and from Adams et al. 2015, for the years 1126-2015, smoothed with a 20-year moving average (plotted on last year in the 20-year period).

Colorado River Comparisons. The Colorado River reconstruction at Lees Ferry updates the existing reconstructions of the natural flows at this gage from Woodhouse et al. (2006) and Meko et al. (2007). Because we updated the tree-ring chronologies used in Woodhouse et al. (2006) for this study, we expect the 2006 reconstructions (two versions, one preserving less low frequency, Lees A, and one preserving more, Lees B) to be quite similar to the reconstructions updated for this study. The 2007 reconstruction utilized some very long chronologies, not all of which were updated for this study, so we expect this reconstruction to be less similar to the new ones. The correlations shown in Table 9 support these expectations. In particular, Lees B and the updated reconstruction (most skillful version) are strongly correlated, while correlations for the most skillful Lees and Lees A and Lees (2007) are slightly lower, but still quite strong (Table 9b and c). Correlations are slightly lower for the Lees long reconstruction and the 2006 and 2007 reconstructions (Tables 9a, b, and c).

An evaluation of the statistical properties of the set of reconstructions, compared to the natural flow record, shows a high degree of similarity in measures of mean, median, maximum, upper and lower quartiles, and standard deviation (Figure 15). There are greater differences between the minimum values, with the Lees long reconstruction showing the least extreme minimum value. However, the lower quartile values are quite similar among the reconstructions. There are some differences in autocorrelations (at lag 1), which reflect choices made in the treatment of the tree-ring data (Figure 16). Specifically, more low frequency information was intentionally retained in Lees B and the new reconstructions compared to the Lees A reconstruction. The autocorrelation value in the gage record is closely matched in the Lees B and 2007 reconstructions, while the most skillful reconstruction has a somewhat higher autocorrelation value than the gage record. As a result, more persistence is likely to be present in this reconstruction than is the actual river system. This persistence in manifested in several events of ten years or longer in this reconstruction, compared to Lees (2007) (Figure 17). The Lees long reconstruction has the most year to year persistence. Overall, the smoothed reconstructions show that the updated and previous versions of the reconstructions are quite similar (Figure 18).

Table 9. Correlations between different reconstructions of the Colorado River at Lees Ferry and with the Lees Ferry observed (natural) flow record, for the periods a. 1116-2005, b. 1497-1997, and c. 1906-1997. All correlations are significant at $p < 0.05$. Lees Long and Lees Sk (most skillful) are from this project. Lees A and Lees B are from Woodhouse et al. (2006); Lees (2007) is from Meko et al. (2007).

a. 1116-2005						
	Lees Long	Lees (2007)				
Lees Long	1	0.82				
Lees (2007)	0.82	1				
b. 1490-1997						
	Lees Long	Lees (2007)	Lees-A	Lees-B	Lees Sk	
Lees Long	1	0.83	0.77	0.82	0.82	
Lees (2007)	0.83	1	0.91	0.91	0.9	
Lees-A	0.77	0.91	1	0.92	0.88	
Lees-B	0.82	0.91	0.92	1	0.96	
Lees Sk	0.82	0.9	0.88	0.96	1	
c. 1906-1997						
	Lees Long	Lees (2007)	Lees-A	Lees-B	Lees Sk	Lees Obs
Lees Long	1	0.81	0.74	0.79	0.8	0.74
Lees (2007)	0.81	1	0.92	0.92	0.91	0.87
Lees-A	0.74	0.92	1	0.96	0.93	0.89
Lees-B	0.79	0.92	0.96	1	0.97	0.91
Lees Sk	0.8	0.91	0.93	0.97	1	0.91
Lees Obs	0.74	0.87	0.89	0.91	0.91	1

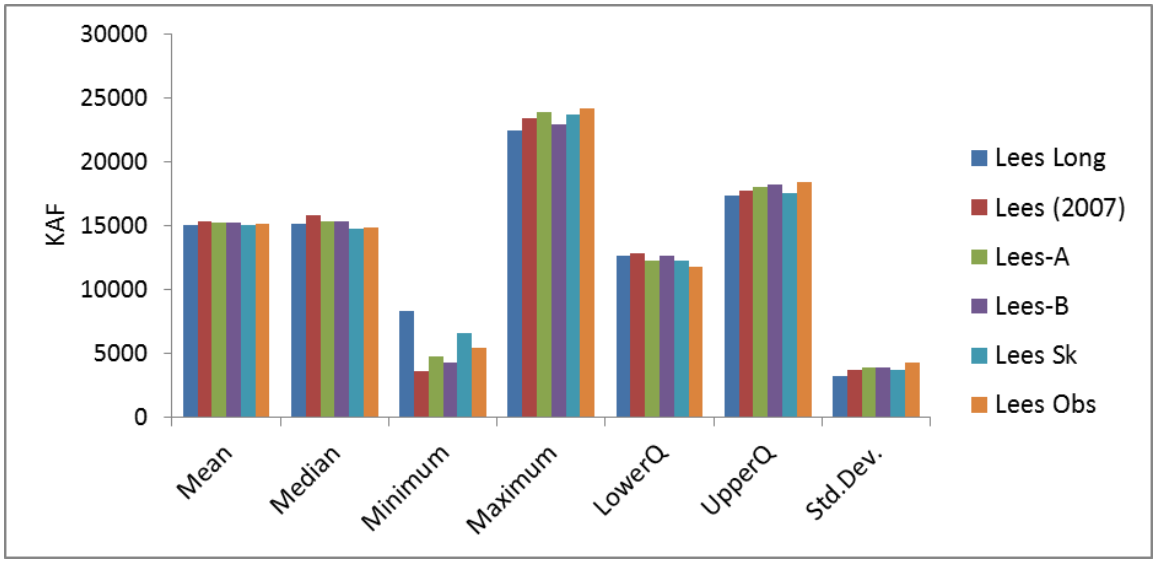

Figure 15. Statistical comparison between the previous Colorado River reconstructions (2006, Lees A and B, and 2007), the Lees reconstructions for this project, Lees long and Lees Sk (most skillful), and the observed (natural) Lees flow record, 1906-1997. Statistics include the mean, median, minimum and maximum, lower and upper quartile, and standard deviation values.

Figure 16. Autocorrelation values at lag 1 for previous Lees reconstructions (2006, Lees A and B, and 2007), the Lees reconstruction for this project, Lees long and Lees Sk (most skillful), and the observed (natural) Lees flow record, 1906-1997. The autocorrelation value represents the correlation between one year's flow and the prior year's flow. For example, in the observed record (Lees Obs) the autocorrelation value is 0.23, so over this record, the annual flow is weakly correlated with the prior year flow.

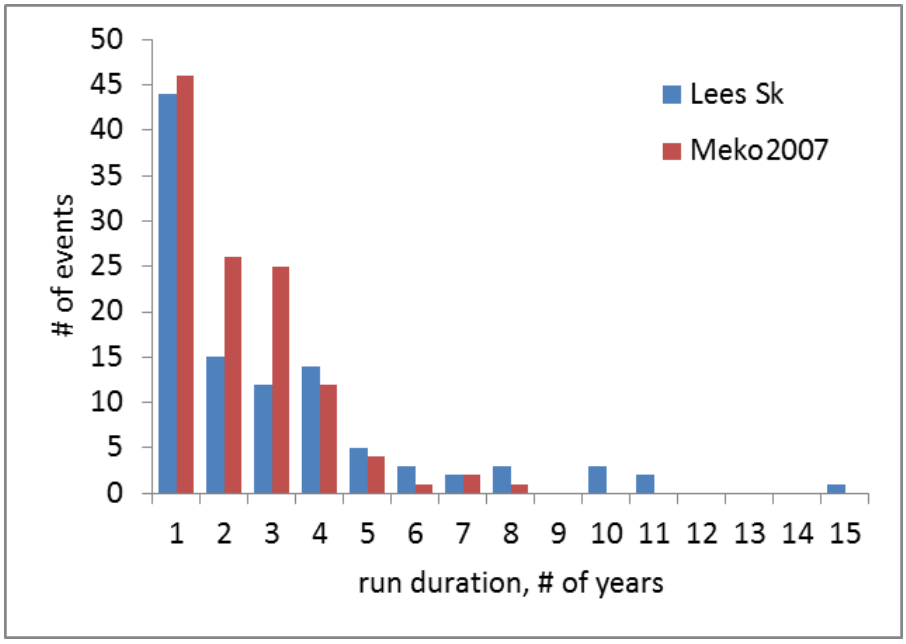

Figure 17. Single and consecutive below average (based on instrumental record mean) flow years, for Lees Sk (most skillful) and Lees (2007) reconstructions, 1416-2005.

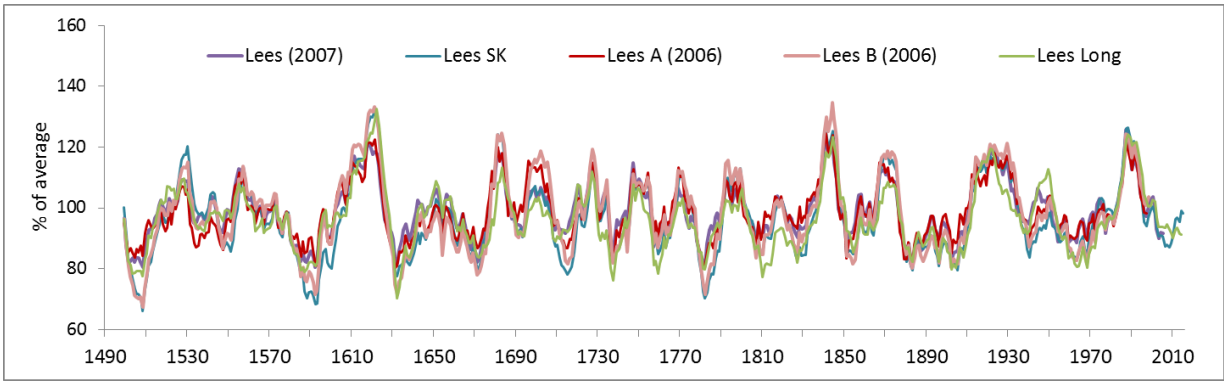

Figure 18. Colorado River smoothed (10-year moving average) reconstructions of 2006, Lees A and B (1490-1997), and 2007 (1490-2005) versions, and the reconstruction for this project, Lees long and Lees Sk (most skillful), (1490-2014). Units are percent of average, based on instrumental record mean.

3.5 Instrumental-Period Statistics in Context

Statistics of reconstructed flow or precipitation can be used to infer whether the short period covered by the instrumental, or observed, hydrologic records was wetter or drier (or more or less variable) than the longer period covered by tree rings. The mean, median, standard deviation, skew, and lag-1 autocorrelations of observations and reconstructions are listed in Tables 10 and 11 for the most skillful and longest reconstructions, respectively. These tables have three rows for each of the eight basins. The first two rows compare the statistic of observations and reconstructions for their overlap period. The third row has the statistics for the full-length reconstruction. A comparison of the statistics in the second and third rows for a basin is useful for placing instrumental-period flow statistics in a long-term context.

Consider, for example, the most skillful reconstruction for San Gabriel Dam precipitation and how the reconstruction compares with the observed record. (Table 10). Over the common period 1938-2015, the mean and the median are somewhat higher, and the standard deviation, skew, and the lag-1 autocorrelation are lower than for the observed record. In most cases, the differences are relatively small, indicating that the reconstruction is quite similar to the observed record with respect to these measures. In the case of the standard deviation, the reconstruction process by design leads to under-estimation of this metric because some fraction of the variance of precipitation or discharge in unexplainable with tree rings.

Comparison of reconstruction statistics for the instrumental and full reconstruction periods for San Gabriel Dam give equivocal results on whether the 1938-2015 instrumental period has been wetter or drier than the full period, 1405-2016, since the mean indicates it was wetter while the median indicates it was drier. The standard deviations suggest that precipitation has been more variable over 1938-2015 than over 1405-2016, as well as slightly more skewed (more extreme precipitation years) and more negatively autocorrelated (less year-to-year persistence in precipitation).

As a second example for assessing statistical properties in the long-term context, consider the most skillful reconstruction for the Colorado River (Table 10). Both the mean and median indicate that the instrumental period, 1906-2015, is wetter than the long-term period, 1416-2015. The mean for the instrumental period is 3.5% higher than the long-term mean, and the median for the instrumental period is 5.5% higher than the long-term median. On the other hand, the standard deviations suggest that the instrumental period has been slightly less variable than the full period. The skew for the instrumental period is also lower than for the reconstruction. The difference is small, but suggests an increased tendency for high values of flow or precipitation (relative to low values) in the years before the start of the instrumental period. Finally, the reconstruction indicates that the lag-1 autocorrelation of Colorado River discharge is lower for the instrumental period than over the long-term record, suggesting less persistence in flow, such that annual departures from the mean in one year are less likely to be followed by same-sign departures from the mean the next year.

Table 10. Instrumental-period statistics[c] of precipitation and discharge in context using most skillful reconstructions.

Code	Gage[a]		Period[b]	Mean	Median	StDev	skew	r[1]
SECO	Arroyo Seco, Q	Obs	1911-2015	69252	31700	87535	2.1	-0.03
	(1E-01 acre-ft)	Rec	1911-2015	67930	42217	**70002**	1.88	-0.02
		Rec	1404-2016	59577	46168	**47435**	2.07	0.08
GABE	San Gabriel Dam, P	Obs	1938-2015	28.27	22.71	14.95	1.14	-0.14
	(inches)	Rec	1938-2015	28.51	25.67	**13.44**	1.13	-0.18
		Rec	1405-2016	27.87	26.94	**9.63**	0.86	-0.08
ANA	Santa Ana River, Q	Obs	1901-2015	57655	37901	50534	1.68	0.2
	(acre-ft)	Rec	1901-2015	56959	41434	**38335**	0.89	0.23
		Rec	1404-2016	50791	42276	**29987**	1.08	0.24
ARROW	Lake Arrowhead, P	Obs	1942-2015	38.71	34.11	19.89	1.16	-0.09
	(inches)	Rec	1942-2015	38.92	35.48	**17.11**	1.16	-0.25
		Rec	1426-2016	37.99	36.83	**11.8**	0.89	-0.16
OJAI	Ojai, P	Obs	1901-2014	20.69	18.81	9.94	1.12	-0.07
	(inches)	Rec	1901-2014	20.87	18.87	**8.97**	1.11	-0.02
		Rec	1391-2016	19.74	18.86	**6.76**	0.94	0.04
CUYA	Cuyamuca, P	Obs	1888-2014	35.61	34.31	13.54	0.71	0.03
	(inches)	Rec	1888-2014	35.72	33.49	**10.73**	0.52	0.05
		Rec	1404-2016	34.6	34.12	**8.86**	0.24	0.09
KERN	Kern River, Q	Obs	1930-2015	67851	51573	45223	1.4	0.11
	(1E01 acre-ft)	Rec	1930-2015	68155	60025	**40688**	1.28	0.14
		Rec	1404-2016	65833	61441	**31288**	1.12	0.27
COLO	Colorado River, Q	Obs	1906-2015	14804	14514	4277	0.14	0.25
	(1E03 acre-ft)	Rec	1906-2015	14834	14801	3786	-0.01	0.31
		Rec	1416-2015	14331	14031	3977	0.12	0.4

[a]Name of observed (Obs) or reconstructed (Rec) series, preceded by letter code; all series are water-year totals of either river flow (Q) or precipitation (P).

[b]Time period for computation of statistics; for Obs, period is overlap of available data of observations and reconstructions; for Rec, period is full length of reconstruction available.

[c]Statistics: sample mean, median, standard deviation, skew, and lag-1 autocorrelation; units for first three statistics are given below the series name; last two statistics are dimensionless. **Bold values** indicate the standard deviations of reconstructions for the instrumental period and reconstruction period of the are statistically significant (α=0.05).

Generally, the results summarized here suggest that in this region California precipitation and river discharge over the instrumental period have been more variable and with less year to year persistence than for the long-term record. This result holds true without exception whether assessed by the most skillful (Table 10) or longest (Table 11) reconstructions. The standard deviation of the reconstruction for the recent period is larger than the standard deviation for full-length reconstruction, and the lag-1 autocorrelation is lower for the instrumental period than for the full reconstruction period. A test of ratio of variances applied to the most skillful reconstructions indicates that variability has been significantly (α=0.05) greater in the instrumental period than in the long term for all California basins; the same test applied to the longest reconstructions indicates significant difference in variability only for San Gabriel Dam and Lake Arrowhead (bold font in Tables 10 and 11). A test of difference of means applied to the reconstructions failed to show a significant difference in means for the full-length period and the instrumental period in any of the basins for either the most skillful or longest reconstructions.

Table 11. Instrumental-period statistics[c] of precipitation and discharge in context using longest reconstructions. Remainder of caption as in Table 10.

SECO	Arroyo Seco, Q	Obs	1911-2015	69252	31700	87535	2.1	-0.03
	(1E-01 acre-ft)	Rec	1911-2015	66733	44557	49648	1.24	0.09
		Rec	1125-2015	65763	47127	44099	1	0.21
GABE	San Gabriel Dam, P	Obs	1938-2015	28.27	22.71	14.95	1.14	-0.14
	(inches)	Rec	1938-2015	28.2	24.12	**11.21**	1.26	-0.18
		Rec	1126-2015	28.11	24.48	**9.45**	1.04	-0.04
ANA	Santa Ana River, Q	Obs	1901-2015	57655	37901	50534	1.68	0.2
	(acre-ft)	Rec	1901-2015	55299	38238	34237	0.87	0.22
		Rec	1125-2015	52182	39594	30762	0.93	0.28
ARROW	Lake Arrowhead, P	Obs	1942-2015	38.71	34.11	19.89	1.16	-0.09
	(inches)	Rec	1942-2015	38.94	34.66	**15.65**	1.38	-0.25
		Rec	1126-2015	39.46	35.54	**13.21**	1.04	-0.13
OJAI	Ojai, P	Obs	1901-2014	20.69	18.81	9.94	1.12	-0.07
	(inches)	Rec	1901-2014	20.68	18.53	7.03	0.77	0.03
		Rec	1126-2015	20.3	18.79	6.19	0.64	0.1
CUYA	Cuyamuca, P	Obs	1888-2014	35.61	34.31	13.54	0.71	0.03
	(inches)	Rec	1888-2014	35.55	33.84	8.56	0.25	0.13
		Rec	1126-2015	34.37	33.93	8.19	0.1	0.23
KERN	Kern River, Q	Obs	1930-2015	67851	51573	45223	1.4	0.11
	(1E01 acre-ft)	Rec	1930-2015	66657	54730	35771	1.45	0.14
		Rec	1125-2015	67593	62084	31687	1.11	0.29
COLO	Colorado River, Q	Obs	1906-2014	14813	14543	4296	0.14	0.25
	(1E03 acre-ft)	Rec	1906-2014	14797	14765	3203	0.11	0.35
		Rec	1116-2014	14281	13995	3210	0.16	0.32

An alternative way of putting instrumental-period statistics in context is by comparing the single statistic (e.g., mean) for the segment of reconstruction covering the instrumental period with the statistic computed for all other segments of the reconstruction with the same length as the instrumental period. Graphical summaries of such assessments for the mean and standard deviation for all basins are shown in Figures 19a-d. Summaries for the most skillful reconstructions are shown in Figure 19a (mean) and Figure 19b (standard deviation). Similar summaries for the longest reconstructions are shown in Figure 19c (mean) and Figure 19d (standard deviation).

Consider, for example, the results for San Gabriel Dam precipitation using the most skillful reconstructions (upper right panel, Figures 19a and 19b). The instrumental period for this gage is the 78-year period 1938-2015, while the most skillful reconstruction begins in the early 1400s. The three or four non-overlapping wettest and driest 78-year means of the reconstruction are compared with the mean for the instrumental period in Figure 19a. The wettest 78-year period was reconstruction was 1866-1943, while the driest was 1430-1507. The instrumental period lies toward the lower end of the wettest reconstructed 78-year periods. For the other gages, the instrumental period is also among the wettest periods, but is not unprecedented in wetness. Over a longer period of time (Figure 19c, the longest reconstructions extending to the 1100s), the instrumental period generally appears less wet in a long-term context, and falls toward the lower end of the wettest periods (e.g., San Gabriel) or near the highest of the driest periods (e.g., Arroyo Seco, Lake Arrowhead, Kern River).

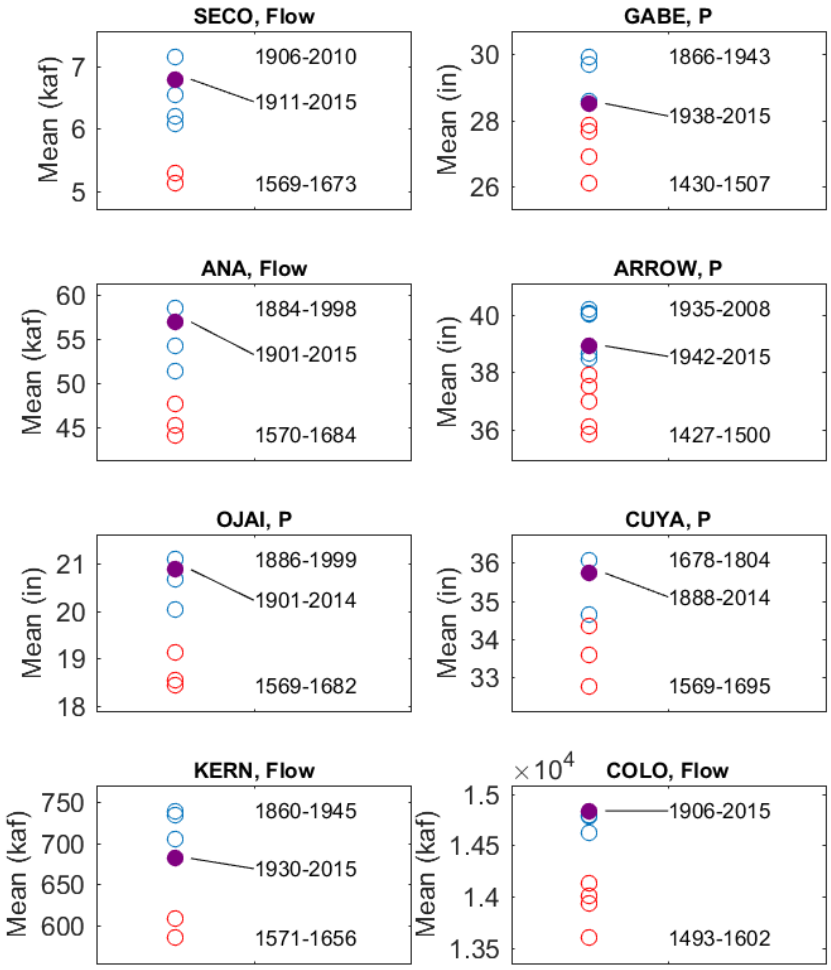

Figure 19a. Windowed means for the most skillful reconstructions. Mean flow or precipitation for the wettest and driest several *m*-year non-overlapping time periods are compared with the mean for the instrumental period. Y-axis units are inches for precipitation and thousands of acre-feet (kaf) for full natural flow. Time window *m* is equal to the length of the instrumental period. Wet periods in blue circles, dry period in red circles, and instrumental period in solid dark purple circle (with reference line). Years of instrumental period and most extreme wet and dry periods annotated. For example, consider the Kern flow reconstruction (lower left). The instrumental period, defined here as the overlap of the reconstruction and the gaged record, is 1930-2015, or 86 years. The mean reconstructed flow for this period is intermediate, and does not place the instrumental period among the wettest or driest 86-year periods of the long-term reconstruction. The driest 86-year period was 1571-1656 and the wettest 86-year period was 1860-1945.

In a similar assessment of variability for the most skillful reconstructions, using the standard deviation as a measure, the instrumental-period ranks near the top of the subsets of most variable periods in all basins except the Colorado River (Figure 19b). For the Santa Ana River and the Kern, the instrumental period is in fact the most variable of all periods of the same length. The Colorado River reconstruction does not share this characteristic, with a standard deviation over the instrumental period that is among the lowest. When the analysis is repeated for the longest reconstructions, the instrumental period for California Basins is generally still among the more variable periods, but is less extreme (Figure 19d). Again, the exception is the Colorado River, in which the instrumental period standard deviation appears between those with the highest and lowest standard deviations.

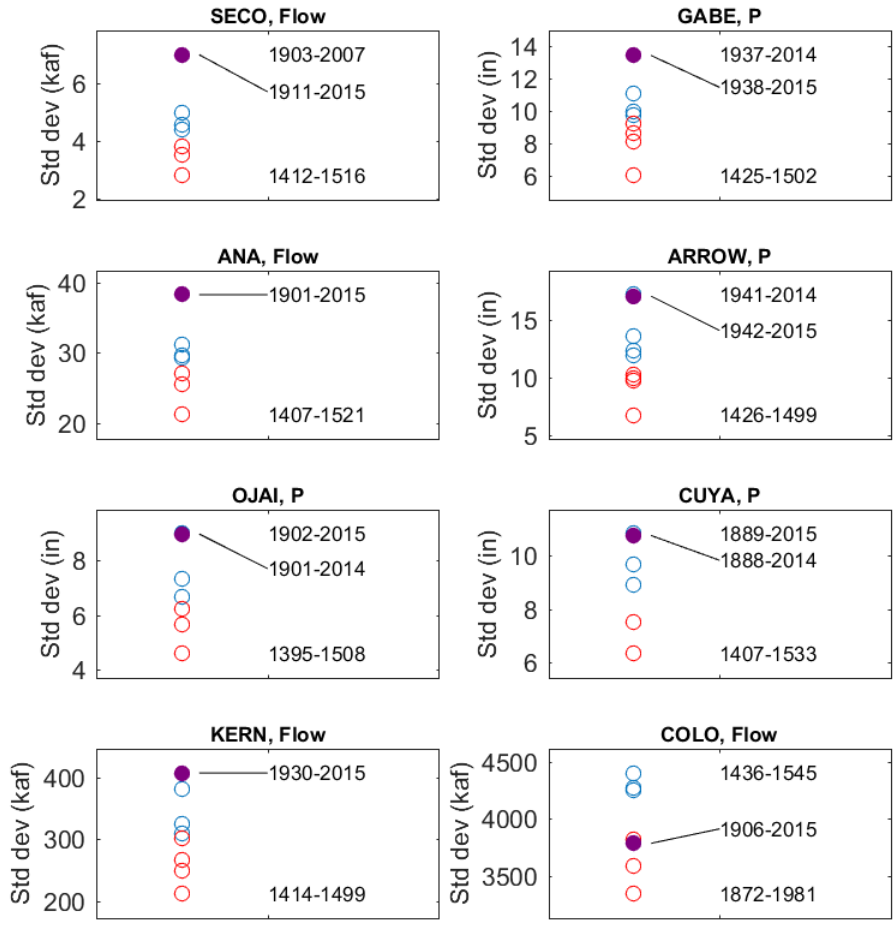

Figure 19b. Windowed variance for the most skillful reconstructions. Standard deviation of flow or precipitation for the most variable and least variable several *m*-year non-overlapping time periods compared with the standard deviation for the instrumental period. Time window *m* equal to the length of the instrumental period. Periods of high variability in blue circles, periods of low variability in red circles, and instrumental period in solid dark purple circle (with reference line). Plot annotation as in Figure 19a. For example, the least-variable 86-year period (equal to length of overlap of gaged record with reconstruction) for the Kern was 1414-1499, while the most variable was the instrumental period itself, 1930-2015. All records except the Colorado (lower right), are characterized by an instrumental period overlapping or defining the most variable 86-year period of the reconstruction.

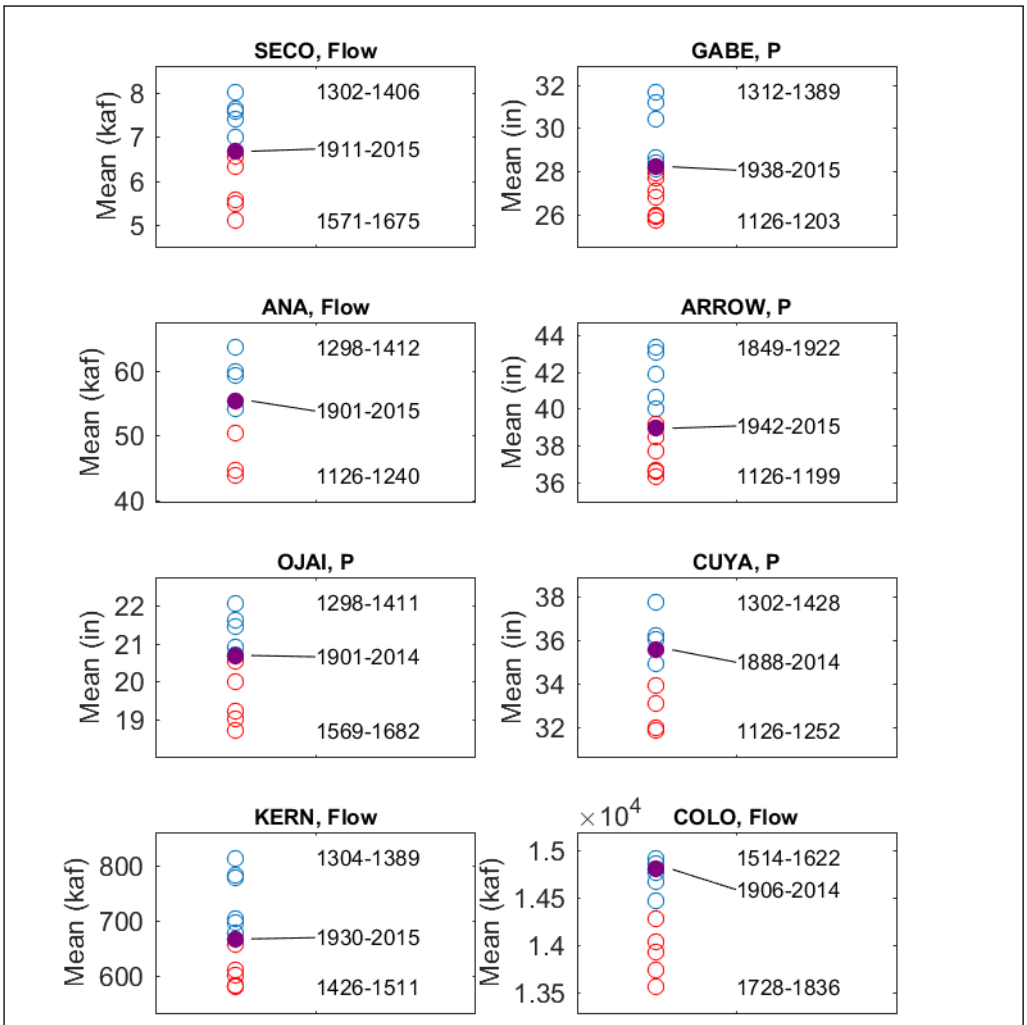

Figure 19c. Windowed means for the longest reconstructions. Mean flow or precipitation for the wettest and driest several *m*-year non-overlapping time periods compared with the mean for the instrumental period. Plot components are defined in caption of Figures 19a and b, which has corresponding plots for the most skillful reconstructions.

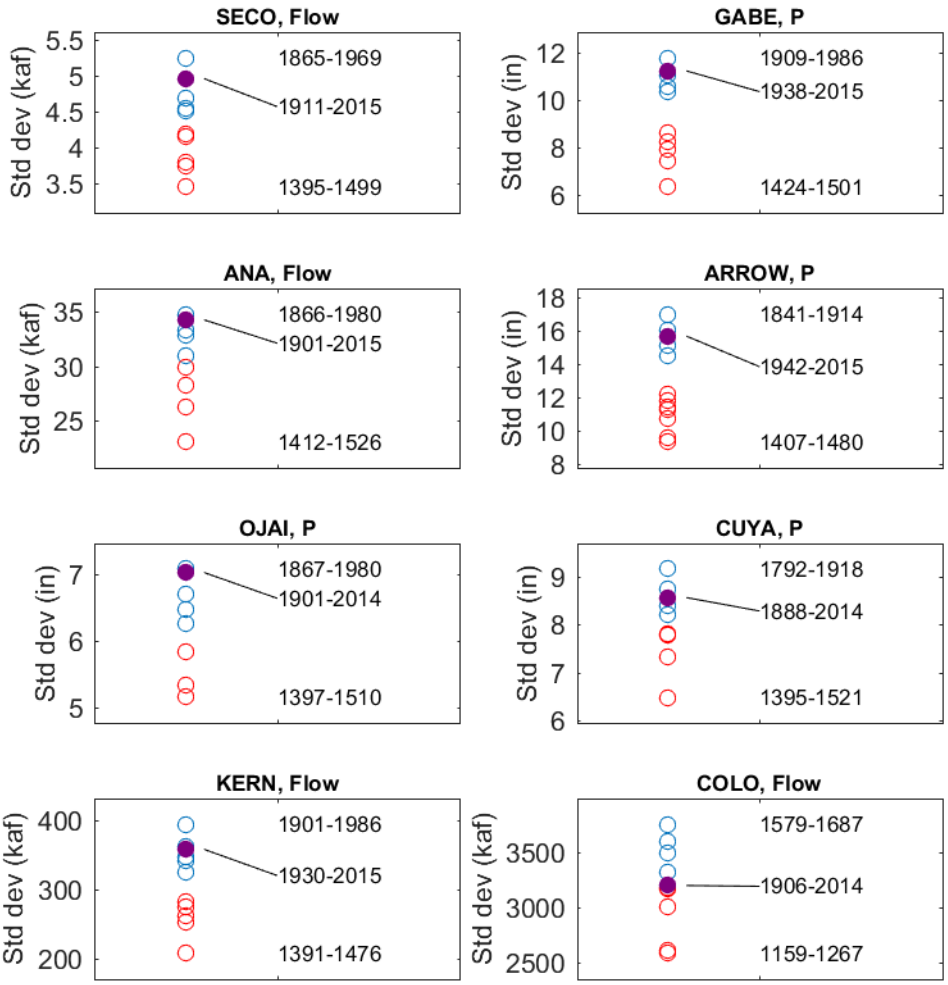

Figure 19d. Windowed variance for the longest reconstructions. Standard deviation of flow or precipitation for the most variable and least variable several *m*-year non-overlapping time periods compared with the standard deviation for the instrumental period. Plot components are defined in caption of Figures 19a and b, which has corresponding plots for the most skillful reconstructions.

3.6 Covariance of moisture variations in basins of Colorado, Southern California and Northern/California/Central Valley of California

The relationships between three key water supply regions for southern California over past centuries can be investigated by comparing hydroclimate reconstructions for the three regions. A particular focus is on sustained droughts that impacted all three regions.

An examination of streamflow reconstructions for the Sacramento River Index (Sacramento, Feather, American, and Yuba Rivers) and the Colorado River at Lees Ferry, along with San Gabriel precipitation (to represent southern California) provides some insights on concurrence of drought events across the three regions (Figure 20). Periods of drought (three or more consecutive years of near to below average conditions; 110% or less) are evident across the three regions throughout the past six centuries, but most events are limited to three or four years. Sets of years with concurrent drought across three basins in which the average annual value is 75% of average or less have occurred approximately twice a century. However, these region-wide events range from four events in the 18th century, to one event in the

20th century (the 15th century is incomplete) (Figure 20). While the majority of these widespread drought events last only three years, there are two nine-year events, 1452-1460 and 1775-1783. An 11-year period from 1451-1461 slightly exceeds the average annual threshold of this analysis at 78%, but is notable for its length. Clearly, these widespread drought events are relatively rare, but they do occur periodically. While there have been only two cases of 9-year concurrent drought in about six hundred years, the statistical probability of one of these events occurring in the future is quite low, but not out of the question.

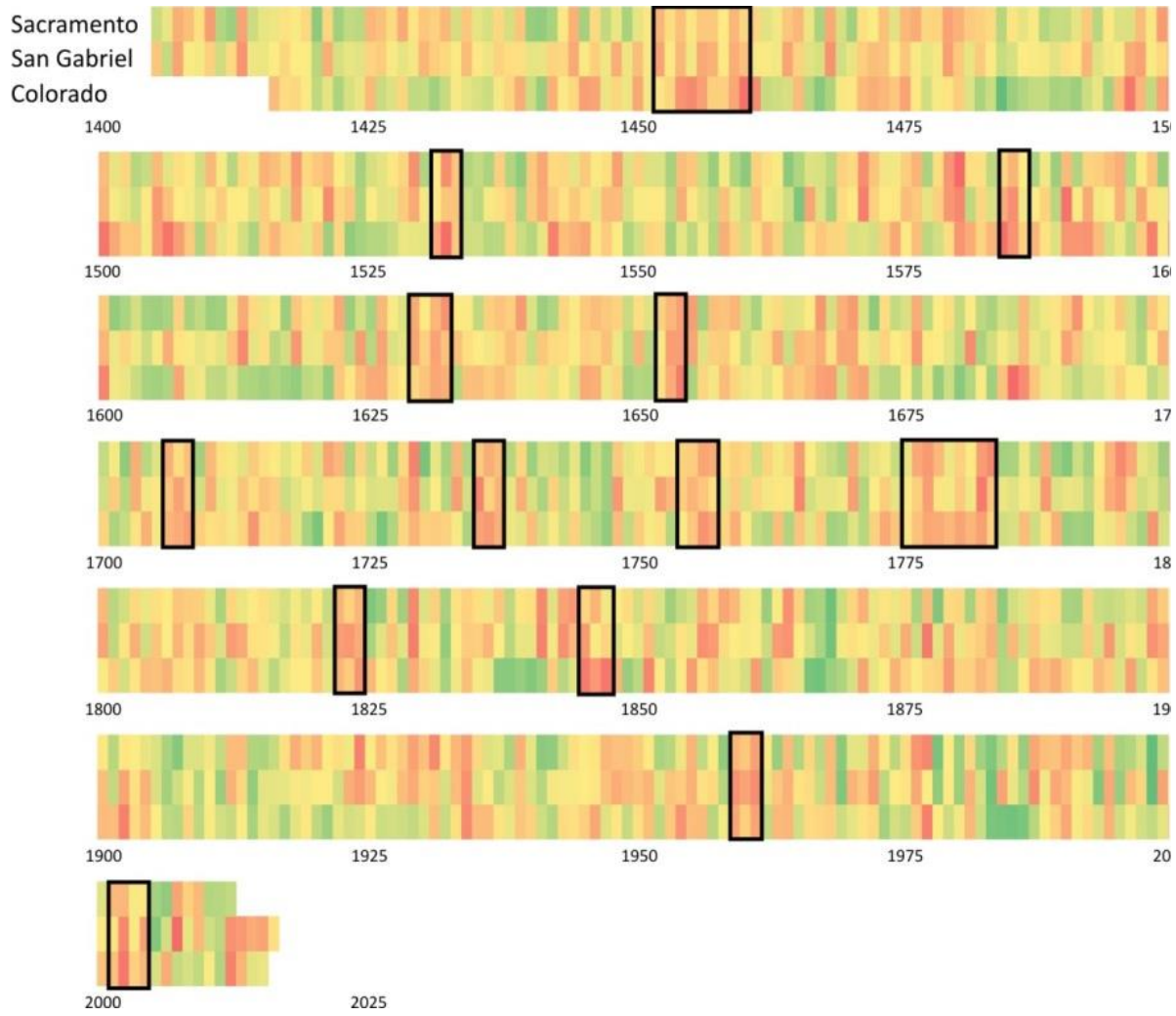

Figure 20. Annual values for the Sacramento River Index (1405-2012, top row), San Gabriel precipitation (1405-2016, middle row), and the Colorado River at Lees Ferry (1416-2015, bottom row) reconstructions. Plots are organized chronologically by century from top to bottom. Years are color coded, grading from wettest/highest flow (dark green) to driest/lowest flow (red). Sets of years in which all values are 110% of average or less in all records, lasting three years or more, with an annual average value of 75% or less are shown with black outlines. The exception to this is the extended 11-year period, 1451-61, with average annual values of 78%.

While concurrent droughts do occur, they do not impact each basin in exactly the same way. These dry periods tend to overlap, with variable duration and overall magnitude from region to region. For example, the 11-year period from 1451-1461 was nine years of consecutively below average flow in the upper Colorado River basin, while it was broken by one above average years in the Sacramento basin and by four separate years in southern California (Figure 21). It was one of the most severe periods of drought in the upper Colorado River basin (in terms of duration and deficit). In the Sacramento basin, although persistent (including a 7-year run of below average conditions), average annual deficits were quite modest. In southern California, within two 2-year intervals, deficits were relatively severe, but recovery years moderated the overall severity of drought over this time period.

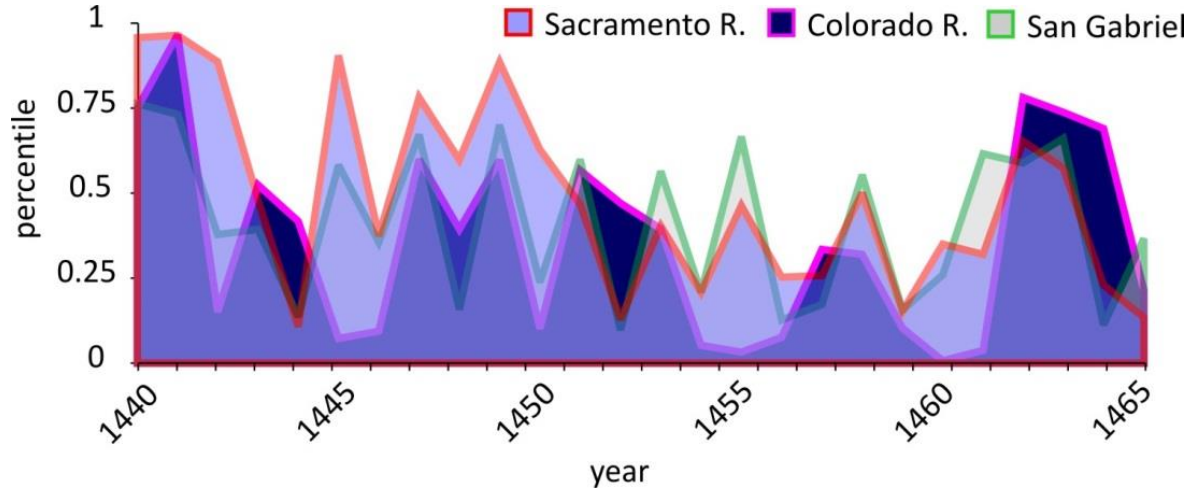

Figure 21. The extended 11-year period of drought, 1451-61, which impacted all three basins. Values are percent of average (based on instrumental data mean), 1440-1465.

Droughts are multi-dimensional, and considering duration, cumulative deficits, and average annual intensity (cumulative deficit/years in drought run) separately and together provides a more detailed picture of drought across these three regions. Ranked values of these three measures, plotted for each basin, show patterns of variability across the region (Figure 22). There is a high degree of variability from basin to basin, but during some periods, common characteristics are evident. For example, the period from 1570-1590 (Figure 22a) exhibits frequent and intense droughts in all three regions, whereas the mid-1700s had relatively long periods without events in any of the basins, interspersed with an occasionally severe drought event (Figure 22b). The 1860s-1870s was a period of mostly short droughts of moderate intensity in the Colorado and San Gabriel reconstruction, with a marked absence of events in the Sacramento reconstruction (Figure 22c).

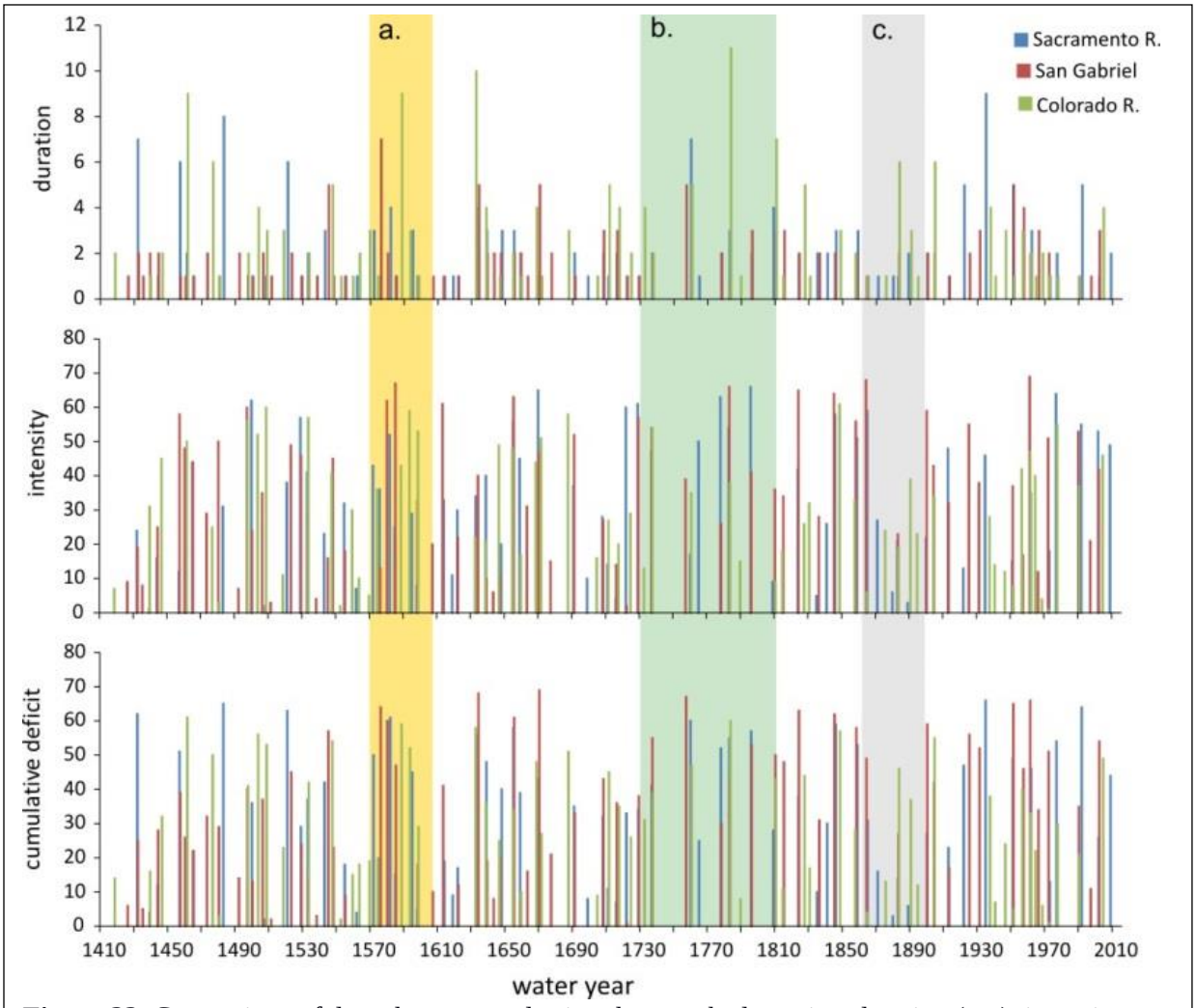

Figure 22. Comparison of drought measured using three ranked metrics: duration (top), intensity (middle), and cumulative deficit (bottom), for the Sacramento River index, San Gabriel water year precipitation, and Colorado at Lees Ferry water year flow. Higher values indicate greater magnitude of overall drought conditions. Bars mark the last year in the drought period. Vertical bars indicate a) 1450s drought, and periods of b) clustering of severe drought in all three basins and for all three metrics, c) more sparse events, but interspersed with extremes by all three measures, and d) shorter events and more moderate drought conditions.

Another view of covariation of droughts as well as wet periods in the three regions is given by the wavelet-transform coherency (WTC), which is introduced in the Data and Methods section (2.4). The WTC summarizes the correlation between a pair of time series as a function of time and frequency. WTCs from a cross-wavelet analysis of the most skillful reconstructions of San Gabriel Dam precipitation, Sacramento River annual flows and Colorado River annual flows (same series as analyzed above for drought) are plotted in Figures 23 - 25. Figure captions provide annotations and more in-depth description of how to interpret the figures and results.

The WTC for the two California series (San Gabriel vs Sacramento) is significant and in-phase over most of the concave region of WTC plot (this region is open to interpretation, marked by thin black line) in Figure 23. Coherency is significant for large regions of time-frequency space from periods of less than 4 years to periods of more than 128 years. This is expected because the same atmospheric circulation ridges and troughs often drive similar wet or dry climate episodes in these regions. Some influence on the WTC from sharing of a few tree-ring predictors could also be contributing to the coherence. The period after about 1850 is particularly interesting for strong, continuous coherence bands at short (~6 yr), median (~20 yr) and long (~128 yr) periods. The covariation of the series at multi-decadal periods or wavelengths is visible also in the time series plots of the two series smoothed with a Gaussian filter (bottom of Figure 23). Notable shared wet events, or high peaks, occur in the mid-1500s, early 1700s, and early 20th century. The most prominent shared dry event is the late 1500s. Some periods are remarkable for their contrast in the two regions. The most exceptional is the all-time high in the early 1600s on the Sacramento opposite near normal conditions in the San Gabriel series. Another contrast is the less severe shift from wet to dry conditions over the first few decades of the 20th century in the San Gabriel series than on the Sacramento. Such contrasts probably reflect periods of persistent anomalous north-south positions of storm tracks.

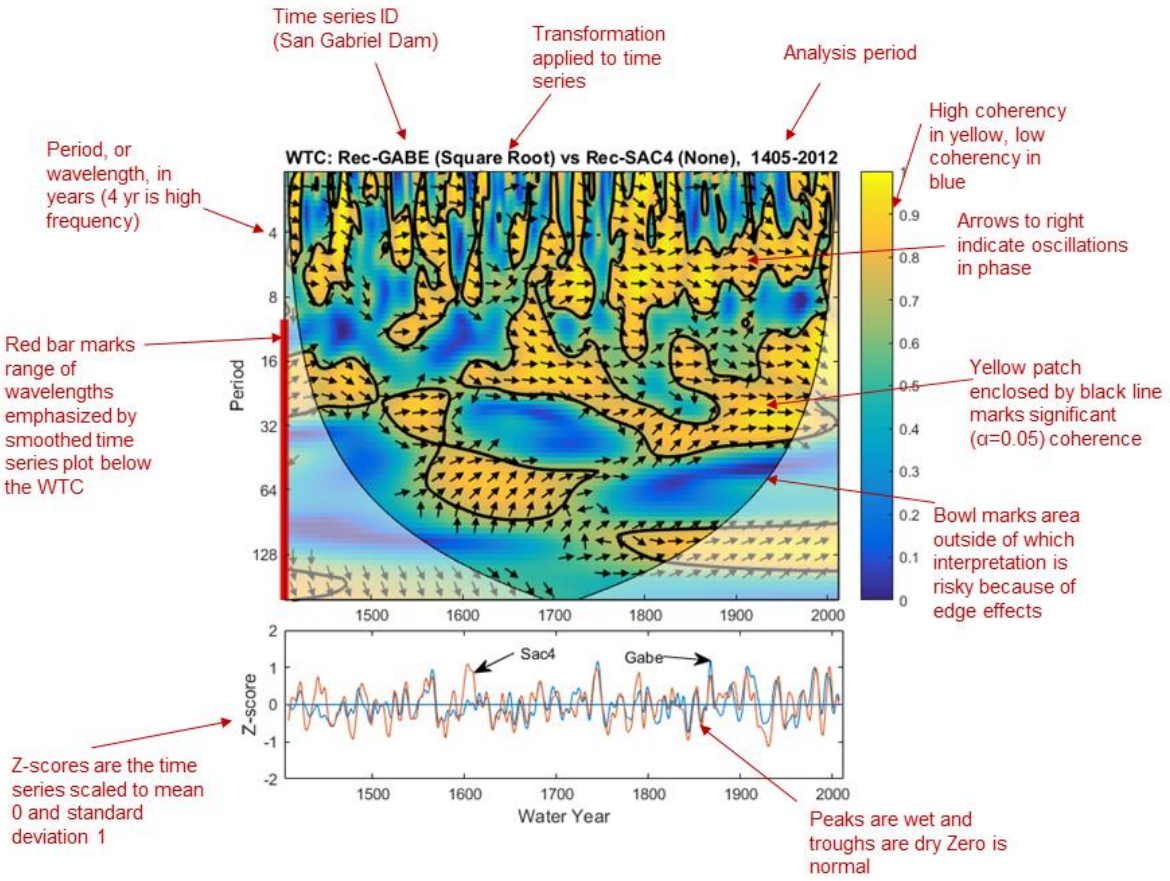

Figure 23. Wavelet-transform coherency (WTC) of most skillful reconstructions of San Gabriel Dam precipitation and Sacramento River natural flow. The WTC is plotted above, and the smoothed time series are plotted below. Coherency is color-mapped, as indicated by the scale at right. High coherence is analogous to high correlation at a specific period. Black lines enclose coherency significant at α=0.05. Direction of arrows indicates phase relationship of the oscillations in the series. Arrow to the right mean oscillations are exactly in-phase. Arrows to the left mean oscillations are exactly out of phase (e.g., peaks in one series coincide with troughs in the other). Angle of arrow with horizontal indicates degrees out of phase (0° is arrow to right, 180° is arrow to left). Arrows pointing upward to the right mean that oscillations at period *P* years in the second series (here, Sac4) lead oscillations in the first series (here, Gabe) by *m* years, where $m = P(x°/360°)$, and x° is the angle of the arrow from the horizontal. Conversely, arrows pointing downward to the right mean oscillations in the first series lead oscillations in the second series by the computed number of years. For example, the arrows pointing upward to the right in the yellow patch near a period of 50 years and year 1600 mean that oscillations near the 50-yr wavelength in Sacramento River Streamflow at that time lead oscillations in San Gabriel Dam precipitation by about 50(45/360) = 6.25 years.

The WTCs for the Colorado River reconstructions against each of the two California reconstructions (Figures 24, 25) show much less coherency at short periods than between the two California reconstructions. The WTC for the Colorado vs San Gabriel has an almost continuous (through time) band of high coherency near periods of 50-70 years, and this coherence is reflected in the smoothed time series plots (Figure 25, bottom). Low-frequency linkage of reconstructed variations is generally stronger between the Colorado River and Southern California (Figure 25) than between the Colorado River and the Sacramento River (Figure 24). After about 1850, the smoothed time series plots show stronger tracking of the Colorado River series by the San Gabriel series than by the Sacramento series. The sharp low-frequency dive from wetness to extreme dryness early in the 20th century on the Sacramento is not shared by the Colorado River or the San Gabriel series. On the other hand, some periods of the record show greater agreement of the Colorado with the Sacramento than with Southern California. An example is the all-time wet peak in the Sacramento in the early 1600s, which corresponds (slightly offset) to a major wet peak on the Colorado, but to near normal conditions in Southern California (time series plots in Figures 23 - 25).

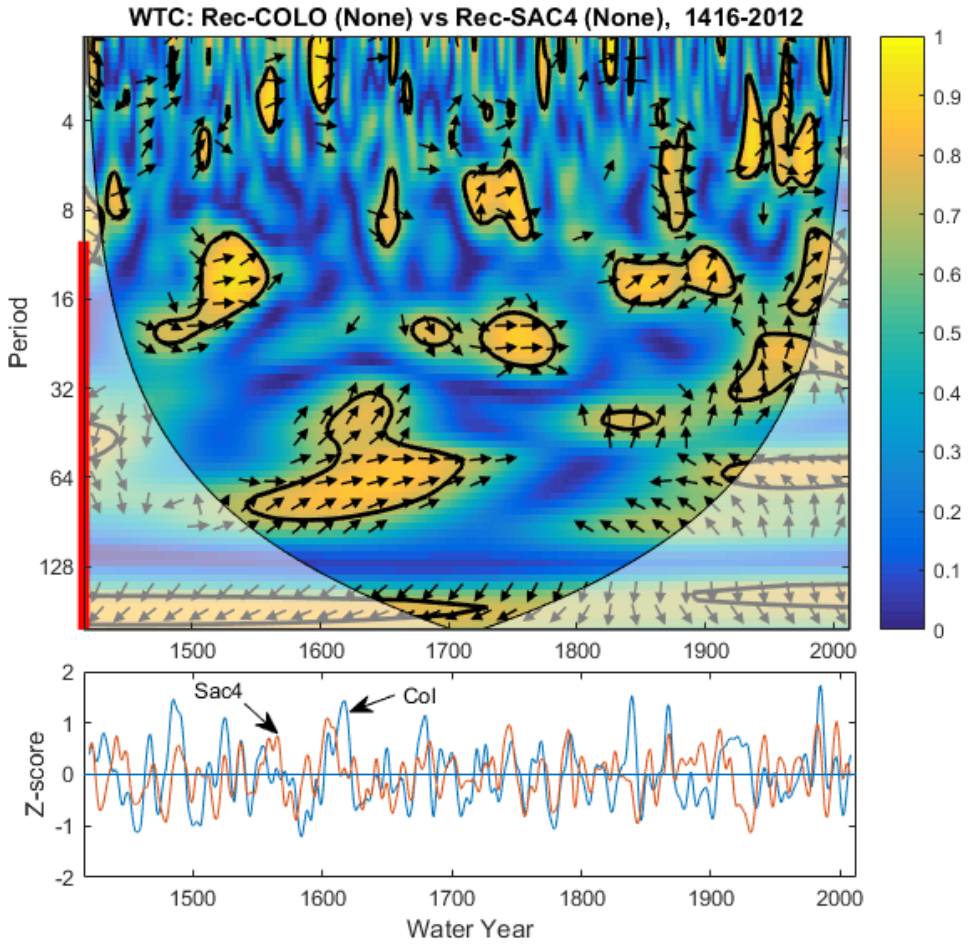

Figure 24. Wavelet-transform coherency (WTC) between reconstructions of natural flow of the Sacramento River (4 rivers runoff) and natural flow of the Colorado River at Lees Ferry. See caption of Figure 23 for guidance on interpretation.

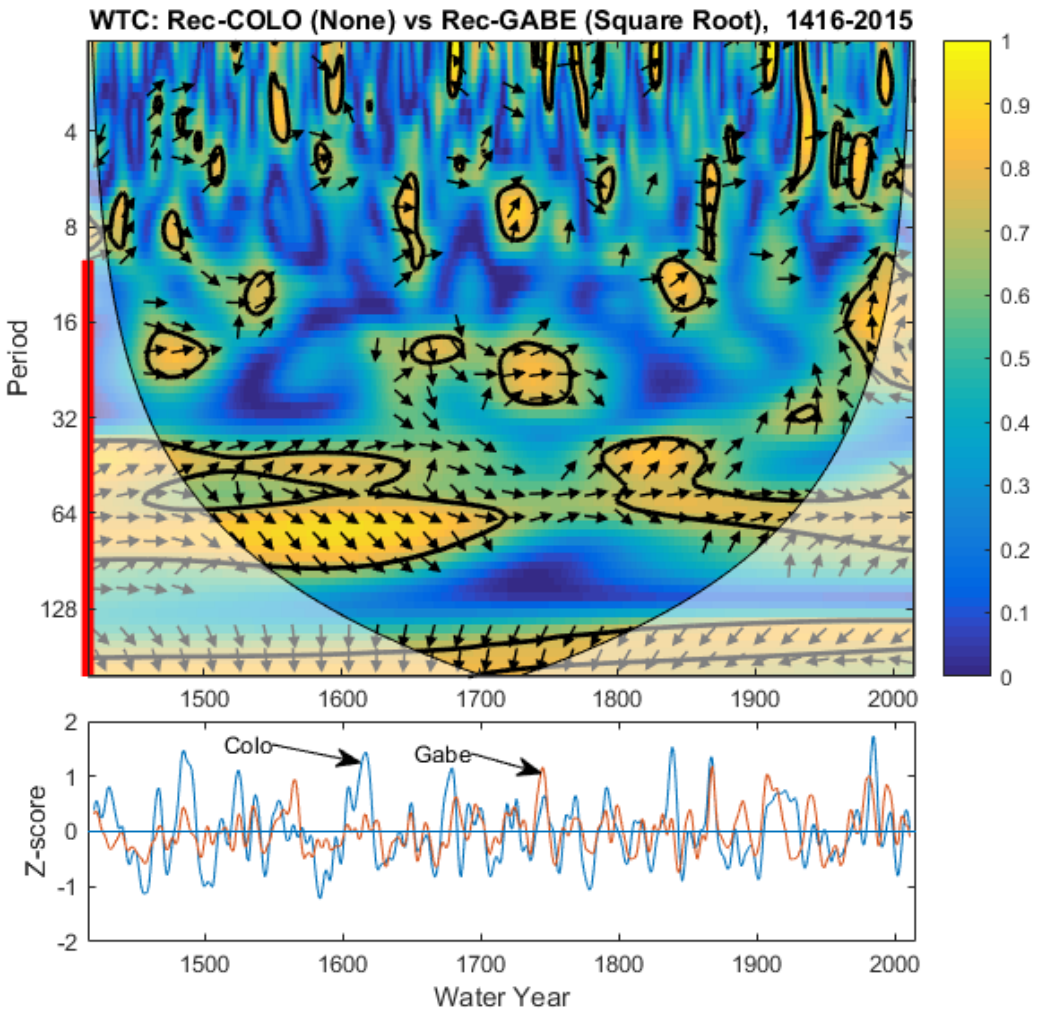

Figure 25. Wavelet-transform coherency (WTC) between reconstructions of natural flow of the Colorado River at Lees Ferry and precipitation at San Gabriel Dam. See caption of Figure 23 for guidance on interpretation.

3.7 Western North America Context for Southern California Drought

We identified six extremely dry 10-yr periods in southern California, and created maps of reconstructed drought values for the western US averaged over each time period. The maps are based on gridpoint data from the North American Drought Atlas (Cook et al. 2010) (Figure 26). The time series at each gridpoint is averaged for each 10-yr period, and then maps represent interpolated conditions between gridoints. The five lowest ranking 10-yr drought periods in the San Gabriel Dam precipitation reconstruction were selected (Table 4a). The fifth lowest (1629 – 1638) 10-yr period coincided with the driest seven-year event based on the runs analysis (Figure 5). A sixth period (1662 – 1671) was included because it corresponded with the fifth driest 20-yr period in the moving average rankings.

In each map, drought in southern California corresponds with drought conditions in other regions of the western US. Many of the periods also exhibit contrasting wet and dry conditions in different portions of the western US, along with variations in the drought intensity in different portions of the western US. Three periods (1662 – 1671; 1805 – 1814; 1947-1956) correspond with drought in the Southwest and southern Rocky Mountains. In this pattern, northern California has average conditions, and the Pacific Northwest and northern Rockies are moderately wet. The decades of 1450-1459 and 1571 – 1580 also follows this dipole type pattern, but wetter areas are farther to the north, with drought conditions in California and Oregon. The years of 1579 – 1580 have been identified as some of the driest years across the west coast of north America in other reconstructions of western US hydroclimate (though not entirely independent because of shared tree-ring chronologies) (e.g., Meko et al. 2001; Wise 2016), in agreement with the results shown here.

A different pattern emerges during the drought period from 1629 – 1638. During these years, drought conditions in southern California correspond with drought in northern Rockies and farther east, but not in the Southwest. The Southwest is relatively wet during this period, and exhibits a strong contrast with the climate of the northern Rockies. Northern California is moderately dry at this time. In contrast, the drought period 1947 – 1956 has a similar dipole pattern as other drought periods, but in these years, the drought is most intense in New Mexico and west Texas. In southern California, drought conditions were less intense, but drought conditions were prolonged, lasting up to several consecutive years below the instrumental mean.

One interesting feature in the drought maps is the mildness of drought conditions during the 1805 – 1814 drought episode. During this episode, closer inspection of the time series data reveals that drought conditions were consistently below the mean value, but none of the individual years were extreme. There was also one wet year (1811) within the time period. The prolonged drought contributed to the low ranking, rather than the severe conditions in any particular year. As described above, this pattern corresponds with moderate drought in the Southwest and Rocky Mountains.

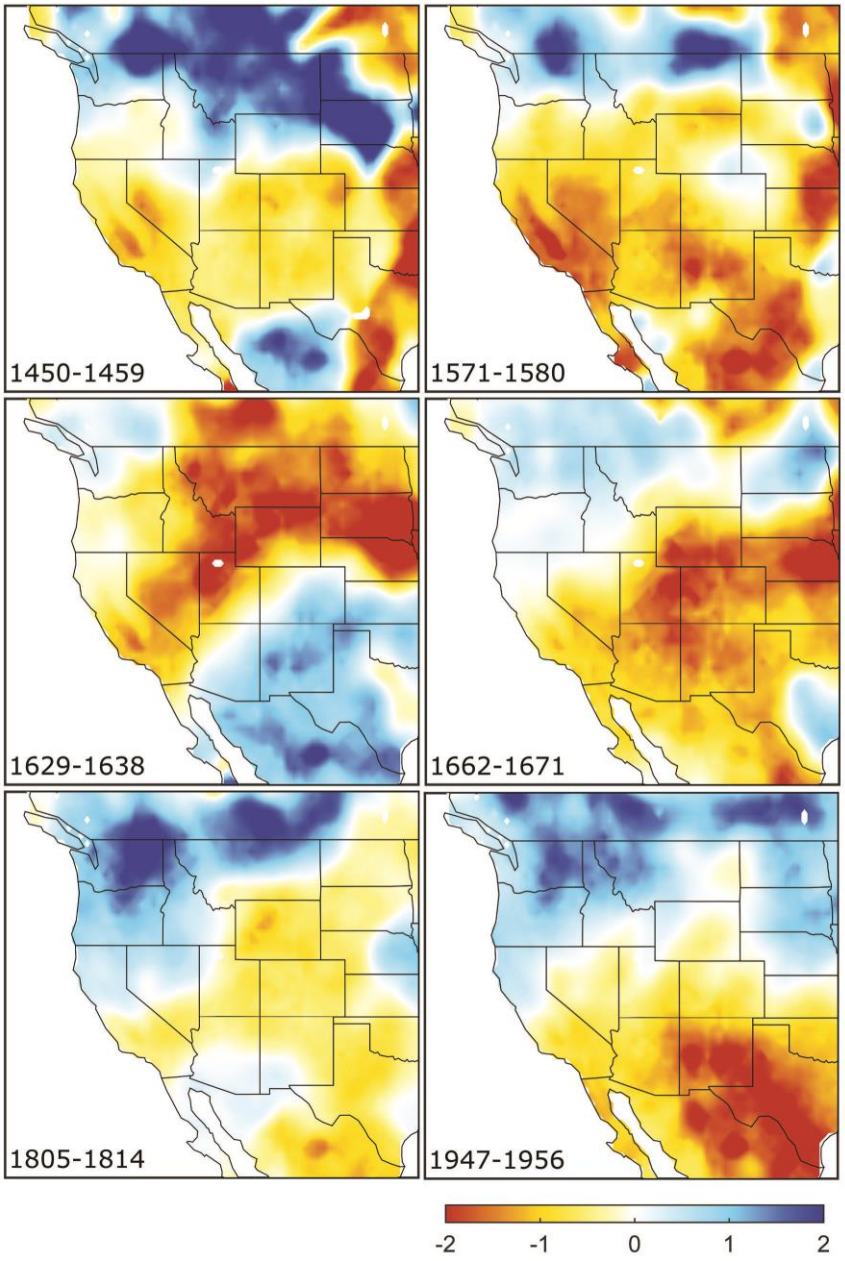

Figure 26. Composite drought maps for western US based on data from the North American Drought Atlas (Cook et al., 2010). Drought values at a 0.5° spacing obtained from the atlas were averaged over 10-year periods and then spatially interpolated to create the color maps. The scale for drought index ranges from moderately dry (-2) to moderately wet (+2). The time periods mapped represent the five lowest-ranking 10-yr drought periods based on moving averages identified in the San Gabriel Dam Precipitation record. A sixth period (1662 - 1671) was selected because it corresponded with fifth-driest 20-yr drought period based on moving averages.

4. Conclusions

A set of eight tree-ring based reconstructions of hydroclimate were generated for this study for use in water-resources planning and operation. These include reconstructions of southern California streamflow (Santa Ana, Arroyo Seco) and precipitation (Ojai, San Gabriel Dam, Lake Arrowhead), along with streamflow reconstructions for the Kern and the Colorado Rivers.

- Field collections and laboratory work yielded an updated set of moisture-sensitive tree-ring chronologies for the reconstructions, which now extend close to the present (2016 for the California reconstructions and 2015 for the Colorado River reconstruction).
- Two versions of reconstructions were generated: a most skillful set, with time coverage to the early 1400s, and a longest set, with time coverage to the early 1100s.
- The most skillful reconstructions explain a larger part of the instrumental record variance, ranging from 54% to 79%, while the longest reconstruction explain somewhat less (42% to 67%)
- The Colorado River at Lees Ferry reconstructions update previous reconstructions from 2006 and 2007
- The skillful version of the Colorado River reconstruction is almost identical to the Lees B (Woodhouse et al. 2006), but contains slightly more persistence that the Lees B reconstruction, which closely matched the persistence in the gage (natural flow) record.

The streamflow and precipitation reconstructions are useful for placing the period of the instrumental records in a long-tern context. The longer records allow an assessment of the statistical characteristics of the instrumental period, such as the mean and standard deviation, to determine if the period upon which water resource planning has been based is representative of a longer period of time.

- Results of the statistical comparisons suggest that southern California and Kern precipitation and river discharge over the instrumental period have been more variable and with less year to year persistence than for the long-term record.
- Variability has been significantly greater in the instrumental period than in the past six centuries for all California basins, while the instrumental period means are not significantly different than in the past nine centuries.
- The variance of Colorado River flows, in contrast, has been low in a long-term context, although the past century was among the wettest centuries of the past 600 years. Neither variance nor the mean in the instrumental period are significantly different than over the long term.

An evaluation of possible cycles (defined as variations that are rhythmic but not necessarily regular) in the reconstructions was undertaken to determine if the centuries-long record revealed some information that was not detectable in the shorter instrumental record. To summarize:

- A moisture cycle near a wavelength of 13-15 years is present in recent decades in both southern California and the Upper Colorado River basin in the instrumental record, but is not a consistent feature over the multi-century time frame of the reconstructions.
- The most skillful reconstructions for all 4 streamflow series (Colorado, Kern, Arroyo Seco and Santa Ana) have a spectral peak near 22 years, but wavelet analysis shows that this peak represents a quasi-cyclic variation (variable wavelength) rather than regular cycle.
- Spectral and wavelet analysis of the longest versions of reconstructions identify a consistent cyclic variation at a wavelength somewhat longer than 100 years (146-yr spectral peak). This feature is not present in the Colorado River reconstruction.

A focus of this project was on drought and the long-term perspective provided by the reconstructions of streamflow and precipitation. The duration of droughts (defined as consecutive years below the instrumental record average) was of particular interest, but cumulative deficit and average annual intensity were also considered. Because this set of reconstructions complements existing

reconstructions for northern California, this study also examined regional patterns of drought and the concurrence of drought in key water supply regions for California, the Sacramento and Colorado River basins, along with circulation features relate to regional drought. Some of the main finds are as follows:

- Droughts of long duration occurred in the past, and the longest droughts ranged from 8 – 13 years in the San Gabriel and Kern River most skillful reconstructions. Based on moving averages, extreme dry periods occurred the mid-1100s, mid-1400s, late 1500s and mid-late 1600s. In some cases, shorter, consecutive-year droughts in the 20th/21st centuries were more severe than the paleorecord.
- Concurrent droughts have occurred periodically across the main water supply regions for southern California (northern California, the upper Colorado River basin, and southern California). While the majority of these widespread drought events are short in duration, two nine-year events have occurred, 1452-1460 and 1775-1783.
- Although widespread drought events do occur, the characteristics of drought (duration, annual intensity, and cumulative deficit) vary across northern and southern California and the upper Colorado River basin, so that in periods of concurrent dryness, the overall severity of conditions varies regionally as well.
- Analysis with the drought reconstructions from North American Drought Atlas shows that the most severe decadal-scale droughts in Southern California are associated with more than one spatial pattern of continental drought in the western United States. Two distinctly different patterns are a 1) southwest-northeast alignment t oriented toward the Upper Colorado River Basin, and 2) a southerly alignment, with severe drought in Mexico or Texas.

To summarize, these new reconstructions now complete a set of hydroclimatic (streamflow or precipitation) reconstructions for California. With the updated Colorado River reconstruction, they provide a resource for evaluating the instrumental period in a long term context. Because these reconstructions represent a larger range of natural variability than 20th-21st century instrumental record, they provide an extended baseline for assessing possible future conditions.

5. Acknowledgments

The following individuals contributed to field work in southern California: Brewster Malevich, Chris Zemp, Andrew Cunningham, Mark Losleben, Cody Russell, and Cedar Welsh. Special thanks to Mark Borchert, retired USFS fire ecologist, for helping with logistics and field collections for the update of Lake Peak in the San Gorgonio Wilderness. Special thanks also to Emanuele Ziaco (UNR) for updating the Log Cabin Mine chronology on the east side of the Sierras, and providing the cores for our project.

The following individuals contributed to lab work and chronology development, including sample preparation, crossdating, measurement, quality control and chronology development: Maya Antoun, Jordan Krcmaric, Brewster Malevich, Chris Zemp, Andrew Cunningham and Oya Karamehtoglu. Jordan Krcmaric was especially helpful with data analysis. Maya Antoun made important contributions to organizing samples and metadata for archiving. Brewster Malevich contributed to many phases of the Southern California project, including assistance with site selection, compiling gage data, fieldwork, lab work and chronology development. We thank Chris Zemp for updating the TreeFlow website with the new chronologies. We thank Sarah Frederick for creating the layout of the guidebook and proof reading the TreeFlow web pages.

Special thanks to Dan Griffin for collaboration in the field, and for providing updated blue oak chronologies for five sites. We value Dan's input for site selection, research ideas and interpreting temporal and spatial patterns of drought for southern California. Tony Caprio assisted and provided valuable site information for updating foxtail pine sites in the Kern River watershed. He also generously provided older ring-width data for merging with our collections to create long foxtail pine chronologies important for the Kern River reconstruction. Troy Knight, a former student at LTRR whose PhD thesis centered on dendroclimatology in eastern Utah, contributed unpublished data to strengthen the chronology for Beef Basin, Utah. Chris Baisan assisted with fieldwork in eastern Utah, helped with crossdating and provided samples from the LTRR archive.

We thank contributors to the International Tree-Ring Data Bank (ITRDB) for making their chronologies freely available for studies such as ours (see Appendix B for individual attributions). Specifically, thanks are due to Franco Biondi for development of chronologies in southern California. We also thank the Los Angeles County Department of Public Works for providing the San Gabriel Dam precipitation data.

This work was made possible by funding from the California Department of Water Resources (CADWR). We thank Jeanine Jones of the CADWR for her encouragement and support.

6. References

Adams, K.D., Negrini, R.M, Cook, E.R. and Rajagopal, S. 2015. Annually resolved late Holocene paleohydrology of the southern Sierra Nevada and Tulare Lake, California. *Water Resources Research* 51, 9708–9724, 10.1002/2015WR017850.

Akaike, H., 1974: A new look at the statistical model identification. *IEEE Transactions on Automatic Control*, 19 (6), 716–723.

Benjamin, J. R. and C. A. Cornell (1970), *Probability, Statistics and Decisions for Civil Engineers*, McGraw-Hill Book Company, New York, 704 p.

Biondi F, Kozubowski TJ, Panorska AK (2002) Stochastic modeling of regime shifts. *Clim Res* 23:23–30.

Bloomfield, P. (2000), *Fourier Analysis of Time Series: An Introduction*, second ed., John Wiley & Sons, New York, 261 pp.

Box, G., G. M. Jenkins, and G. Reinsel, 1994: *Time Series Analysis: Forecasting & Control*. 3d ed., Prentice Hall.

Cleveland, W. S. (1979), Robust locally weighted regression and smoothing scatterplots, *J. Am. Stat. Assoc*., 74, 829–836.

Cook, E. R., P. J. Krusic, R. H. Holmes, and K. Peters (2007), *Program ARSTAN, Version 41d*, 2007, www.ldeo.columbia.edu/tree-ring-laboratory.

Cook, E. R. and K. Peters, 1981: The smoothing spline: a new approach to standardizing forest interior tree-ring width series for dendroclimatic studies. *Tree-ring bulletin*, 41, 45–53.

Cook, E. R., R. Seager, R. R. J. Heim, R. S. Vose, C. Herweijer, and C. Woodhouse (2010), Megadroughts in North America: Placing IPCC projections of hydroclimatic change in a long-term palaeoclimate context, *J. Quat. Sci*., 25, 48–61, doi:10.1002/jqs.1303.

Grinsted, A., J. C. Moore, and S. Jevrejeva (2004), Application of the cross wavelet transform and wavelet coherence to geophysical time series, *Nonlinear Proc. Geoph*., 11, 561–566.

Holmes, R., 1983. Computer assisted quality control in tree-ring standardization. *Tree-Ring Bulletin*, 43, 69–75.

Martinez, W. L., and A. R. Martinez (2005), *Exploratory Data Analysis with MATLAB*, Chapman & Hall/CRC, New York, 405 pp.

Meko, D. (1997), Dendroclimatic reconstruction with time varying predictor subsets of tree indices, *J. Clim*., 10(4), 687–696.

Meko, D. M., M. D. Therrell, C. H. Baisan, and M. K. Hughes, 2001: Sacramento River flow reconstructed to A.D. 869 from tree rings. *Journal of the American Water Resources Association*, 37 (4), 1029–1039.

Meko, D.M., C.A. Woodhouse, C.H. Baisan, T. Knight, J.J. Lukas, M.K. Hughes, and M.W. Salzer, 2007. Medieval drought in the upper Colorado River basin. *Geophysical Research Letters* 34m L10705, doi: 10.1029/2007GL029988.

Meko, D. M., and C. A. Woodhouse (2011), Dendroclimatology, dendrohydrology, and water resources management, In: *Tree Rings and Climate: Progress and Prospects* (eds. M.K. Hughes, T.W. Swetnam, H.F. Diaz). Springer, pp. 231-261.

Meko, D. M., C.A. Woodhouse, and R. Touchan (2014), *Klamath/San Joaquin/Sacramento Hydroclimatic Reconstructions from Tree Rings*. Final Report to California Department of Water Resources, Agreement 4600008850. 72 pp.

Mitchell, J. M., Jr, B. Dzerdzeevskii, H. Flohn, W. L. Hofmeyr, H. H. Lamb, K. N. Rao, and C. C. Walleen (1966), *Climatic change, technical note no. 79*, Report of a working group of the Commission for Climatology No. 195 TP 100, WMO, Geneva, Switzerland, 81 pp.

Myers, R. H. (1990), *Classical and Modern Regression with Applications*, Doxbury, Pacific Grove, California, 488 pp.

Osborn, T. J., K. R. Briffa, and P. D. Jones (1997), Adjusting variance for sample-size in tree-ring chronologies and other regional mean timeseries, *Dendrochronologia*, 15, 89– 99.

Schulman, E., 1945. Tree-ring hydrology of the Colorado River Basin. *University of Arizona Bulletin* XVI (4), University of Arizona, Tucson, 51 pp.

Salas, J. D., J. W. Delleur, V. Yevjevich, and W. L. Lane (1980), Applied Modeling of Hydrologic Time Series, *Water Resources Publications*, P.O. Box 630026, Highlands Ranch, Colorado, USA 80163-0026, 485 pp.

Stine, Scott (1994), Extreme and persistent drought in California and Patagonia during mediaeval time, *Nature*, 369, 546–549.

Stockton, C.W. and Jacoby, G. C.: 1976, *Long-Term Surface Water Supply and Streamflow Levels in the Upper Colorado River Basin*, Lake Powell Research Project Bulletin No 18, Inst. of Geophysics and Planetary Physics, University of California, Los Angeles, 70 pp.

Stokes, M. A., and T. L. Smiley (1996), *An Introduction to Tree-Ring Dating*, 73 pp., Univ. of Ariz. Press, Tucson. (originally published 1968, University of Chicago Press).

Torrence, C., and G. P. Compo (1998), A practical guide to wavelet analysis, *Bull. Amer. Meteorol. So*c., 79, 61–78.

Wigley, T. M. L., K. R. Briffa, and P. D. Jones (1984), On the average value of correlated time series, with applications in dendroclimatology and hydrometeorology, *J. Clim. Appl. Meteorol*., 23, 201–213.

Wise E.K. 2016. Five centuries of U.S. West Coast drought: Occurrence, spatial distribution, and associated atmospheric circulation patterns. *Geophysical Research Letters* 43, 4539–4546. doi:10.1002/2016GL068487.

Woodhouse, C.A., S.T. Gray, and D.M. Meko. 2006. Updated streamflow reconstructions for the Upper Colorado River basin. *Water Resources Research* 42(5): W05415.

Appendix A. Observed Flows and Precipitation

Refer to Table 1 and text of report for definition of individual series
P is precipitatio (inches); Q is full natural flow (thousands of acre-ft)

water year	Q Arroyo	P SanGab	Q SantaAna	P LakeArrow	P Ojai	P Cuyam	Q Kern	Q Colo
1887								
1888						22.4		
1889						53.39		
1890						62.21		
1891						62.43		
1892						38.58		
1893						40.71		
1894						14.35		
1895						56.98		
1896						23.6		
1897						36.11		
1898						28.65		
1899						22.07		
1900						28.86		
1901			47.16		21.69	41.78		
1902			25.06		14.86	37.37		
1903			66.38		23.54	37.62		
1904			24.66		13.53	23.42		
1905			59.81		22.74	57.3		
1906			121.77		23.66	59.23		18214.7
1907			164.42		37.45	40.91		21234.3
1908			59.34		20.42	34.83		11774
1909			89.15		27.75	39.85		21841.4
1910			96.08		23.78	33.6		14736.7
1911	3.14		102.6		30.01	31.16		15125.1
1912	1.19		43.14		13.07	32.47		19082.1
1913	0.72		32.44		18.24	32.46		14472.2
1914	32.98		94.96		39.53	33.48		21066.8
1915	8.63		137.75		24.02	55.19		14137.6
1916	1.48		249.88		29.68	61.47		19187.5
1917	5.58		70.33		20.76	35.92		23849.3
1918	5.59		84.62		26.86	29.73		15750.7
1919	1.52		37.95		12.82	30.83		12951.5
1920	3.64		81.29		15.54	38.5		21928
1921	3.17		52.05		18.5	30.77		22703.1
1922	25.45		190.5		26.67	46.53		18669.6
1923	3.2		62.9		19.35	37.24		18343.7

1924	0.84		36.51		6.88	28.42		14639.1
1925	1.08		28.49		11.99	36.1		13410.8
1926	6.2		48.28		21.68	36.98		16114
1927	6.8		112.64		26.23	66.98		18551.9
1928	1.29		19.64		16.25	20.83		17577.9
1929	1.41		26.3		13.21	40.61		21407.1
1930	1.64		34.69		14.01	38.14	331.57	15283.5
1931	1.48		21.84		17.29	28.18	184.13	8631.72
1932	5.32		86.1		26.06	50.6	696.03	17545.5
1933	2.79		26.15		11.64	40.72	427.2	12130.1
1934	2.97		22.02		13.78	20.91	230.12	6627.51
1935	9.02		46.3		22.45	37.84	455.89	12280
1936	3.91		37.42		20.36	39.33	747.7	14485.4
1937	11.93		150.84		29.14	65	1107.78	14161.8
1938	21.87	44.32977	193.04		33.97	48.72	1288.42	17920.1
1939	4.69	29.41008	59.08		14.44	44.07	451.46	11718.1
1940	3.99	20.10999	41.69		15.46	30.11	694.97	9380.28
1941	25.22	53.3	105.34		45.25	65.92	1245.64	18319.3
1942	2.46	17.58996	42.47	32.19	17.16	31.44	750.26	19428.3
1943	21.26	47.56003	77.03	60.8	28.07	37.77	1002.67	13624.5
1944	13.74	33.23004	52.2	46.47	24.16	40.39	577.92	15512.5
1945	5.82	28.89009	64.2	52.15	18.9	41.24	806.76	13912.7
1946	4.98	28.88035	49.16	42.13	13.84	35.29	646.41	11062.7
1947	5.9	29.30988	34.38	43.23	15.37	28.98	425.27	15916.3
1948	1.2	13.88002	22.51	28.9711444	9.34	28.77	331.72	15880.2
1949	1.27	16.1	30.58	38.34	11.12	34.31	295.07	16662.2
1950	1.52	20.61	23.37	34.2	16.71	32.33	434.24	13317.9
1951	0.54	12.69	14.8	20.6	10.1	26.71	528.28	12485.8
1952	11.5	49.19	78.1	70.65	35.72	53.73	1392.99	20900
1953	1.5	16.71	26.4	25.18	13.85	26	540.763	11204
1954	3.04	25.6	51.2	44.45	19.4	40.8	503.176	8368.14
1955	1.3	19.88	26	34.5	16.59	26.01	355.811	9795.47
1956	2.2	24.32	18.52	29.07	18.78	23.42	870.49	11505.1
1957	1.19	21.82	25.21	35.4	13.83	29.34	438.647	20159.8
1958	11.29	45.95	86.71	63.13	40.07	49.25	1057.54	16899.9
1959	1.61	15.82	19.79	20.88	12.22	18.6	276.534	9232.54
1960	0.78	14.24	18.93	25.72	13.48	27.66	279.179	11974.8
1961	0.8	11.57	11.63	19.46	8.97	12.13	174.99	9247.78
1962	6.61	33.73	39.43	43.64	30.4	34.43	653.654	17769.4
1963	1.8	17.37	13.88	24.57	17.5	22.98	737.823	9169.05
1964	1.39	15.73	17.83	27.27	11.69	33.04	323.11	10355.5
1965	2.239	22.32	23.19	35.39	19.22	27.87	697.863	18433.7
1966	14.56	39.56	66.39	51.66	23.2	37.49	399.603	11139.8
1967	16.98	47.42	109.4	72.22	31.92	47.04	1576.05	11787

1968	5.18	19.04	33.49	30.79	14.57	28.48	489.596	13307.3
1969	41.8	65.09	233.41	98.24	47.23	46.72	2226.73	14543.5
1970	4.13	20.35	35.32	22.49	16.32	20.48	604.213	15040.9
1971	4.48	21.16	26.79	28.78	14.31	30.25	429.092	14867.4
1972	1.54	13.15	25.93	28.4	11.22	20.98	256.778	12398.4
1973	8.18	36.24	62.41	45.88	32	52.13	912.298	19270.8
1974	5.26	25.33	32.76	34.25	19.49	23.59	788.363	12965.3
1975	2.77	21.8	24.05	30.92	22.44	34.79	558.051	16563.8
1976	2.371	20.33	21.45	37.67	15.74	34.49	237.793	11199.8
1977	1.873	18.8	15.079	25.41	11.05	25.14	186.015	5436.47
1978	26.435	62.6	130.28	93.03	48.04	54.82	1523.86	14892.8
1979	6.44	30.38998	109.27	47.6	24.38	42.28	678.004	17609.8
1980	21.76	58.22	206.65	66.99102564	29.96	72.4	1549.91	17312.2
1981	2.55	16.38	33.45	21.05265899	14.52	21.8	458.657	8647.97
1982	5.81	33.7	48.68	47.0478465	19.22	39.21	1102.67	16718.4
1983	31.576	58.46	147.658	71.41	42.87	74.43	2317.93	23717.8
1984	3.65	15.63	37.31	26.48361891	13.06	28.44	889.275	24192.6
1985	2.412	23.71	27.59	34.01	12.03	33.02	677.717	21040
1986	4.947	34.19	45.461	50.81	22.32	40.57	1359.5	22305.4
1987	0.981	11.46	21.376	23.74	7.74	21.73	402.671	16554.7
1988	3.11	30.13	18.88	40.39	17.95	31.06	291.418	11638.2
1989	1.882	20.55	18.316	29.7	11.59	22.45	388.367	9529.57
1990	0.809	15.45	10.627	26.1	9.02	20.97	204.308	8965.07
1991	2.644	21.99	28.67	35.36	19.19	34.63	383.631	12326.5
1992	13.536	36.51	39.547	45.24	27.4	34.74	288.096	11077.5
1993	30.36	64.5802	161.04	90.88	42.25	60.47	833.587	18681.8
1994	2.389	16.95	35.244	28.7	13.72	32.28	335.364	10586.5
1995	17.954	50.16	125.53	74.51	42.41	57.48	1281.82	19859.1
1996	5.034	27.85994	38.968	32.95	16.93	19.94	921.196	14053.1
1997	3.911	30.40007	37.901	40.97878773	21.03	26.6	1199.32	21184.6
1998	20.365	54.63981	123.823	69.05	48.57	54.32	1530.53	16968.6
1999	2.118	14.23997	22.127	18.88843132	12.46	21.35	473.181	16451.9
2000	3.044	21.10993	16.951	24.92	18.84	19.35	464.485	10541.3
2001	3.216	23.10983	14.14	22.28	20.54	14.39	371.423	11025.4
2002	0.473	10.93002	2.987	8.4	7.27	9.45	355.821	5869.16
2003	2.277	26.05	21.407	40.46	22.23	34.48	575.196	10451.9
2004	1.29	18.06989	10.008	21.51	13.65	20.14	399.718	9444.49
2005	37.886	72.36012	120.743	84.65	47.31	52.97	1089.5	17111.2
2006	5.236	28.17993	60.711	39.24	25.37	26.12	1043.82	12627.7
2007	0.617	10.62	10.884	8.81	7.42	14.9	274.07	12565.1
2008	5.753	31.81004	34.149	46.06	11.84	27.42	502.431	16312.2
2009	1.87	19.18987	23.687	8.46	11.46	19.78	456.813	14304
2010	9.712	33.41993	52.957	20.12201213	21.49	37.83	794.932	12330.4
2011	14.079	42.23	96.997	31.31903325	24.89	44.26	1395.03	20063.2

2012	2.908	16.74	23.772	20.72382206	10.37	24.29	383.394	8223.92
2013	1.304	12.96	9.461	17.50644503	8.71	19.51	220.172	8850.57
2014	1.372	14.23	8.339	23.33381716	9.51	16.75	177.552	14137.1
2015	1.629	17.23	10.108	27.02774126			129.841	

Appendix B. Tree-Ring Metadata

Metadata for the 46 site chronologies. Tables (2 pages), followed by key (2 pages)

Code	N	SiteName	lePrefix	First	Last	EPS	Species	Lat	Lon	Elevm	PI	DataFrom
B27	1	Rock Springs Ranch Up	B27c	1379	2016	1404	QUDG	36.490	-120.878	1067	r	our files, Griffin
B32	2	Wright Mountain Updat	B32c	1409	2016	1460	QUDG	36.340	-120.520	1219	r	our files, Griffin
BFB	3	Beef Basin Update	BFBM#ec	350	2015	585	PSME	37.928	-109.794	2270	t	our files, ITRDB and Knig
BIG	4	Bigrock Campground	BIG#e	1393	2015	1575	PSMA	34.396	-117.828	1481	q	our files
BMC	5	Black Mountain	BMC#e	-210	2012	965	SEGI	36.104	-118.655	1950		Our files
KR2	6	Kern River	ca621c	1585	2003	1640	QUDG	35.532	-118.628	715		ITRDB
JOA	7	San Joaquin River Mil	ca627c	1710	1996	1770	QUDG	37.030	-119.675	137		ITRDB
BFA	8	Boreal Plateau	ca636#e	831	1992	1065	PIBA	36.450	-118.550	3420		ITRDB
UWL	9	Upper Wright Lakes	ca637#e	-215	1992	640	PIBA	36.620	-118.370	3519		ITRDB
DEN	10	Dennison Peak	ca651c	1601	2003	1660	QUDG	36.286	-118.776	1132		ITRDB
DMS	11	Dead Mule Saddle	ca653c	1468	2003	1493	QUDG	35.908	-118.667	1237		ITRDB
KAW	12	North Fork Kaweah Riv	ca659c	1494	2004	1550	QUDG	36.549	-118.893	701		ITRDB
SJR	13	San Joaquin Experimer	ca664c	1557	2004	1582	QUDG	37.090	-119.747	345		ITRDB
CTN	14	Crabtree North (Sierr	CTNM#e	941	2015	1125	PIBA	36.558	-118.363	3285	q, u	our files, Caprio
CTS	15	Crabtree South (Sierr	CTSM#e	1150	2015	1195	PIBA	36.543	-118.368	3254	q, u	our files, Caprio
DJU	16	Dutch John Update	DJUM#e	1365	2015	1366	PIED	40.953	-109.454	2190	t	our files, ITRDB
DOU	17	Douglas Pass Update	DOUM#e	1382	2015	1490	PSME	39.597	-108.812	2560	t	our files, ITRDB
EVG	18	Evans Grove Merged	EVGM	-350	2011	1100	SEGI	36.776	-118.818	2183	i	Our files
FCU	19	Fry Creek Update	FCUM#e	1617	2015	1695	PSMA	33.346	-116.880	2083	t	our files, ITRDB
FIG	20	Figueroa Mountain Upc	FIGc	1293	2016	1318	QUDG	34.742	-119.987	971	r	our files, Griffin
GFE	21	Guyot Flat East (Sier	GFEM#e	890	2015	1075	PIBA	36.519	-118.348	3327	q, u	our files, Caprio
GFN	22	Guyot Flat North (Sie	GFN	1080	2015	1190	PIBA	36.528	-118.358	3276	q	our files
GFS	23	Guyot Flat South (Sie	GFSM#e	931	2015	1065	PIBA	36.504	-118.346	3158	q, u	our files, Caprio
HLC	24	Hard Luck Campground	HLC	1645	2015	1705	PSMA	34.675	-118.841	890	q	our files

Code	N	Site Name	Prefix	First	Last	EPS	Species	Lat	Lon	El	PI	Data From
KAI	25	Kaiser Pass Merged	KAIM	720	2011	980	JUOC	37.306	-119.110	2685	g	Our files; Caprio
KSU	26	Keen Camp Summit (Upc	KSUM#e	1458	2015	1515	PSMA	33.682	-116.692	1463	t	our files, ITRDB
LCM	27	Log Cabin Mine Update	LCMM#e	1420	2016	1467	PSMA, PIJE	37.950	-119.150	2499	t	our files, ITRDB, Ziaco (
LCU	28	Lion Canyon Upate	LCUM#e	1494	2015	1535	PSMA	33.626	-116.715	1478	v	our files, LTRR archive
LGU	29	Mount Laguna Update	LGUM#e	1648	2015	1685	PSMA	32.869	-116.419	1813	t	our files, ITRDB
LOB	30	Los Lobos Creek Updat	LOBc	1333	2016	1390	QUDG	34.923	-119.240	1017	r	our files, Griffin
LPK	31	Lake Peak Update (Tos	LPKM#e	340	2015	800	PIFL	34.116	-116.812	3017	v	our files, LTRR archive
LSC	32	Little Sycamore Canyc	LSCc	1378	2016	1455	QUDG	34.510	-118.430	1128	r	our files, Griffin
MHC	33	Mountain Home	MHC#e	1297	2012	1575	SEGI	36.240	-118.672	1970		Our files
MPS	34	Maple Springs Update	MPSM#e	1657	2015	1695	PSMA	33.732	-117.548	1283	t	our files, ITRDB
MWC	35	Mount Wilson Combinec	MWC#e	1190	2015	1325	PSMA	34.261	-118.107	1481	q	our files
NPC	36	North Park Update	NPCM#e	1486	2015	1491	PIED	40.956	-106.338	2450	t	our files, ITRDB
PMN	37	Pine Mountain Update	PMNM#e	1333	2015	1425	PSMA	34.673	-119.372	1176	t	our files, ITRDB
PT2	38	Peterson 552 Update	PT2M#e	1628	2015	1715	PSMA	34.108	-116.976	1412	t	our files, ITRDB
PT9	39	Peterson 539 Update	PT9M#e	1692	2015	1775	PSMA	33.999	-116.758	1412	t	our files, ITRDB
PUM	40	Pumphouse Update	PUMM#e	1175	2015	1200	PIED	39.955	-106.525	2385	t	our files, ITRDB
RCK	41	Red Creek Update	RCKM#e	1270	2015	1541	PIED	38.558	-107.210	2835	t	our files, ITRDB
RED	42	Red Canyon Update	REDM#e	1336	2015	1416	PIED	39.703	-106.735	2164	t	our files, ITRDB
RRT	43	Red Reef Trail	RRT	1411	2015	1595	PSMA	34.502	-119.116	1412	q	our files
SBP	44	Siberian Pass Trail (	SBPM#e	783	2015	1190	PIBA	36.467	-118.272	3332	q, u	our files, Caprio
TRG	45	Trail Gulch Update	TRGM#e	996	2015	1141	PIED	39.715	-106.979	2210	t	our files, ITRDB
WIL	46	Wild Rose Update	WILM#e	1000	2015	1116	PIED	39.012	-108.245	2636	t	our files, ITRDB

Headings of metadata columns

Code = site code, usually 3 characters, unique to the site
N site number
SiteName.... self-explanatory
FilePrefix = the part of the crn and rwl filename before the suffix
First = first year of data in the chronology
Last = last year of data in the chronology
EPS = first year EPS>0.85 for the chronology
Species = 4 letter species code
Lat = latitude in decimal degrees
Lon = longitude in decimal degrees (west negative)
Elev = representive elevation of site (meters a
PI = Principal Investigator for the collection (see codes above)
DataFrom = where we obtained the rwl data

Principal Investigator Code	
a	Meko & Touchan, SJK
b	Meko & Touchan, SJK project; Meko, Sacramento River
c	Meko & Touchan, SJK; Meko, Sacramento River; Fritts 1980s
d	Woodhouse, SJK
e	Woodhouse, SJK; Meko Sacramento River; Fritts 1980s
f	Woodhouse, SJK; Meko, Sacramento River
g	Woodhouse, SJK; Caprio 1990s; Fritts 1980s
h	Stahle, blue oak project
i	Woodhouse, SJK; Ferguson and others, 1964
j	Meko & Touchan, SJK; Hughes, 1992
k	Woodhouse, SJK; Fritts 1980s
l	Meko, Sacramento River
m	Meko & Touchan, SJK; Baisan/Swetnam
n	King
o	Graumlich
p	Meko & Touchan, SJK; Hughes 2013
q	Meko & Woodhouse, SoCal
r	Meko & Woodhouse, SoCal + Griffin 2016
s	Meko & Woodhouse, SoCal + Biondi 2016
t	Meko & Woodhouse, SoCal and ITRDB
u	Caprio, 1990's Sequoia NP collection
v	Meko & Woodhouse, SoCal, LTRR Archive
First group in a row is most recent collection	
SJK = Sacramento/San Joaquin/Klamath project funded by CADWR in 2013	
SoCal = Southern California project funded by CADWR in 2015	
files prefix:	
AAA = our collection, unedited	
AAAM = merged	
AAA#e = edited	
AAAM#e = merged and edited	
AAAc	culled dataset (MATLAB)

Appendix C. Tree-Ring Site Cross-Reference to Models.

Cross-reference table of tree-ring chronologies to reconstruction models. The four numbers for each basin (last 8 columns) and chronology (row) indicate whether a chronology was included (1) or not included (0) in the reconstruction model. From left to right, these models are Rec1, Rec2, Rec3, and Rec4 as defined in the report. The "longest" reconstruction uses only Rec1. The "most skillful" reconstruction is a spliced version of Rec2 and Rec3. Only the last year of the "most-skillful" reconstruction is contributed by Rec4. Chronologies are numbered as in the table of tree-ring metadata (Appendix B). As an example of interpretation, to identify the sites used in the "longest" Colorado River reconstruction, refer to the first sub-column under "COLO." Number "1" occurs in just rows 3 and 46, indicated that chronologies BFB and WIL were used. Chronologies used at any time in the "most skillful" version of COLO are those with a "1" in any of the last 3 sub-columns under COLO. These are the 9 sites: 3, 16, 17, 36, 40, 41, 42, 45, and 46.

N	CODE	SPECIES	SECO	GABRIEL	ANA	ARROW	OJA	CUYAM	KERN	COLO
1	B27	QUDG	0111	0111	0111	0111	0011	0111	0111	0000
2	B32	QUDG	0011	0011	0000	0011	0010	0011	0011	0000
3	BFB	PSME	0000	0000	0000	0000	0000	0000	0000	1111
4	BIG	PSMA	0000	0000	0000	0000	0000	0000	0000	0000
5	BMC	SEGI	0000	0000	0000	0000	0000	0000	0000	0000
6	KR2	QUDG	0000	0000	0000	0000	0000	0000	0000	0000
7	JOA	QUDG	0000	0000	0000	0000	0000	0000	0000	0000
8	BFA	PIBA	0000	0000	0000	0000	0000	0000	0000	0000
9	UWL	PIBA	0000	0000	0000	0000	0000	0000	0000	0000
10	DEN	QUDG	0000	0000	0000	0000	0000	0000	0000	0000
11	DMS	QUDG	0000	0000	0000	0000	0000	0000	0000	0000
12	KAW	QUDG	0000	0000	0000	0000	0000	0000	0000	0000
13	SJR	QUDG	0000	0000	0000	0000	0000	0000	0000	0000
14	CTN	PIBA	1110	1110	1110	1110	1110	1110	1110	0000
15	CTS	PIBA	0110	0110	0000	0110	0110	0000	0110	0000
16	DJU	PIED	0000	0000	0000	0000	0000	0000	0000	0011
17	DOU	PSME	0000	0000	0000	0000	0000	0000	0000	0010
18	EVG	SEGI	0000	0000	0000	0000	0000	0000	0000	0000
19	FCU	PSMA	0000	0000	0000	0000	0000	0000	0000	0000
20	FIG	QUDG	0111	0111	0111	0111	0111	0111	0111	0000
21	GFE	PIBA	0000	1110	1110	0000	0000	1110	1110	0000
22	GFN	PIBA	0110	0110	0000	0110	0110	0110	0110	0000
23	GFS	PIBA	1110	1110	1110	1110	1110	0000	1110	0000
24	HLC	PSMA	0010	0010	0010	0010	0010	0000	0000	0000
25	KAI	JUOC	0000	0000	0000	0000	0000	0000	0000	0000
26	KSU	PSMA	0010	0010	0010	0010	0000	0010	0010	0000
27	LCM	PSMA	0000	0001	0000	0001	0000	0000	0001	0000
28	LCU	PSMA	0000	0010	0010	0010	0010	0010	0010	0000
29	LGU	PSMA	0000	0000	0000	0000	0000	0000	0000	0000
30	LOB	QUDG	0111	0111	0111	0111	0111	0111	0111	0000
31	LPK	PIFL	1110	1110	1110	1110	1110	1110	1110	0000
32	LSC	QUDG	0011	0011	0011	0011	0011	0011	0011	0000
33	MHC	SEGI	0000	0000	0000	0000	0000	0000	0000	0000
34	MPS	PSMA	0000	0000	0000	0000	0000	0010	0000	0000
35	MWC	PSMA	0000	0110	0110	0000	0110	0110	0110	0000
36	NPC	PIED	0000	0000	0000	0000	0000	0000	0000	0011
37	PMN	PSMA	0010	0000	0000	0110	0010	0000	0010	0000
38	PT2	PSMA	0000	0000	0000	0000	0000	0000	0000	0000
39	PT9	PSMA	0000	0000	0000	0000	0000	0000	0000	0000
40	PUM	PIED	0000	0000	0000	0000	0000	0000	0000	0111
41	RCK	PIED	0000	0000	0000	0000	0000	0000	0000	0011
42	RED	PIED	0000	0000	0000	0000	0000	0000	0000	0111
43	RRT	PSMA	0000	0000	0000	0000	0000	0000	0000	0000
44	SBP	PIBA	0110	0110	0110	0110	0110	0110	0110	0000
45	TRG	PIED	0000	0000	0000	0000	0000	0000	0000	0111
46	WIL	PIED	0000	0000	0000	0000	0000	0000	0000	1111

Appendix D. Statistical Methods

This appendix provides details of statistics and modeling. All methods described in this appendix were implemented in Matlab.

D1. Descriptive Statistics

Descriptive statistics used in the study are the mean, median, standard deviation, skew and lag-1 autocorrelation. These statistics are described in most standard texts on statistics in hydrology or the atmospheric sciences (e.g., Panofsky and Brier 1968; Salas et al. 1980; Wilks 1995; Haan 2002). Let $x_1, x_2, \ldots, x_N$ be a time series of length N.

The **mean** is a measure of the central tendency of the time series. The mean is also called the arithmetic average, and is one of several possible estimates of the "typical" values of a time series. The mean is computed as

$$\bar{x} = \frac{1}{N}\sum_{i=1}^{n} x_i \tag{1}$$

The **median** is another measure of the central tendency of a time series, and is defined as the "middle" value of the series. It is defined such that half the N values of the time series are larger than the median and half are smaller. If the N is odd, the median is equivalent to the middle-ranking member of x. If N is even the median is computed as the average of the two values of x with ranks $N/2$ and $N/2+1$. For example if the time series has length $N = 10$, the median is the average of the 5th largest and 6th largest values. Unlike the mean, the median is insensitive to extreme values of the time series. Therefore, raising the highest value of the series by an arbitrary amount will increase the mean, but have no effect on the median

The **variance** is a measure of spread, or variability, of a time series. The variance is the average of the squared departures of a time series from its mean, and is computed as

$$s^2 = \frac{1}{(N-1)}\sum_{i=1}^{N}(x_i - \bar{x})^2 \tag{2}$$

The denominator in the above equation is N-1 rather than N to ensure that the computed variance s an unbiased estimate of the unknown population variance. Large departures from the mean have an amplified effect on the variance because of the squared term. For example, a departure $(x_i - \bar{x}) = 2$ contributes $2^2 = 4$ to the summation, while a departure twice as large, $(x_i - \bar{x}) = 4$, contributes $4^2 = 16$ to the summation.

The **standard deviation** is the square root of the variance, and so is also a measure of the spread of the series:

$$s = \sqrt{s^2} \tag{3}$$

The standard deviation is perhaps more intuitively meaningful than the variance because the standard deviation is in the units of the time series itself, rather than in squared time series units. If the variance is referred to as the mean square departure (from the mean) of the series, the standard deviation is the root mean square departure.

The **skew** is the average of the cubed departures from the mean, scaled by the cubed standard deviation:

$$g = \frac{\frac{1}{N}\sum_{i=1}^{N}(x_i - \bar{x})^3}{s^3} \tag{4}$$

The cubed departure can be positive or negative, following the sign of the departure itself, and is greatly influenced by outliers, due to the raising of the departure to the 3rd power. A time series with higher departure from the mean on the positive side than on the negative side tends to have a positive skew. Precipitation and streamflow time series often have positive skew, because the departures from mean are limited on the negative side (precipitation or streamflow cannot be less than zero), while very large positive values of precipitation or

streamflow are possible. Statistically, skew is related to the "shape" of a distribution, as might be graphed with histogram. A histogram with a tail extended to the right (large positive departure from mean) is a sign of positive skew, and a histogram with a tail extended to the left (large negative departures from mean) is a sign of negative skew.

The **lag-1 autocorrelation** is the correlation of a time series with itself shifted in time by one time unit. For an annual time series (e.g., water year streamflow), the shift is one year. Lag-1 autocorrelation is computed as

$$r_1 = \frac{\sum_{i=1}^{N-1}\left(x_i - \bar{x}\right)\left(x_{i+1} - \bar{x}\right)}{\sum_{i=1}^{N}\left(x_i - \bar{x}\right)^2} \tag{5}$$

For an annual time series, positive lag-1 autocorrelation means that positive departures from the mean in year *t* tend to be followed by positive departures in year *t*+1, and conversely that negative departures from the mean in year *t* tend to be followed by negative departures in year *t*+1. Lag-1 autocorrelation is therefore a measure of persistence in a time series: tendency of same-sign departures from the mean to persist from one year to the next. Persistence is an important statistical property relevant to the duration of droughts and wet periods. In tree-ring reconstruction of streamflow it is important to recognize that the hydrologic system and the biological system of the tree have different sources of persistence, such that tree-ring estimates of drought duration, say, can be distorted. For example, a tree-ring width series may have persistence caused by carryover in food storage within the tree from year to year that is unrelated to year-to-year climate variations.

D2. Testing for Significant Change in Mean and Variance

A **difference of means test** (Wilks 1995) was used to test the null hypothesis that the mean of the population for the instrumental period reconstruction is the same as the mean of the population for the full-length reconstruction. The test statistic is

$$t = \frac{\bar{x}_1 - \bar{x}_2}{\sqrt{\frac{s_1^2}{n_1} + \frac{s_2^2}{n_2}}} \tag{6}$$

where the sample sizes are n_1 for the instrumental period and n_2 for the full-length reconstruction, $\bar{x}_1$ and $\bar{x}_2$ are the corresponding sample means, and s_1 and s_2 are the corresponding standard deviations. The statistic t is tested for significance with a t-distribution with $n_1 + n_2 - 2$ degrees of freedom. Matlab function **ttest2** was used for the test.

A **ratio of variance test** (Benjamin and Cornell 1970) was applied to test the null hypothesis that the variance of the population for the instrumental period reconstruction is the same as the variance of the population for the full-length reconstruction. In other words, the two samples represented by the reconstructed flows for the instrumental period and the long-term tree-ring period are considered to represent two populations, and null hypothesis is that those populations have the same variance. The test statistic is

$$F = \frac{s_1^2}{s_2^2} \tag{7}$$

where s_1 and s_2 are the two sample standard deviations. The statistic is tested with an F-distribution with numerator degrees of freedom $N_1 - 1$ and denominator degrees of freedom $N_2 - 1$, where N_1 and N_2 are the samples sizes of the two data sets. The closer this ratio is to one, the less likely to reject the null hypothesis. Matlab function **vartest2** was used for the test

Caveats. There are a couple of caveats to consider in the evaluation of the tests described here. The tests assume normally distributed populations, which may not be strictly true. The tests also assume that the two samples are independent, which they are not: the small sample for the instrumental period is also part of the longer sample for the full reconstruction. This latter deviation from the assumptions would tend to make it even more difficult to get a significant t or F. On the other hand, positive autocorrelation of the time series would lower the effective of degrees of freedom for the t-test and F-test and lead to over-estimation of the significance of statistics (Wilks 1995).

D3. Reconstruction Method

Reconstructions for this project were generated in a two-stage process of multiple linear regression (Weisberg 1985; Myers 1990, Wilks 1995) followed by locally weighted regression, or "loess" (Cleveland 1979; Martinez and Martinez 2005). The two-stage approach was introduced in a methods paper framed around a tree-ring reconstruction of precipitation Meko (1997), and later modified and extended in reconstructions of streamflow for the Sacramento River (Meko et al. 2001), Colorado River (Meko et al. 2007), and San Joaquin River (Meko et al. 2014). The predictand (y) for a basin is either river discharge (Q) averaged over the water year, or precipitation (P) summed for the water year. The method described below is applied independently to produce each of the sub-period reconstructions defined as Rec1, Rec2, Rec3 and Rec4 in the main text of this report.

In the first stage, single-site reconstruction (SSR), each tree-ring chronology is individually converted to an estimate of y by stepwise regression. The pool of potential predictors includes the standard site tree-ring chronology concurrent and lagged one year earlier and later than y. Squared terms on the predictors are included in the pool to allow for possible nonlinear relationships between tree-ring variables and y. The SSR model for a particular tree-ring chronology is

$$\hat{y}_t = \hat{a}_0 + \sum_{i=-1}^{1} \hat{b}_i x_{t+i} + \sum_{i=-1}^{1} \hat{c}_i x_{t+i}^2 \qquad (8)$$

Where $\hat{a}_0$, $\hat{b}_i$, and $\hat{c}_i$ are estimated regression coefficients, and x_t is the chronology in year t. The equation is estimated on the calibration period defined by the overlap of the tree-ring chronology and y. Although this model has 6 predictors in the predictor pool, some much smaller subset is generally selected in stepwise regression, such that for the simplest possible model all estimated parameters except $\hat{a}_0$ and one parameters on an x or x^2 term are zero. The variables are entered or removed step-by-step according to the significance of a computed F-statistic (Weisberg 1985). Settings of $p_{\text{enter}} = 0.05$ and $p_{\text{remove}} = 0.05$ were used in the stepwise fitting. This first stage of reconstruction is repeated separately each tree-ring chronology that might reasonably be expected to have a physical relationship with P or Q (e.g., because of geographical proximity), such that a large number of SSRs, $\hat{y}_{t,j}, j = 1, n_1$ is produced, one for each of the n_1 tree-ring chronologies. After the long-term tree-ring data is substituted into the regression equations, each of the single-site reconstructions might cover a different span of years, depending on the time coverage of the chronology itself.

In the second stage, multi-site reconstruction (MSR), a reconstructed value $\hat{y}_t$ is estimated for each year by linear interpolation from a smoothed scatter plot of the observed predictand, y_t, against the average $\bar{\hat{y}}_{\{J\}}$ of some subset $n_2 < n_1$ of the SSRs. Here, {J} denotes the subet, chosen following a set of rules described below in the detailed steps for computer programming of the Matlab reconstruction scripts. Some of the more important criteria in culling the $n_2 < n_1$ SSRs to be used are as follows:

- The SSR model explains at least 10% of the variance of y
- The SSR model has positive reduction-of-error statistic (RE) in leave-5-out cross-validation (Meko 1997)
- The SSR model has positive RE for both validation halves in split-sample calibration/validation
- Representation of multiple species is favored (see rules below)

The scatter plot itself is smoothed by loess (Martinez and Martinez 2005), which is piecewise locally weighted regression that does not assume a linear relationship. Controls are imposed on the fitting such that the fitted loess curve must increase monotonically. The fitting procedure itself is guided by a single smoothing parameter, α, described in the programming steps below. Some modifications of the loess procedure described in Martinez and Martinez (2005) are necessary to deal with the specific problem of reconstruction of a hydrologic time series from tree rings. Most important is the extension of the smoothed scatterplot to the right or left to enable interpolation of $\hat{y}_t$ for some reconstruction year in which $\bar{\hat{y}}_{\{J\}}$ might fall outside its range in the calibration period. This is essentially a "no analog" year. The handling of such years is described in the programming steps at the end of this section.

SSR is intended to deal with lags and curvilinear relationships between y and tree-growth at the level of the

individual tree-ring site. Subsequent MSR has the goal of efficiently combining the signal for *y* in the various chronologies, while screening out chronologies with weak or temporally unstable signals for *y*. Overfitting (Wilks 1995) is unlikely to be a problem with combining the SSRs into a MSR because the MSR model requires estimation of just the single smoothing parameter for loess. While the loess reconstruction method does not yield an "R^2-squared for regression", an ad hoc explained variance statistic, $R^2 = 1 - (\mathrm{SSE}/\mathrm{SST})$, was computed as a single metric for comparison of the "typical" accuracy of these reconstruction with that of other published reconstructions. Here SSE is the sum of squares of departures of observed minus reconstructed *y*, and SST is the sum of squares of departures of observed *y* from its calibration period mean. R^2 multiplied by 100 can be interpreted as "percentage of variance explained" by the model.

A 95% confidence interval is assigned to each reconstructed value using the method of upper and lower smooths (Martinez and Martinez 2005): confidence bands are interpolated from separate loess models fit to the positive and negative cross-validation residuals of the MSR. The width of the resulting confidence bands varies with magnitude of reconstructed discharge or precipitation, and reflects, for example, the amplified uncertainty of reconstruction in wet years (Meko and Woodhouse 2011).

The statistical procedure of reconstruction of is expanded here step-by-step, first for SSR and then for MSR.

1 Single-site reconstruction (SSR). SSR is the filtering and scaling of a single tree-ring chronology, *x*, into an estimate of a predictand *y*. The goal is an SSR with desirable statistical properties resembling those of the observed *y*, and with variance proportional to the strength of the relationship between the *x* and *y*. The SSR procedure moreover is intended to screen out chronologies whose signal for *y* is either weak or temporally unstable, to adjust for possible lagged dependence of *y* on *x*, and for possible curvature in the relationship between *x* and *y*.

1.1 Preliminary stepwise regression

1.1.1 Define calibration period as the overlap of *y* and *x*, possibly shortened by 1 year on the recent end to accommodate a +1 year lag in the model. For example, the calibration value of *y* for 2016 might require a tree-ring value *x* in 2017; if the tree-ring records ends in 2016, the calibration period of the model must be truncated to end with 2015.

1.1.2 Regress *y* on *x* and x^2 lagged -1, 0 and +1 years from *y* in stepwise regression. The predictand *y* for regression is log10(*Q*) for reconstruction of river discharge, and *P* (no transformation) for reconstruction of precipitation. The resulting equation has at most has 6 predictors -- original and squared *x* at lags 0, -1 and +1 years from *y*. Predictors are entered stepwise, with *p*-to-enter of 0.05 and *p*-to-remove of 0.10. If no variables enter stepwise, the default model is assumed to be *y* on *x* without lags or squared terms.

1.1.3 Store the order of entry of predictors in the above preliminary stepwise regression

1.2 Cross-validation of preliminary regression

1.2.1 Repeat the stepwise regression above, using the same order of entry of predictors, and cross-validating (Myers 1990; Michaelsen 1987) at each step by leave-5-out cross-validation. Omitting 5 observations instead of 1 observation and predicting for central observation of the omitted segment ensures that none of the same predictor observations are used for the calibration and validation data when a model includes lags up to ±1 year on the predictor time series (Meko 1997).

1.2.2 Compute and store the cross-validation reduction of error statistic (RE; Fritts et al. 1990) at each step

1.2.3 Mark as the stopping step for the final SSR model the last step before RE begins to decline (cross-validation stopping rule; Myers 1990; Wilks 1995)

1.3 Final SSR

1.3.1 Re-calibrate the model for the stopping step defined in step 1.2.3. If no lag +1 term is needed for the model, the calibration period can be extended by 1 year on the recent end.

1.3.2 Store the regression R^2 as a measure of accuracy of the SSR model

1.3.3 Substitute the long-term tree-ring index into the model to generate the single-site reconstruction (SSR). If no lags in the model, this reconstruction extends from last year of the available tree-ring series back to the first year the chronology reaches the EPS threshold of 0.85 (Wigley et al. 1984).

1.3.4 Validate the SSR model using both leave-5-out cross-validation and split-sample validation. For

split sample validation, the full calibration period is split in half, and the model is fit and validated in turn on separate halves (e.g., Meko and Graybill 1995).

1.3.5 Flag the chronology's SSR as unusable in subsequent steps of the reconstruction if any of the following conditions are true:

1.3.5.1 Calibration overall-*F* statistic not significant at p=0.05 (no signal)

1.3.5.2 R^2<0.10 for SSR model

1.3.5.3 Cross-validation RE≤0

1.3.5.4 Split sample RE≤0 for either half of the validation

1.4 Repeat steps1.2-1.3 for each of the n_1 tree-ring chronologies ($n_1 = 9$ for Colorado River, $n_1 = 37$ for other basins)

1.5 Backtransform the n_1 SSRs to the original units of the predictand; this step is necessary only if the predictand for SSR was transformed (e.g., log10 transform for river discharge)

2 Multi-site reconstruction (MSR). MSR is the combining of the SSRs from individual tree-ring chronologies into a single reconstructed time series. The idea is that averaging SSRs over tree-ring sites will emphasize the common signal and de-emphasize local and non-climatic noise. Because the SSRs as defined have variance proportional to strength of their signal for *y*, no differential weighting is needed: an unweighted average emphasizes those tree-ring sites with stronger signal. Broadly, the MSR is interpolated from a smoothed scatterplot of observed *y* on the average of n_2 SSRs, where $n_2 < n_1$. Which of the original n_1 SSRs are included among the n_2 SSRs for a particular basin and nested model? This depends on several factors. Obviously, to be considered a candidate for a particular nested model (e.g., Rec1) an SSR must completely cover the specified time period for the model. To qualify as a candidate, we also require the SSR have a regression $R^2 > 0.10$, which, for the lengths of calibration period used here, is a stricter requirement than just a significant $(p < 0.05)$ overall-F of regression. Other requirements are that the SSR must a positive RE of cross-validation and a positive RE in both halves of its split-sample validation. These constraints rule out many of the original n_1 SSRs. Remaining SSRs make up the pool of SSRs from which the n_2 SSRs for use in MSR are selected. MSR models are built chronologically (Rec1, Rec2, …) by the steps described in detail below.

2.1 Identify the SSRs for the Rec1 reconstruction model (earliest nested model)

2.1.1 Identify qualified (see above) SSRs covering the common interval, and consider just those SSRs

2.1.2 Identify how many different species are represented in that set of SSRs

2.1.3 For each species represented, include the 3 SSRs with strongest signal as measured by R^2 of the SSR model (see 1.3.2). If fewer than 3 SSRs available, include all of them.

2.1.3.1 Aim is to favor representation from multiple species, and to use those chronologies with the strongest bivariate signal for the predictand *y*

2.1.3.2 Will end up with some subset of n_2 SSRs, where $n_2 < n_1$

2.1.4 Compute the time series of reconstructed predictand averaged over the selected n_2 SSRs; call this average *v*

2.2 Plot the observed predictand, *y,* against *v* in a scatterplot

2.3 Fit a loess model to the scatterplot

2.3.1 Make loess estimates of *y* at 6 points along the abscissa of the scatterplot: minimum, maximum and percentiles 20 40 60 and 80 of *v*.

2.3.2 Begin with a loess smoothing parameter, α=0.6

2.3.3 Fit the loess model. Check that the resulting loess curve is monotonic increasing; if not, increase α by 0.1 (less flexible curve), and check again; repeat until monotonic increasing curve is attained. The resulting is a final value of smoothing parameter, α.

2.4 Validate the loess model

2.4.1 Cross-validate, leaving out 5 observations at each iteration and predicting *y* for the middle year of the omitted segment

2.4.2 Split-sample validate, exchanging the first and last halves of the overlap of *v* and *y*

2.4.3 Check that the final loess model has positive RE of cross-validation and positive RE of split-

sample validation on both halves (temporal stability)

2.5 Extend the loess curve to cover the full range of *v* over the full nested period (not just calibration years)

2.5.1 Identify extreme high and low values in the time series of *v* of SSRs averaged over n_2 tree-ring sites. Usually these extremes lie outside the range of *v* in the calibration period of the fitted loess curve

2.5.2 Extend the loess curve to the left and right on the scatterplot cover the identified high and low extremes of *v*. The loess curve before extension is monotonic increasing and piecewise linear, with segments joining the minimum, 20th, 40th, 60th, 80th percentiles and maximum of v for the calibration period. Call the segments joining these 6 points segment 1-5. Two new straight-line segments (segment 0 on the left and segment 6 on the right) will be added.

2.5.2.1 On the right side, set the slope of segment 6 such that the change in slope from segment 5 to 6 is the same as the change in slope from segment 4 to 5

2.5.2.2 On the left side, set the slope of segment 0 such that the change in slope from segment 0 to segment 1 is the same as the change in slope from segment 1 to segment 2.

2.6 Interpolate the multi-site reconstruction (MSR) from the extended loess curve

For each year of the current nest, or set of tree-ring chronologies with common time coverage, linearly interpolate a reconstructed value of *y* from the extended loess plot of observed *y* against *v*

2.7 Estimate error bars for the MSR (50% confidence band around annual reconstructed *y*)

The method of "upper and lower smooths" (Martinez and Martinez 2005) was used to estimate a 50% confidence band for reconstructed *y*. This method is specifically applicable where, as here, the reconstructed values are estimated from a smoothed scatterplot and the error variance is a function of the size of reconstructed *y*.

2.7.1 Scatterplot the positive cross-validation residuals against the fitted values, or estimated *y*

2.7.2 Fit a piecewise-linear loess model to the scatterplot

2.7.3 Smoothing parameter $\alpha = 0.95$. Use this same setting for all basins and nested models. This setting was selected from exploratory analysis, and is not claimed to be optimal in a statistical sense

2.7.4 Set estimation points at the minimum, maximum, and percentiles 20, 40, 60, and 80 of calibration-period predicted *y*

2.7.5 Extend the loess curve by adding leading and trailing straight-line segments connecting to the lowest (left) and highest (right) reconstructed *y* in the full-length reconstruction. Unlike the extension used for the loess models of the reconstruction itself (see 2.5), the extension is set to horizontal. Thus the confidence interval for extremely low or high reconstructed *y* is assumed to stay at the same width as for the extremes in reconstructed *y* for the calibration period.

2.7.6 Repeat steps 2.7.1-2.7.5 for the negative cross-validation residuals

2.7.7 Linearly interpolate from the 2 smoothed scatterplots (upper and lower smooths) to get estimated upper and lower 50% confidence bands for each year of reconstructed *y*

2.8 Repeat steps 2.1-2.7 for nested models Rec2, Rec3, and Rec4

2.8.1 Each nested model has a specified time coverage (e.g., 1405-2015)

2.8.2 More sites, and SSRs, become available in Rec2 and Rec3; site density declines for Rec4

2.8.3 If an SSR is used in an earlier nested model and that SSR covers the current nested period, include the SSR in the current model. This approach favors continuity in the mix of tree-ring predictors from one period to the next.

2.8.4 The rule of using the 3 "best" SSRs (highest R^2) for each available species is followed at each nest. Any SSRs retained from an earlier model do not count toward this 3. It is therefore possible for an MSR model for Rec2, Rec3 or Rec4 to be represented by more than 3 chronologies of the same species

D4. Spectral Analysis

Spectra are estimated by the smoothed-periodogram method (Bloomfield 2000). Preliminary steps include the following: 1) subtract the mean from the time series, 2) taper the series (5% of each end), and 3) pad the tapered series with zeros to such that its length is a power of two, 3) compute the discrete Fourier Transform, and raw periodogram of the padded tapered time series, and 4) smoothed with convoluted spans of Daniell filters to achieve spectral estimates with the desired bandwidth. The mathematical and statistical operations in these methods are described in Bloomfield (2000).

In testing spectral peaks for significance, it is necessary to specify a "null continuum", which is a baseline spectrum. For a spectral peak to be deemed "significant", the spectrum at that frequency must be significantly greater than the baseline. Depending on the lag-1, or first-order, autocorrelation of the time series, the null continuum for testing significance in this study is set to either white noise or red noise. White noise has variance distributed evenly across frequencies, while red noise has variance distributed preferentially toward low frequencies (spectrum slopes upward to left). If the computed lag 1 autocorrelation of the time series is zero or negative, white noise is used for the null continuum. If the lag-1 autocorrelation is positive, red noise is used for the null continuum.

The bandwidth describes the range of frequencies in the raw periodogram contributing to a spectral estimate a particular frequency. The bandwidth depends on the spans of the individual Daniell filters convoluted to produce the resultant filter applied to smooth the raw periodogram. In this study, a 41-weight resultant filter with a bandwidth of about 0.18 frequency units is used to smooth the raw periodogram for spectral analysis of full-length reconstructions. This filter was arrived at by convolution of five 9-weight Daniell filters. A 13-weight resultant filter with a bandwidth of 0.06 frequency units is used to smooth the raw periodogram for spectral analysis of the observed and reconstructed series for the instrumental period. This filter was arrived at by convolution of three 5-weight Daniell filters.

Red noise theoretical spectra, for null continua, are computed by equations in Wilks (1995). White noise spectra are drawn as horizontal lines such that the total area under the white-noise spectrum corresponds to the variance of the time series itself and equals the area under the spectrum of the time series. Confidence intervals for estimated spectra are computed using a χ^2 distribution with appropriate number of degrees of freedom, adjusted for such factors as padding and trimming of the time series and smoothing by Daniell filters (Bloomfield 2000, p. 184).

D5. Wavelet Analysis

Wavelet and cross-wavelet analyses were done with the aid of the Matlab-based wavelet package developed by Grinsted et al. (2004) and made available for download by the National Oceanography Centre (http://noc.ac.uk/using-science/crosswavelet-wavelet-coherence). Matlab scripts that call the Grinsted et al. (2004) functions and add interpretive graphics were written to produce plots for this report. The primary wavelet graphic used is the continuous wavelet transform (CWT) which display spectral power of a time series as a function of wavelength and time. The primary cross-wavelet graphic used is the wavelet transform coherency (WTC), which plots coherency (similar to correlation) and phase of two time series as a function of wavelength and time. Both the CWT and the WTC allow assessment of significance (α=0.05), and for this use a red-noise background. In other words, the significance is determined relative to a red-null hypothesis for the time series.

As wavelet and cross-wavelet analysis assume normality, our Matlab implementation of the cross-wavelet tool has additional functionality that allows square-root or log-10 transformation of the time series prior to wavelet analysis. The user is able to view histograms of the time series before and after alternative transformation, and to choose transformation of one or both (if cross-wavelet) series before calling the Grinsted et al. (2004) functions.

Wavelet and cross-wavelet plots are augmented by smoothed time series plots designed to emphasize variations at decadal-and-longer wavelengths. The smoothing filter for these plots is a 9-weight Gaussian filter (Mitchell et al. 1966) with a frequency response of 0.50 at a wavelength of about 10 years. The weights for the filter used for all smoothed time series plots in Section 3.3 (Cycles and Quasi-Periodic Behavor) are as follows:

1. 0.027630898004301
2. 0.066282614593644
3. 0.123831607604267
4. 0.180173385402692
5. 0.204162988790191
6. 0.180173385402692
7. 0.123831607604267
8. 0.066282614593644
9. 0.027630898004301

REFERENCES

Benjamin, J. R. and C. A. Cornell (1970), *Probability, Statistics and Decisions for Civil Engineers*, McGraw-Hill Book Company, New York, 704 p.

Bloomfield, P. (2000), *Fourier Analysis of Time Series: An Introduction*, second ed., John Wiley & Sons, New York, 261 pp.

Cleveland, W. S. (1979), Robust locally weighted regression and smoothing scatterplots, *J. Am. Stat. Assoc*., 74, 829–836.

Cook and Kairiukstis (1990), *Methods in Dendrochronology: Applications in the Environmental Sciences*, Kluwer Academic Publishers, Dordrecht, 394 p.

Fritts, H. C., J. Guiot, and G. A. Gordon (1990), Verification, in Cook and Kairiukstis [1990], pp. 178–185, 394 pp.

Grinsted, A., J. C. Moore, and S. Jevrejeva (2004), Application of the cross wavelet transform and wavelet coherence to geophysical time series, *Nonlinear Proc. Geoph*., 11, 561–566.

Haan, C. T. (2002), *Statistical Methods in Hydrology*, second ed., Iowa State University Press, 496 pp.

Martinez, W. L., and A. R. Martinez (2005), *Exploratory Data Analysis with MATLAB*, Chapman & Hall/CRC, New York, 405 pp.

Meko, D. (1997), Dendroclimatic reconstruction with time varying predictor subsets of tree indices, *J. Climate*, 10 (4), 687–696.

Meko, D., and D. A. Graybill (1995), Tree-ring reconstruction of Upper Gila River discharge, *J. Am. Water Resour. Assoc.*, 31 (4), 605–616.

Meko, D. M., M. D. Therrell, C. H. Baisan, and M. K. Hughes, 2001: Sacramento River flow reconstructed to A.D. 869 from tree rings. *Journal of the American Water Resources Association*, 37 (4), 1029–1039.

Meko, D.M., C.A. Woodhouse, C.H. Baisan, T. Knight, J.J. Lukas, M.K. Hughes, and M.W. Salzer, 2007. Medieval drought in the upper Colorado River basin. *Geophysical Research Letters* 34m L10705, doi: 10.1029/2007GL029988.

Meko, D. M., and C. A. Woodhouse (2011), Dendroclimatology, dendrohydrology, and water resources management, In: *Tree Rings and Climate: Progress and Prospects* (eds. M.K. Hughes, T.W. Swetnam, H.F. Diaz). Springer, pp. 231-261.

Meko, D. M., C.A. Woodhouse, and R. Touchan (2014), *Klamath/San Joaquin/Sacramento Hydroclimatic Reconstructions from Tree Rings*. Final Report to California Department of Water Resources, Agreement 4600008850. 72 pp.

Myers, R. H. (1990), Classical and Modern Regression with Applications, Doxbury, Pacific Grove, California, 488 pp.

Michaelsen, J. (1987), Cross-validation in statistical climate forecast models, *J. Clim. Appl. Meteor.*, 26, 1589–

1600.

Mitchell, J. M., Jr, B. Dzerdzeevskii, H. Flohn, W. L. Hofmeyr, H. H. Lamb, K. N. Rao, and C. C. Walleen (1966), *Climatic change, technical note no. 79*, Report of a working group of the Commission for Climatology No. 195 TP 100, WMO, Geneva, Switzerland, 81 pp.

Panofsky, H. A., and G. W. Brier (1968), *Some Applications of Statistics to Meteorology*, The Pennsylvania State University, University Park, Pennsylvania, 224 pp.

Salas, J. D., J. W. Delleur, V. Yevjevich, and W. L. Lane, 1980. *Applied modeling of hydrologic time serie*s. Water Resources Publications, P. O. Box 3841, Littleton, Colorado, 80161, USA, 484 pp.

Torrence, C., and G. P. Compo (1998), A practical guide to wavelet analysis, *Bull. Amer. Meteorol. So*c., 79, 61–78.

Weisberg, S. (1985), *Applied Linear Regression*, 2nd ed., John Wiley, New York, 324 pp.

Wigley, T. M. L., K. R. Briffa, and P. D. Jones (1984), On the average value of correlated time series, with applications in dendroclimatology and hydrometeorology, *J. Clim. Appl. Meteor.*, 23, 201–213.

Wilks, D. S. (1995), *Statistical Methods in the Atmospheric Sciences*, International Geophysics Series, vol. 59, Academic Press, San Diego, 467 pp.

Appendix E

Time series plots for all Socal gages, the San Joaquin River Index, Sacramento River Index and Klamath River. Each plot includes observed vs. reconstructed period, followed by the most skillful and longest reconstructions.

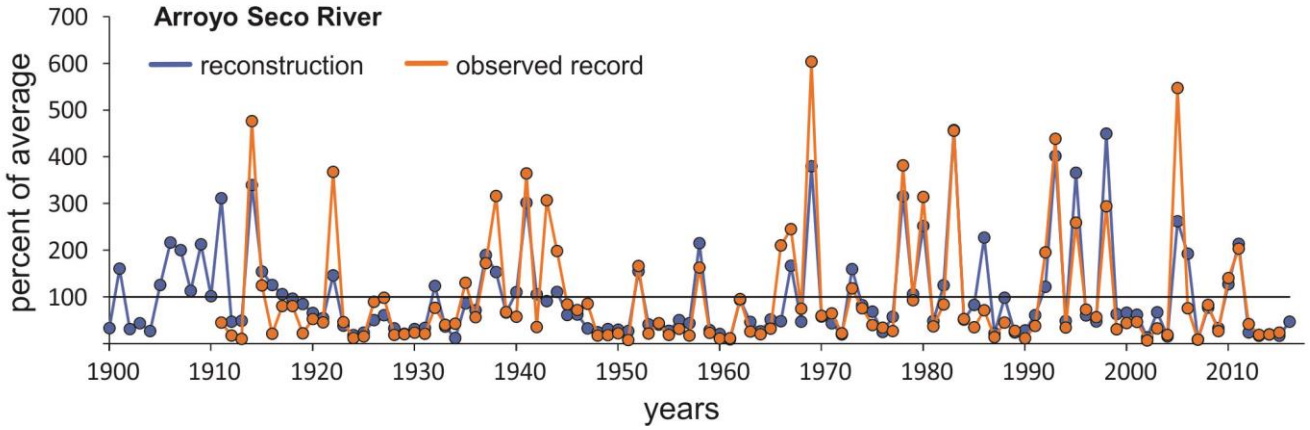

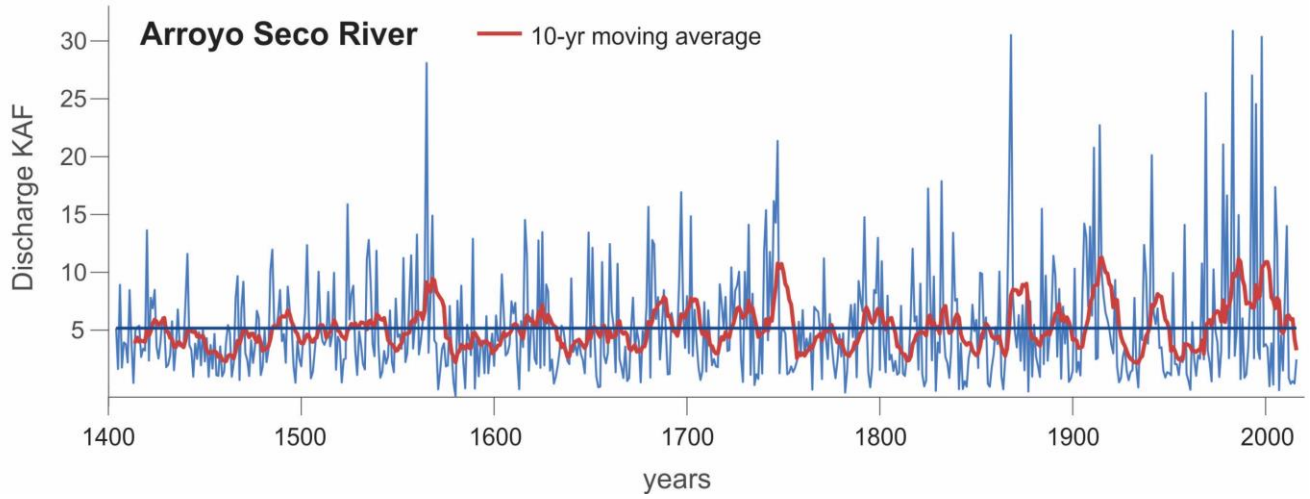

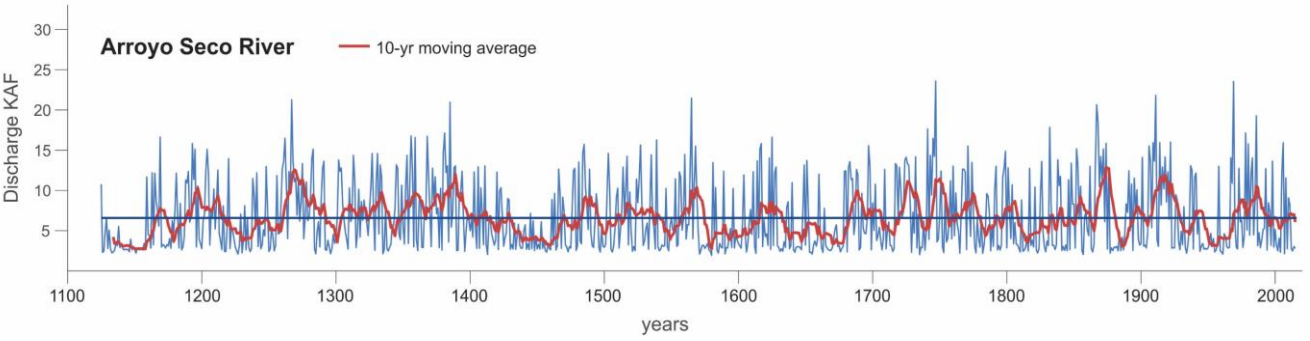

Figure 1. Top Panel: Time plots of observed and reconstructed flow for the **Arroyo Seco River**. Flow is expressed as percent of instrumental mean (inches). Calibration period of reconstructed and observed flow is the 1911-2015. **Middle Panel:** Annual values of most skillful reconstruction with 10-yr moving average (1404 – 2016). **Bottom panel:** Annual values of longest reconstruction with 10-yr moving average (1125 – 2015).

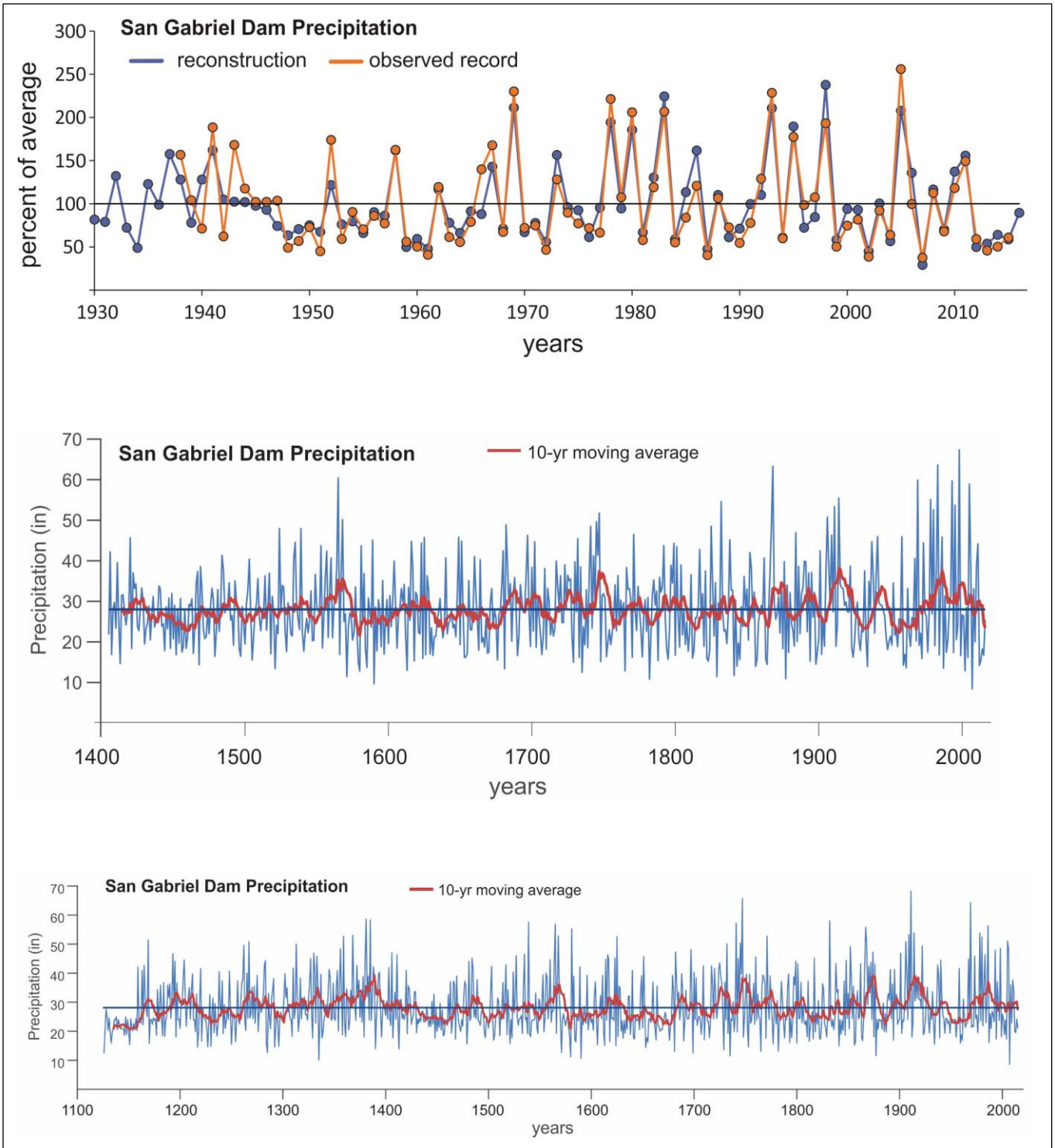

Figure 2. Top Panel: Time plots of observed and reconstructed precipitation for the **San Gabriel Dam**. Precipitation is expressed as percent of instrumental mean (inches). The calibration period for the reconstructed and observed precipitation is the 1938-2015 calibration. **Middle panel:** Annual values of most skillful reconstruction for the San Gabriel Dam with 10-yr moving average (1405 – 2016). **Bottom panel:** Annual values of the longest reconstruction for the San Gabriel Dam with 10-yr moving average (1126 – 2015).

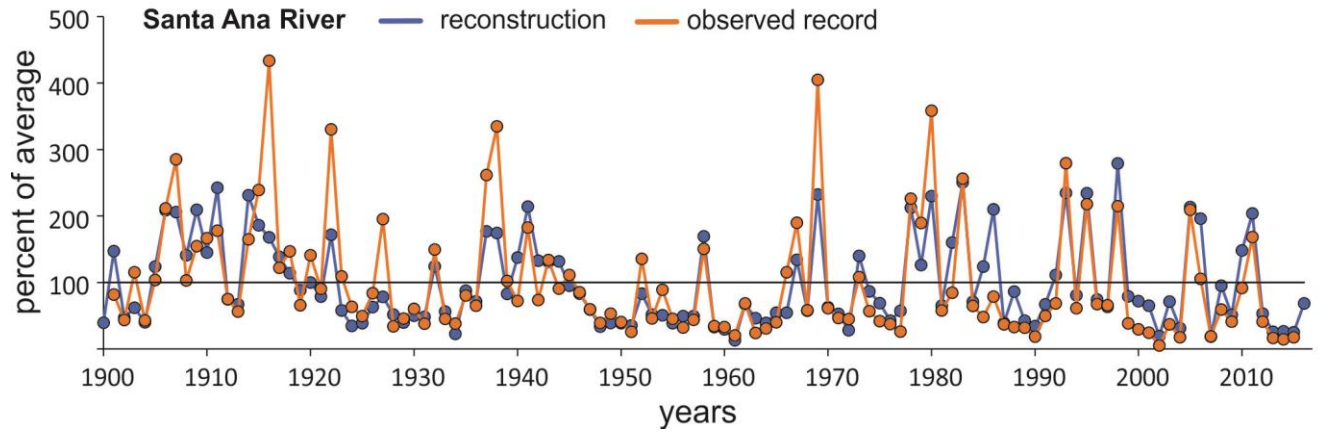

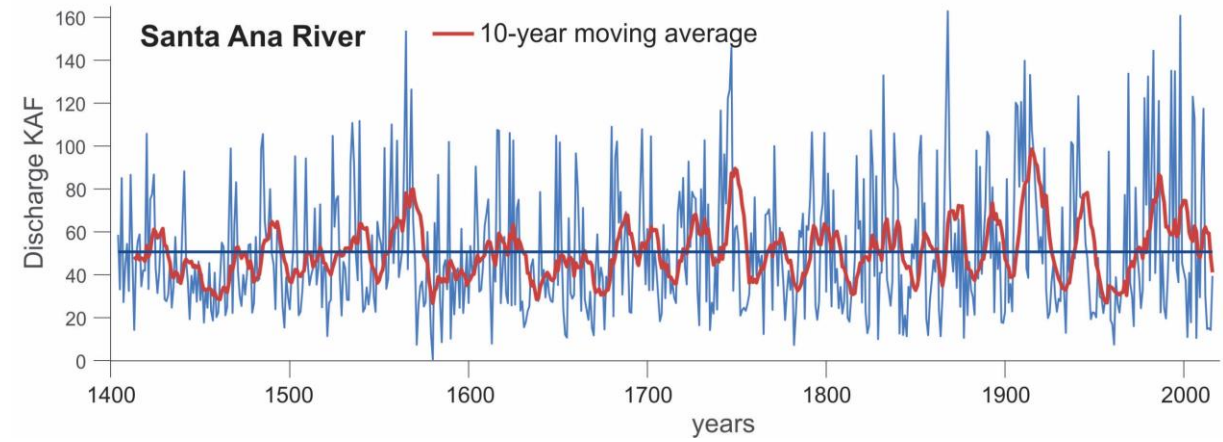

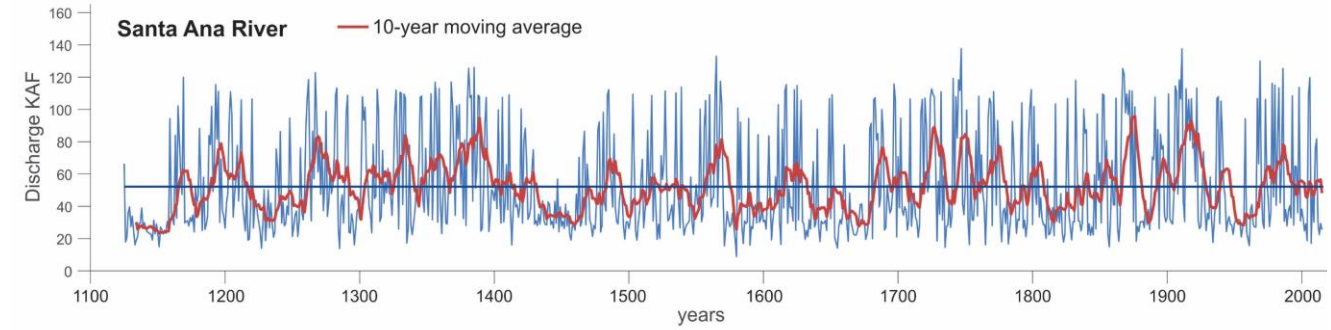

Figure 3. Top Panel: Time plots of observed and reconstructed flow for the **Santa Ana River**. Flow is expressed as percent of instrumental mean (KAF). Calibration period for the reconstructed and observed flow is the 1901 – 2015.

Middle panel: Annual values of most skillful reconstruction with 10-yr moving average (1404 - 2016).
Bottom panel: Annual values of the longest reconstruction with 10-yr moving average (1125 – 2015).

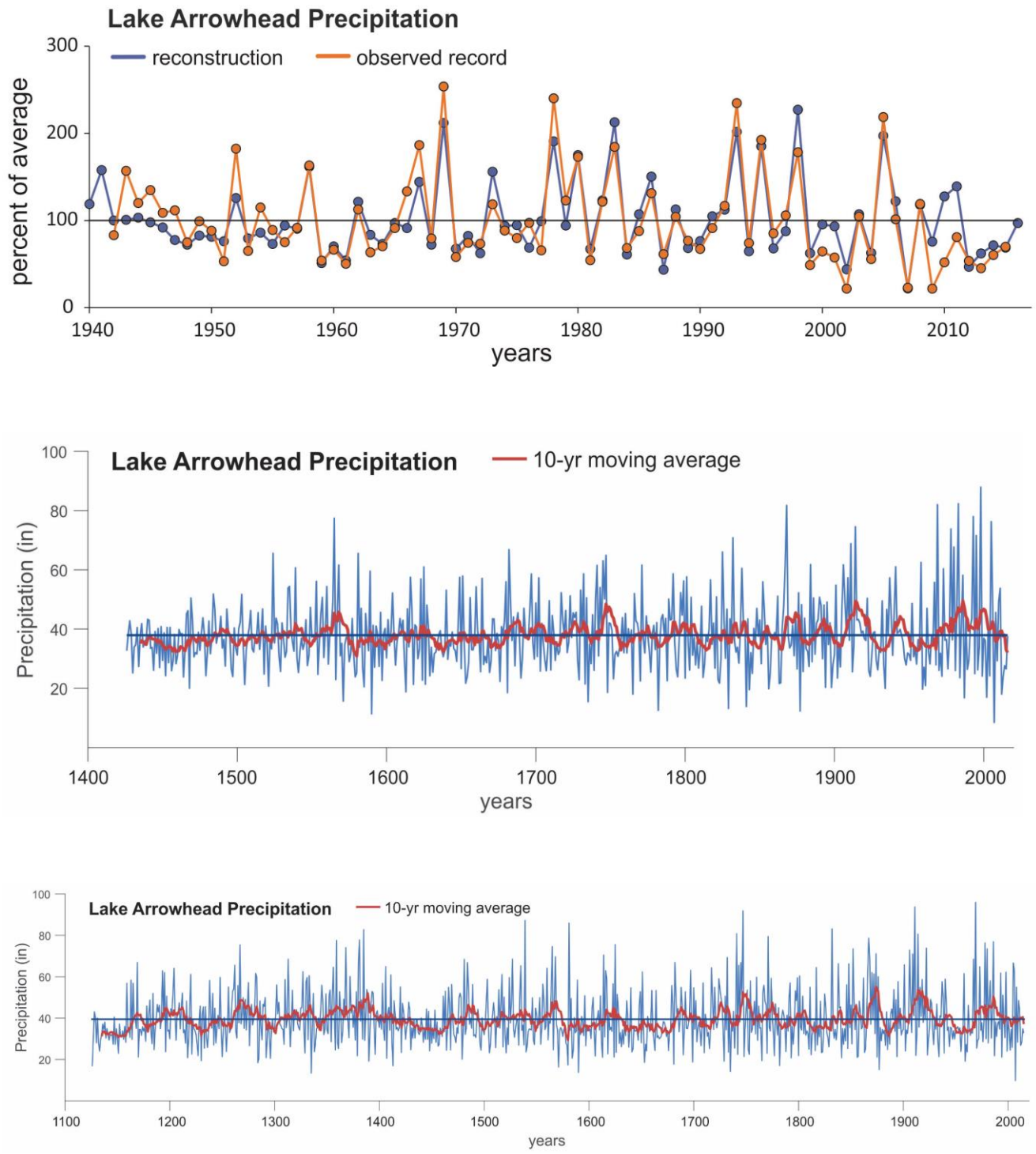

Figure 3. Top Panel: Time plots of observed and reconstructed precipitation for **Lake Arrowhead**. Precipitation is expressed as percent of instrumental mean. Calibration period of reconstructed and observed precipitation is the 1942 – 2015.

Middle panel: Annual values of most skillful reconstruction with 10-yr moving average (1426 – 2016).
Bottom panel: Annual values of the longest reconstruction with 10-yr moving average (1126 – 2015).

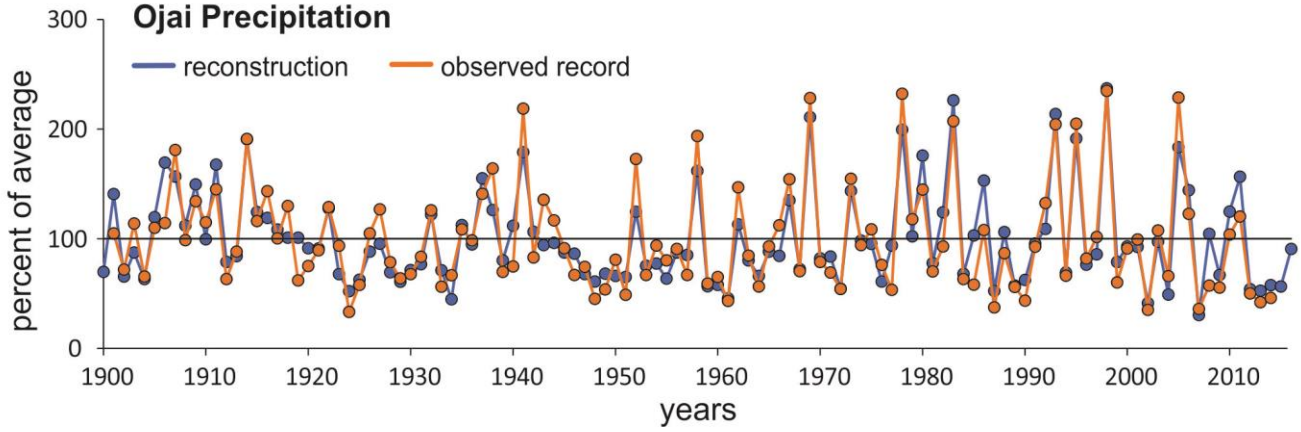

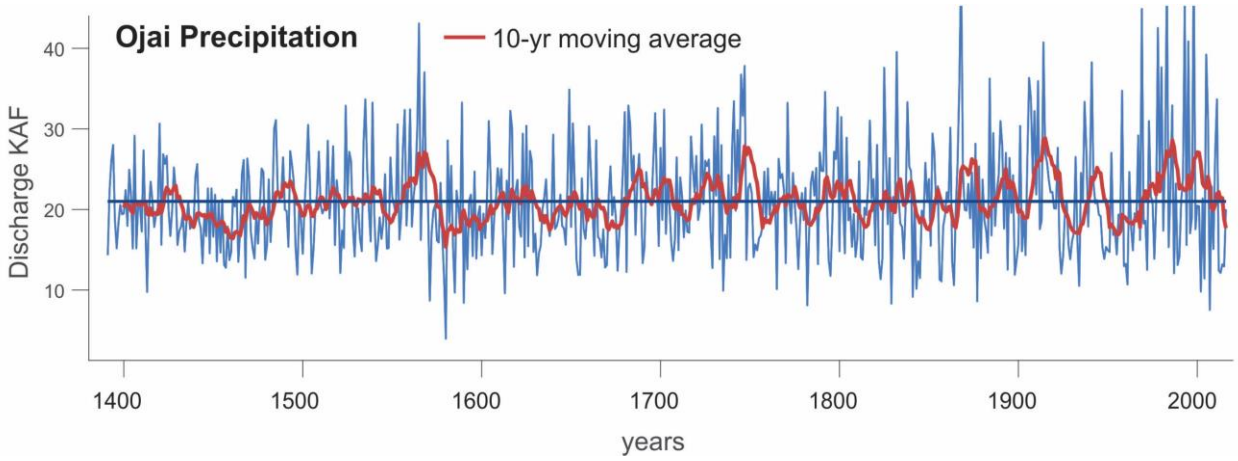

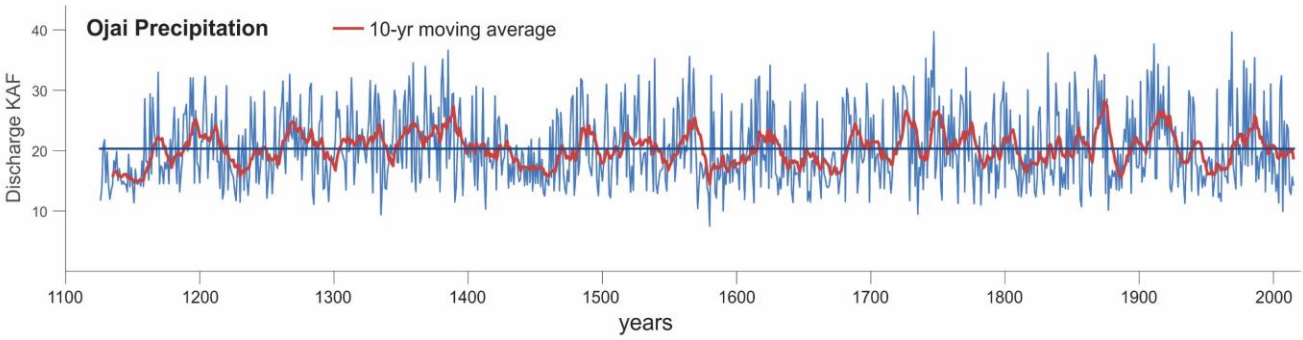

Figure 5. Top Panel: Time plots of observed and reconstructed precipitation for **Ojai**. Precipitation is expressed as percent of instrumental mean. Calibration period of reconstructed and observed precipitation is the 1391 - 2015.

Middle panel: Annual values of most skillful reconstruction with 10-yr moving average (1391 – 2016).
Bottom panel: Annual values of the longest reconstruction with 10-yr moving average (1126 – 2015).

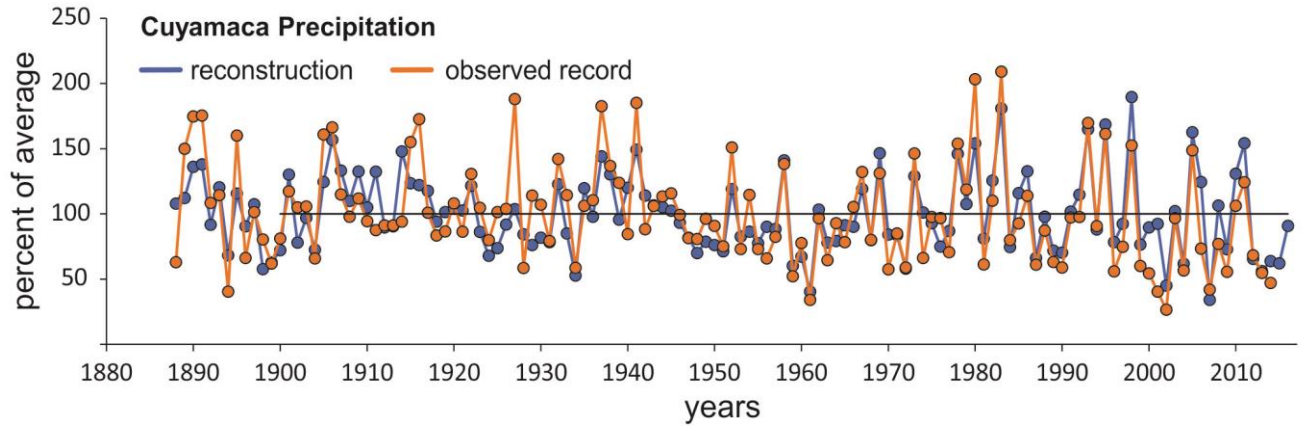

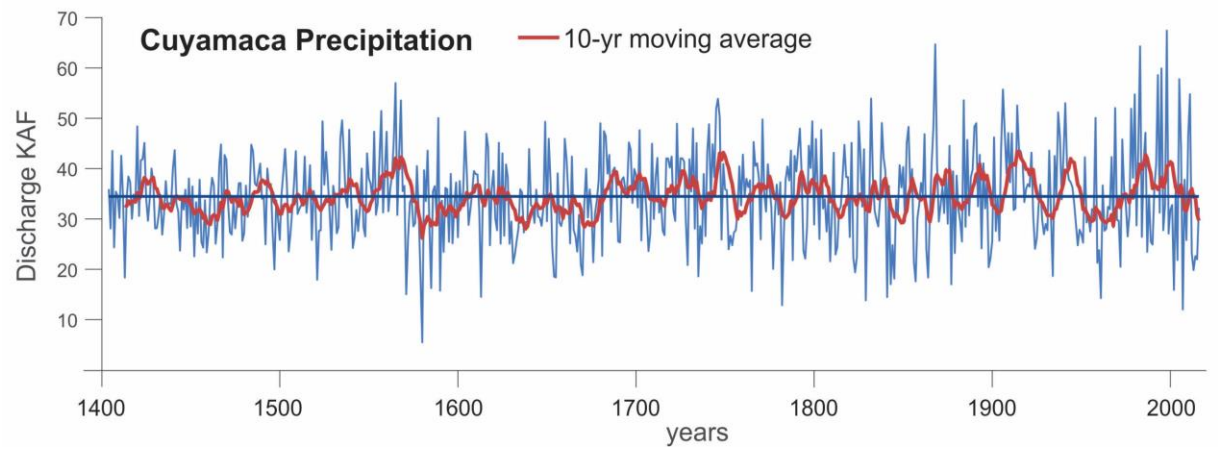

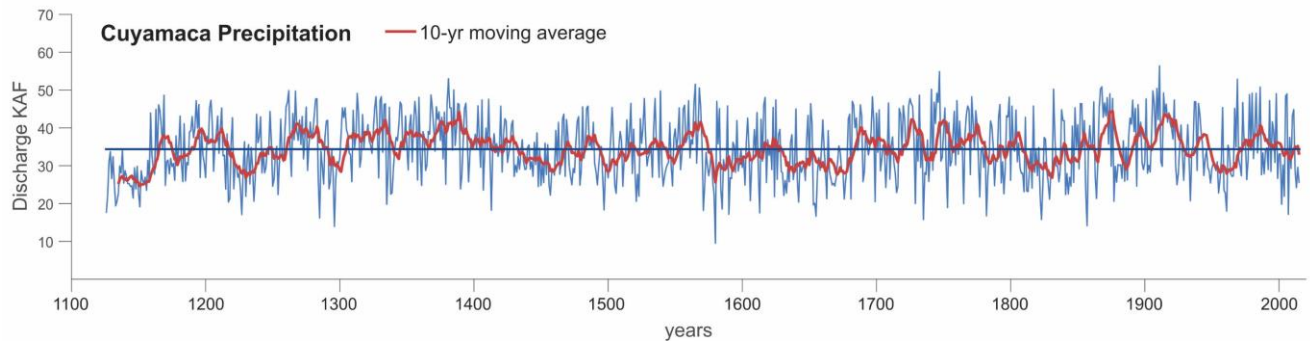

Figure 6. Top Panel: Time plots of observed and reconstructed precipitation for **Cuyamaca**. Precipitation is expressed as percent of instrumental mean. Calibration period of reconstructed and observed precipitation is the 1888-2015.

Middle panel: Annual values of most skillful reconstruction with 10-yr moving average (1404 – 2016).
Bottom panel: Annual values of the longest reconstruction with 10-yr moving average (1126 – 2015).

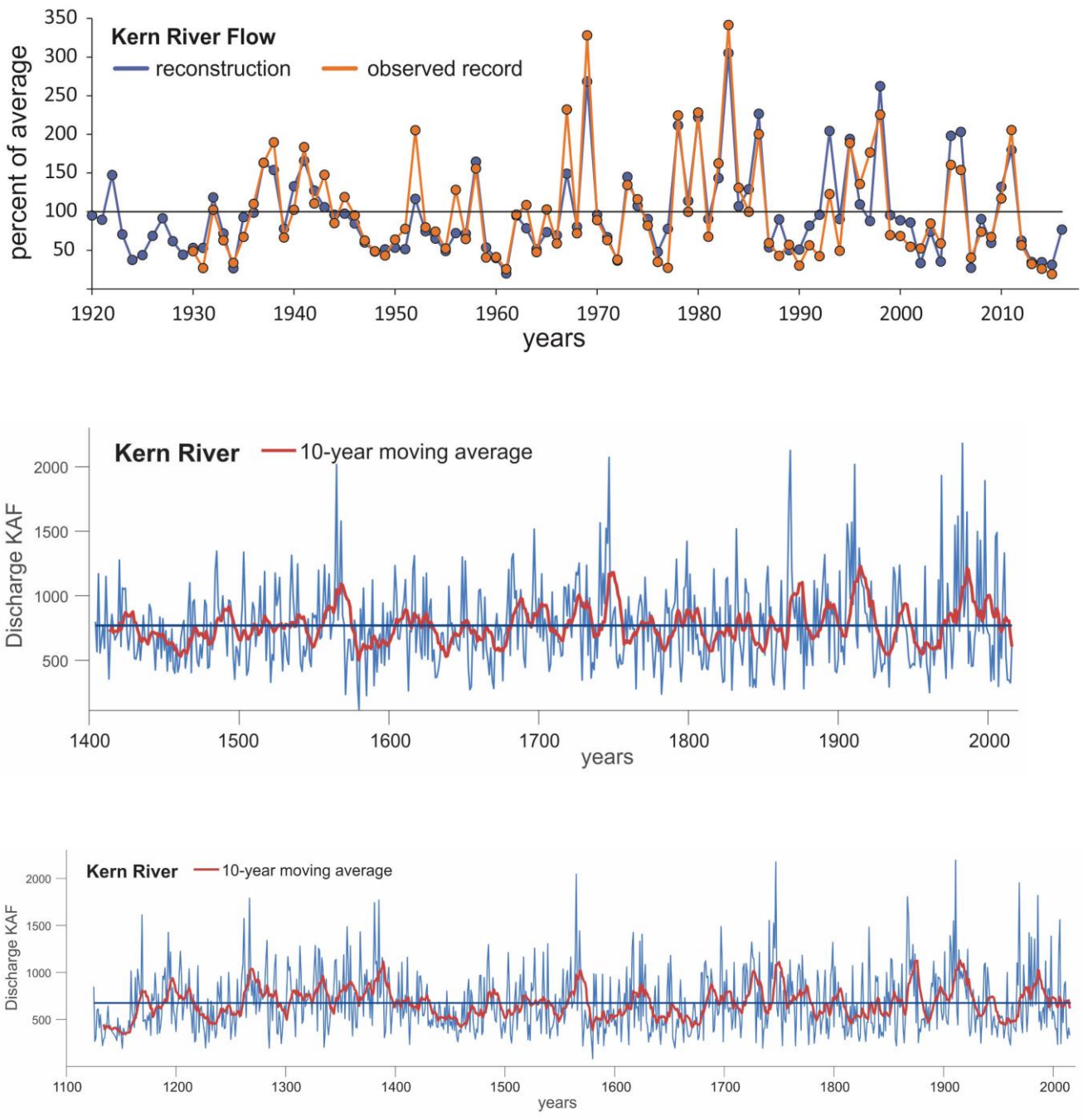

Figure 7. Top Panel: Time plots of observed and reconstructed flow, **Kern River**. Flow is expressed as percent of instrumental mean (KAF). Calibration period of reconstructed and observed precipitation is the 1930-2015.

Middle panel: Annual values of most skillful reconstruction with 10-yr moving average (1404 – 2016).
Bottom panel: Annual values of the longest reconstruction with 10-yr moving average (1125 – 2015).

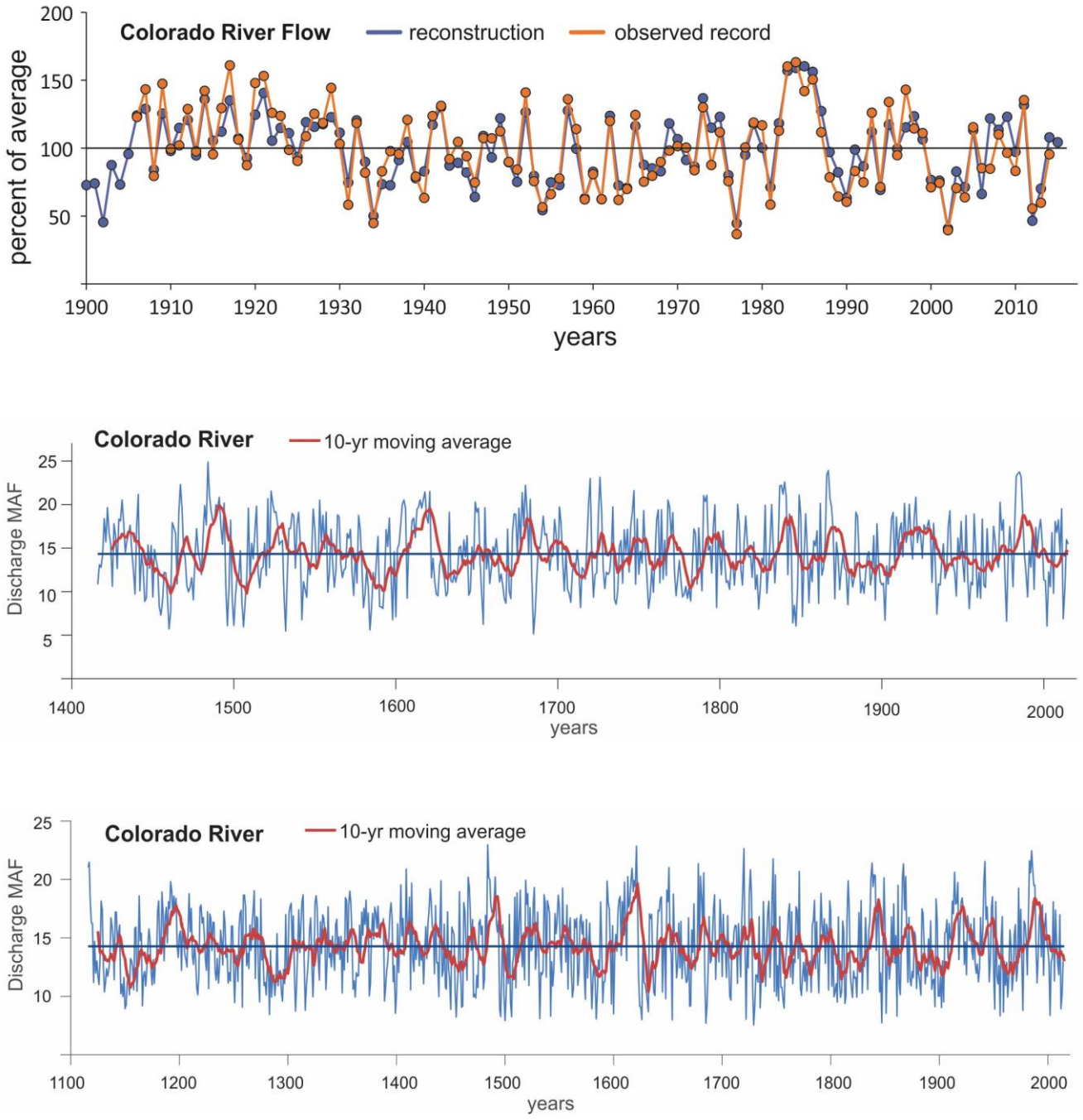

Figure 8. Top Panel: Time plots of observed and reconstructed flow, **Colorado River**. Flow is expressed as percent of instrumental mean (MAF). Overlap period of reconstructed and observed precipitation is the 1906-2014 calibration period of the reconstruction model.

Middle panel: Annual values of most skillful reconstruction with 10-yr moving average (1416 – 2015).
Bottom panel: Annual values of the longest reconstruction with 10-yr moving average (1116 – 2014).

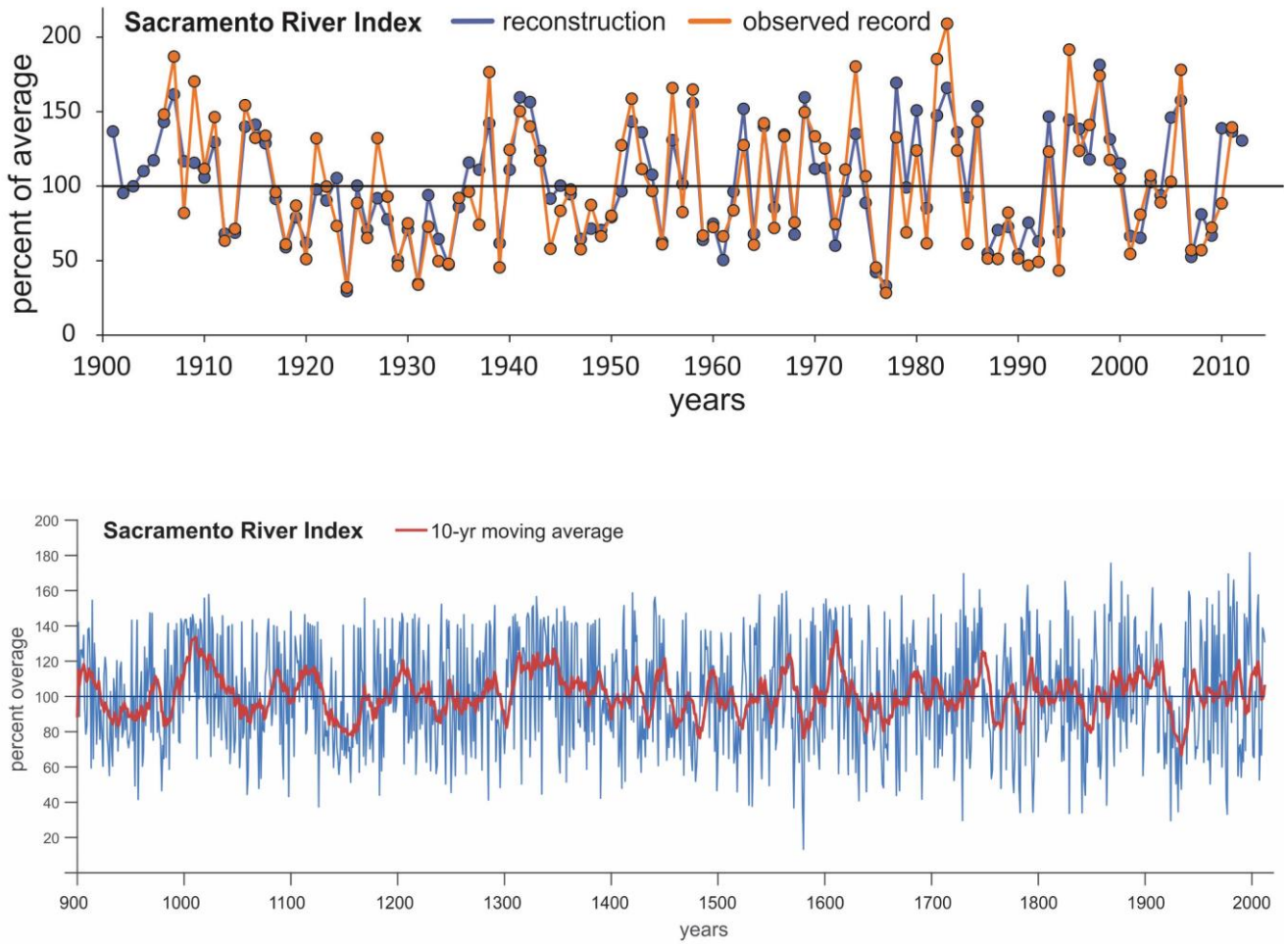

Figure 9. Top Panel: Time plots of observed and reconstructed flow for the **Sacramento River Index**. Flow is expressed as percent of instrumental mean (MAF). Calibration period for the reconstructed and observed precipitation is the 1906-2011.

Bottom panel: The reconstruction with 10-yr moving average (900 – 2012).

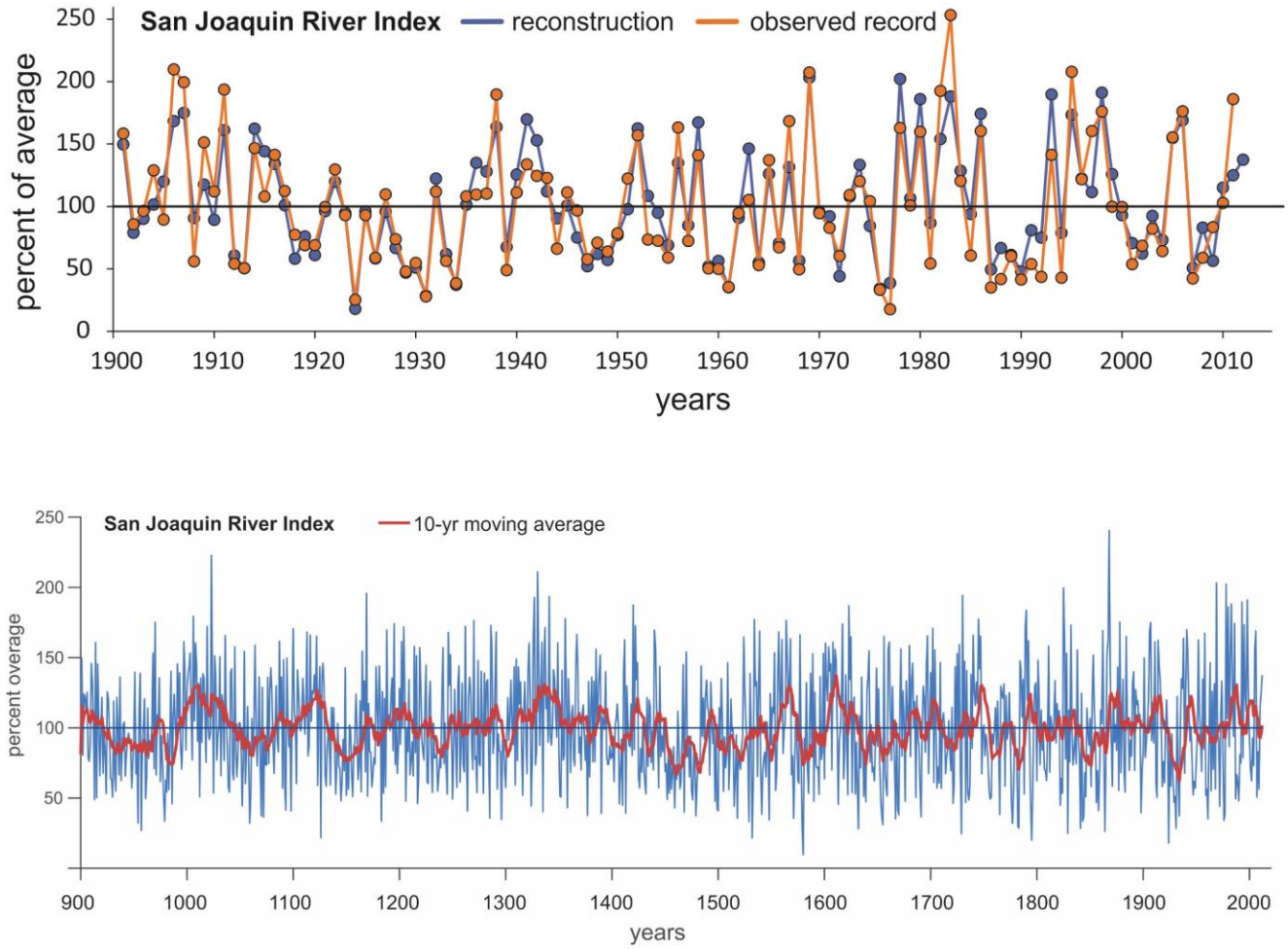

Figure 10. Top Panel: Time plots of observed and reconstructed flow for the **San Joaquin River Index**. Flow is expressed as percent of instrumental mean (MAF). Calibration period for the reconstructed and observed flow is 1901-2011.

Bottom panel: The reconstruction with 10-yr moving average (900 – 2012).

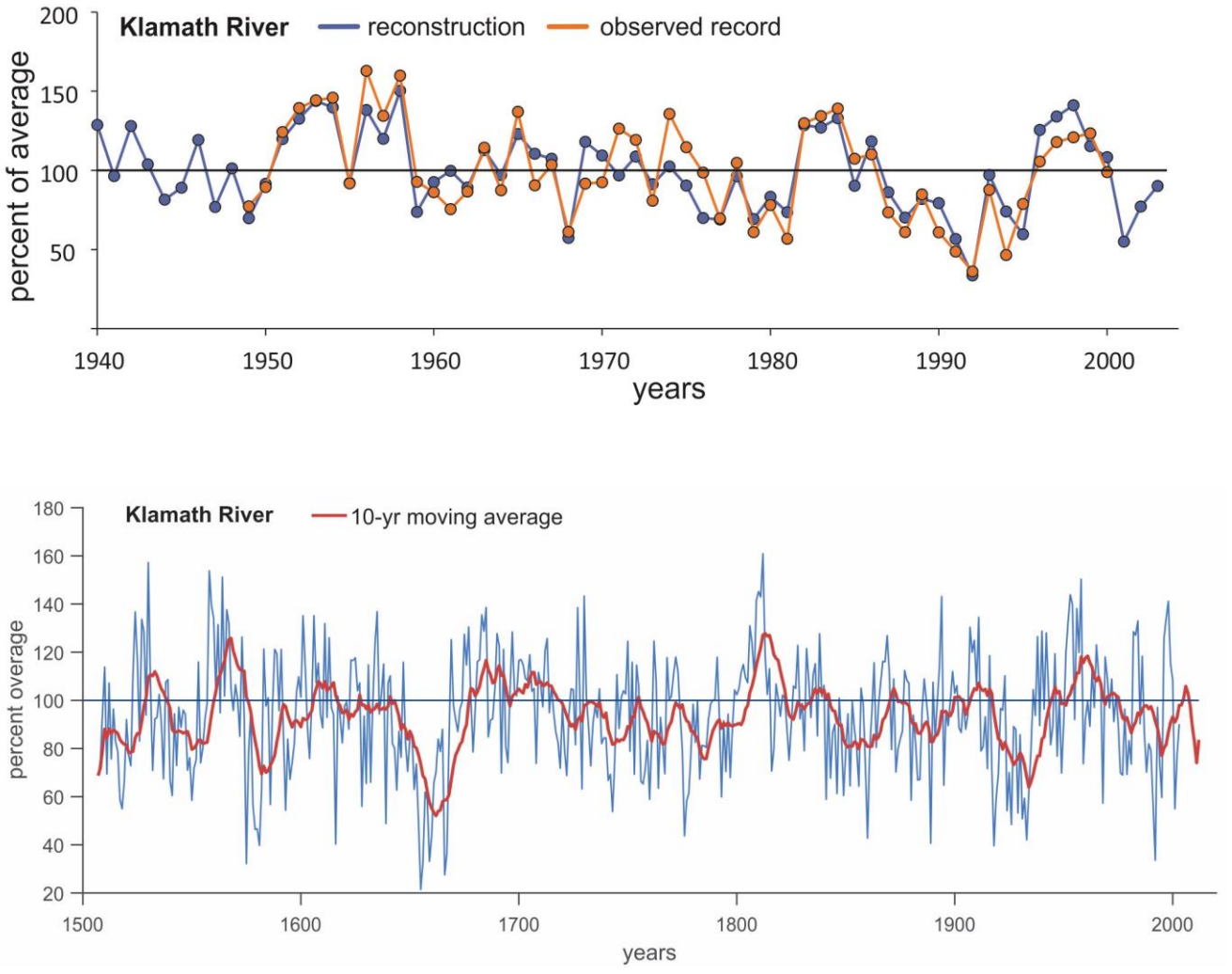

Figure 11. Top Panel: Time plots of observed and reconstructed flow for the **Klamath River**. Flow is expressed as percent of instrumental mean (MAF). Calibration period for the reconstructed and observed flow is 1949 - 2000.

Bottom panel: The reconstruction with 10-yr moving average (1507 - 2003).

Appendix F: Plots of Average drought intensity by duration in years

All California gages and reconstructions

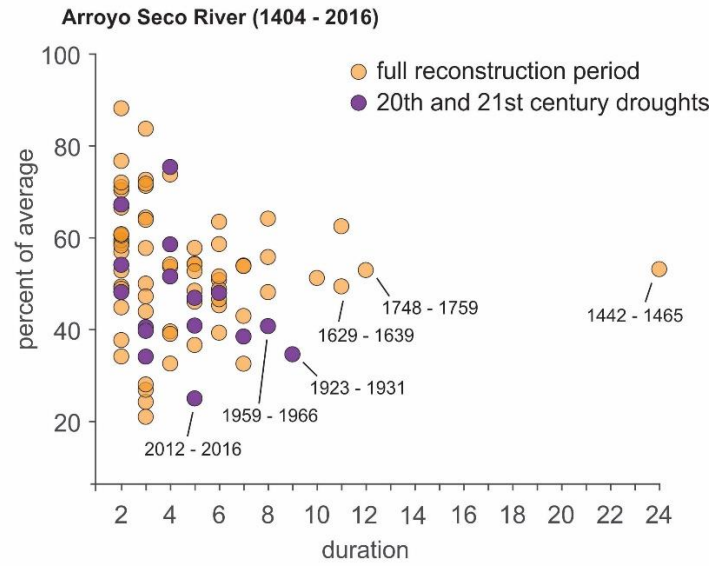

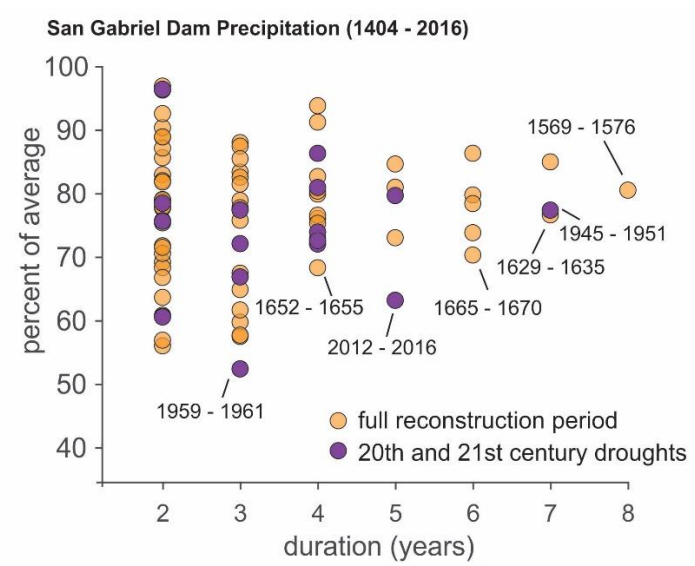

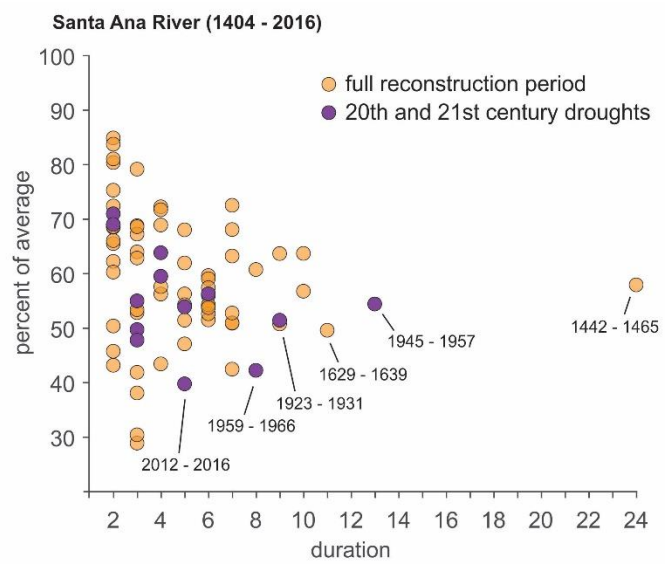

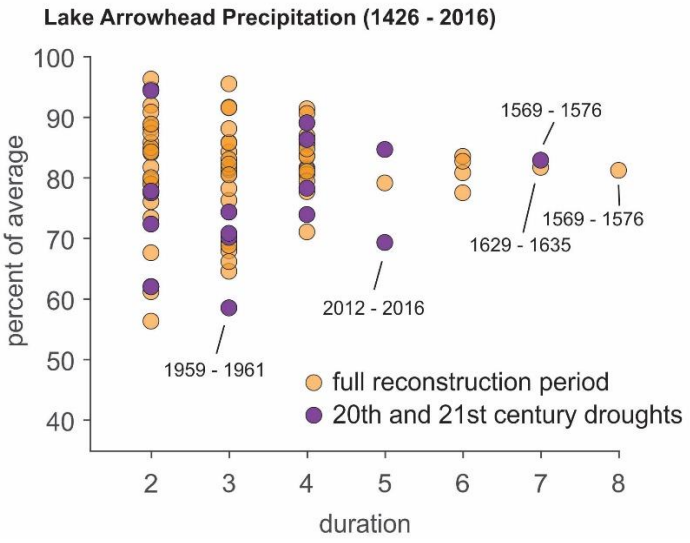

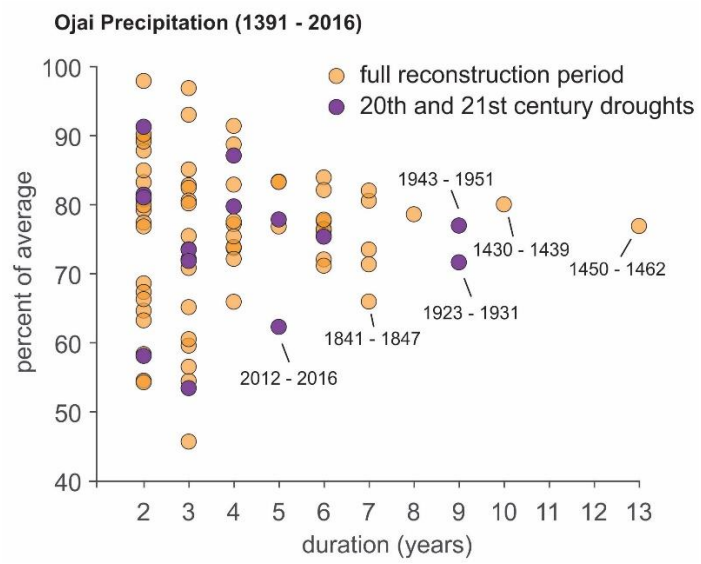
Ojai Precipitation (1391 - 2016)
full reconstruction period
20th and 21st century droughts
percent of average
duration (years)
1943 - 1951
1430 - 1439
1450 - 1462
1923 - 1931
1841 - 1847
2012 - 2016

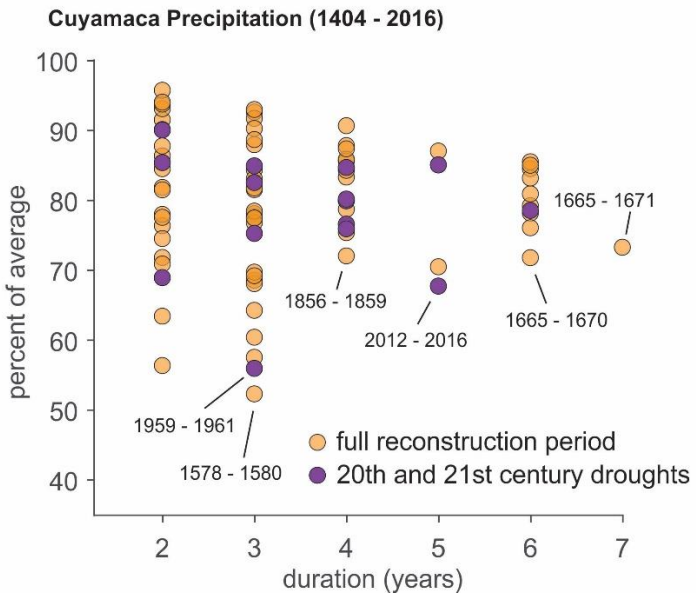
Cuyamaca Precipitation (1404 - 2016)
full reconstruction period
20th and 21st century droughts
percent of average
duration (years)
1665 - 1671
1856 - 1859
1665 - 1670
2012 - 2016
1959 - 1961
1578 - 1580

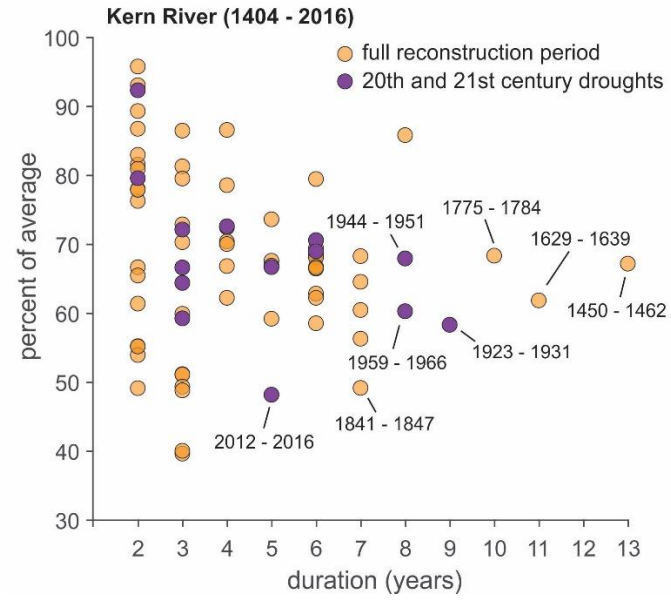
Kern River (1404 - 2016)
full reconstruction period
20th and 21st century droughts
percent of average
duration (years)
1944 - 1951
1775 - 1784
1629 - 1639
1450 - 1462
1959 - 1966
1923 - 1931
1841 - 1847
2012 - 2016

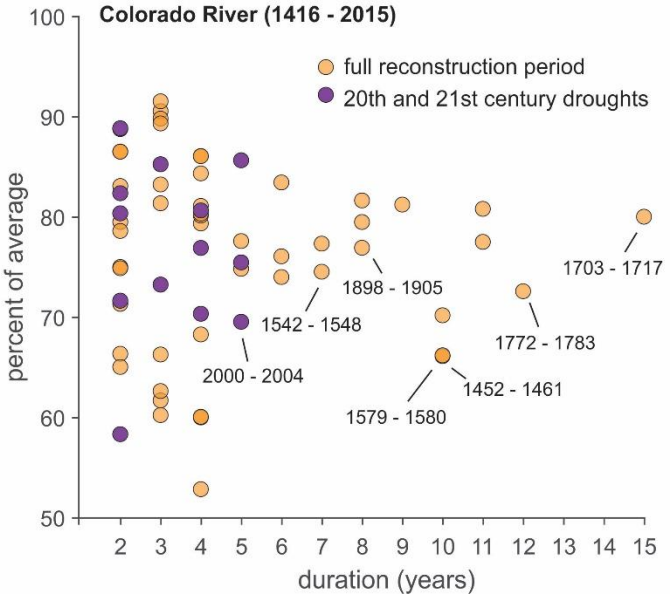
Colorado River (1416 - 2015)
full reconstruction period
20th and 21st century droughts
percent of average
duration (years)
1703 - 1717
1898 - 1905
1542 - 1548
1772 - 1783
2000 - 2004
1452 - 1461
1579 - 1580

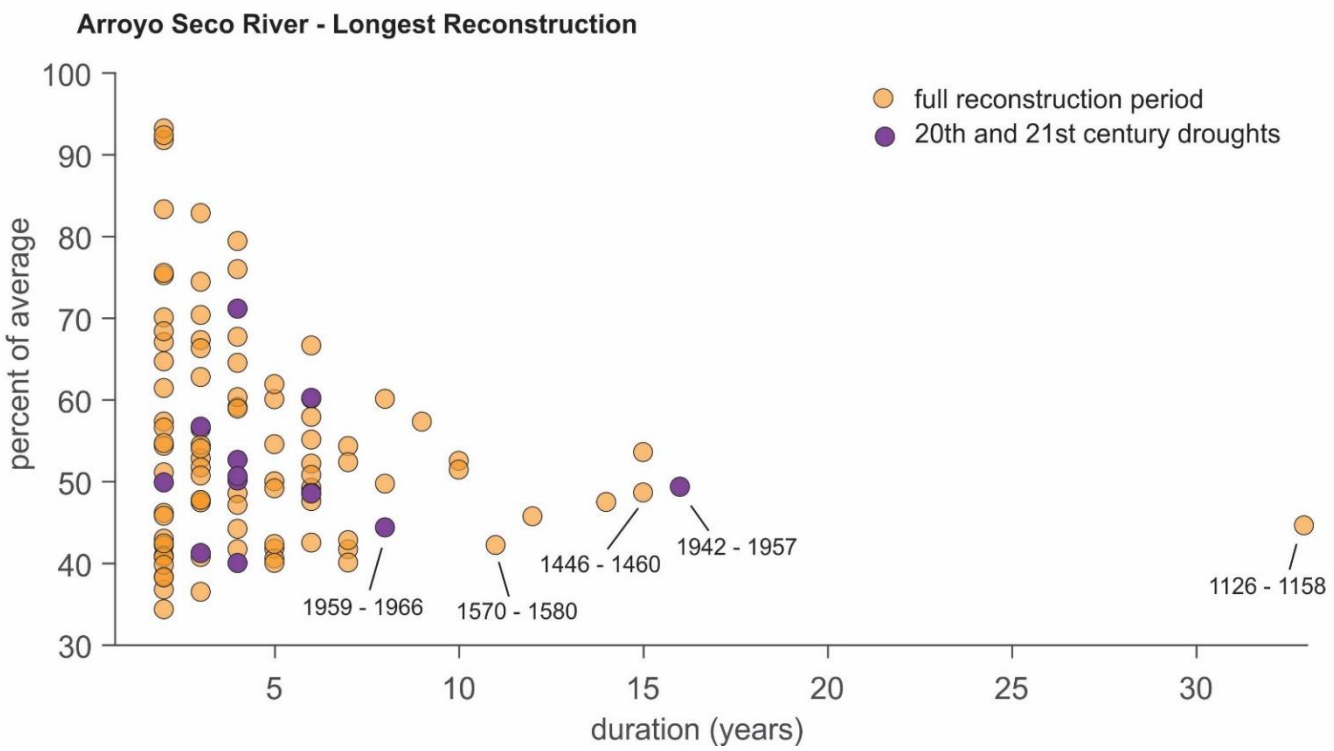
Arroyo Seco River - Longest Reconstruction
full reconstruction period
20th and 21st century droughts
percent of average
duration (years)
1942 - 1957
1446 - 1460
1959 - 1966
1570 - 1580
1126 - 1158

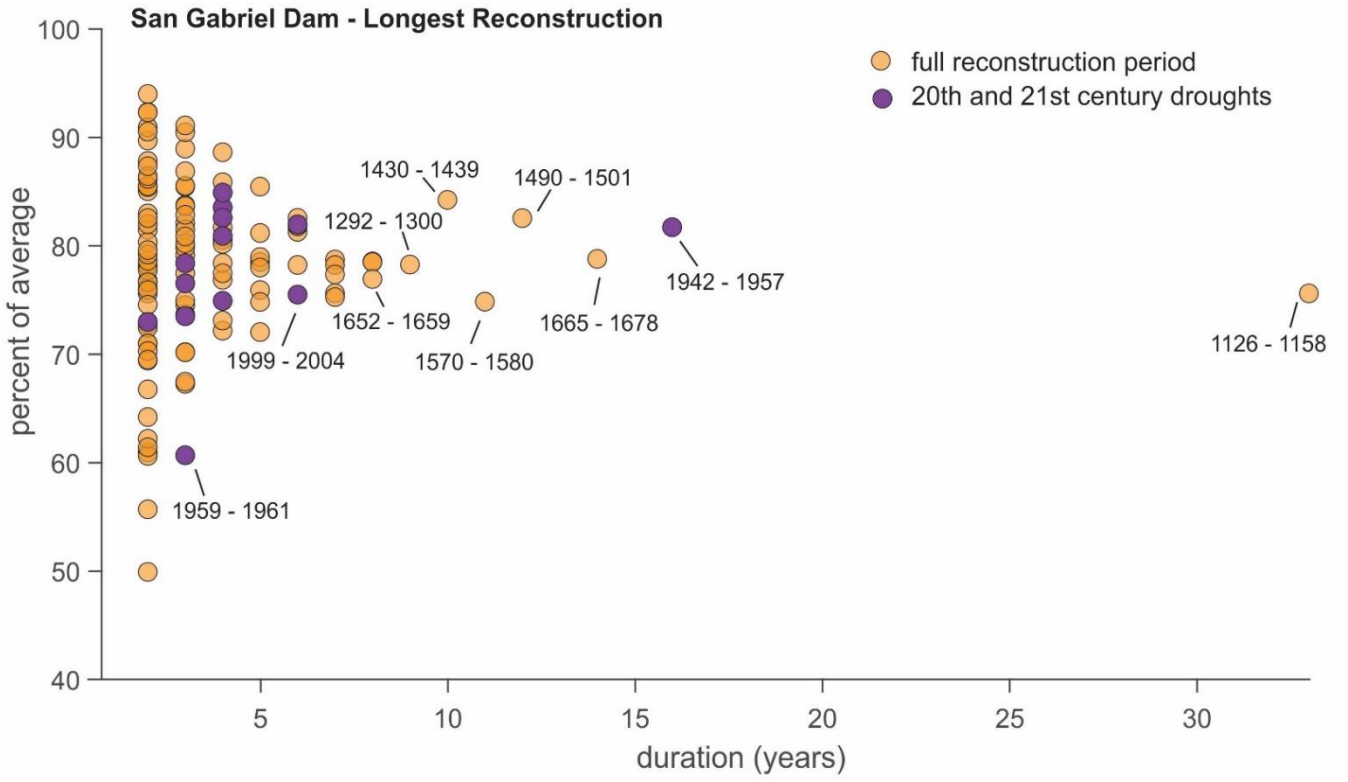
San Gabriel Dam - Longest Reconstruction
full reconstruction period
20th and 21st century droughts
percent of average
duration (years)
1430 - 1439
1490 - 1501
1292 - 1300
1942 - 1957
1652 - 1659
1665 - 1678
1999 - 2004
1570 - 1580
1126 - 1158
1959 - 1961

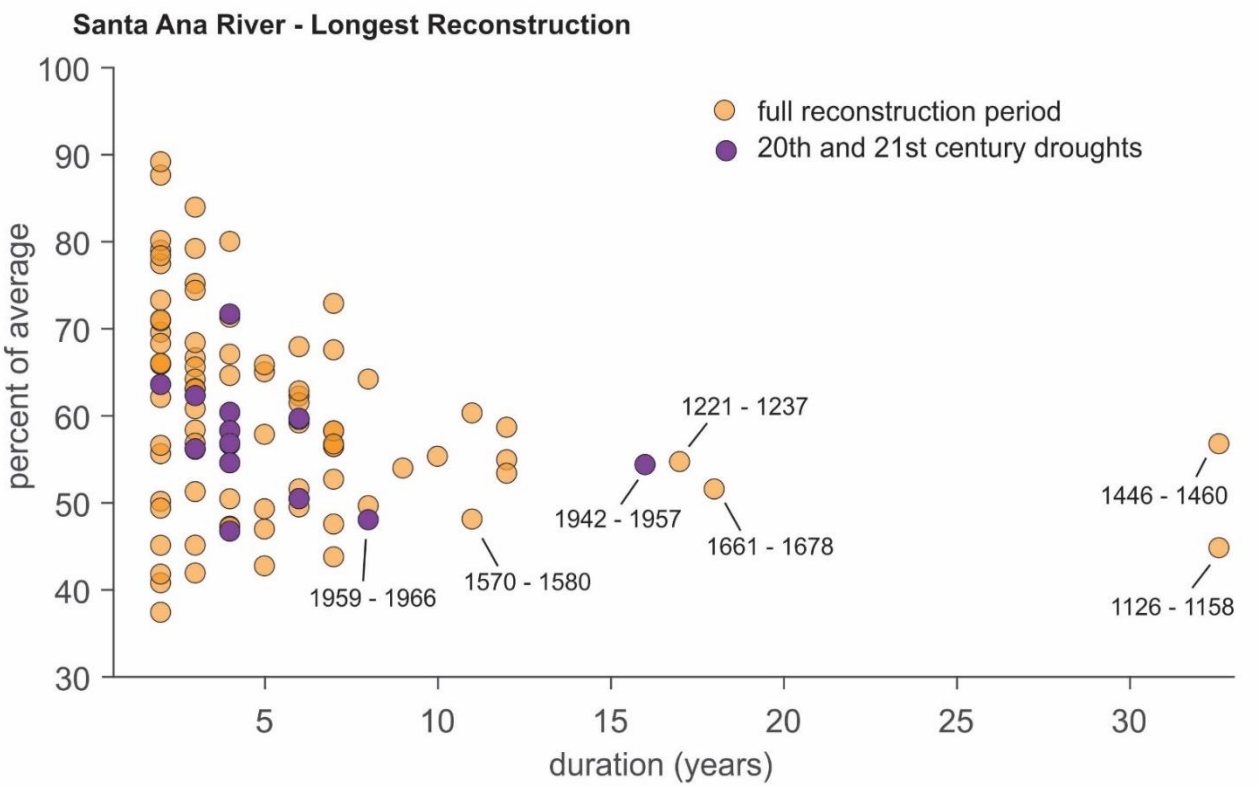
Santa Ana River - Longest Reconstruction
full reconstruction period
20th and 21st century droughts
percent of average
duration (years)
1221 - 1237
1942 - 1957
1661 - 1678
1446 - 1460
1959 - 1966
1570 - 1580
1126 - 1158

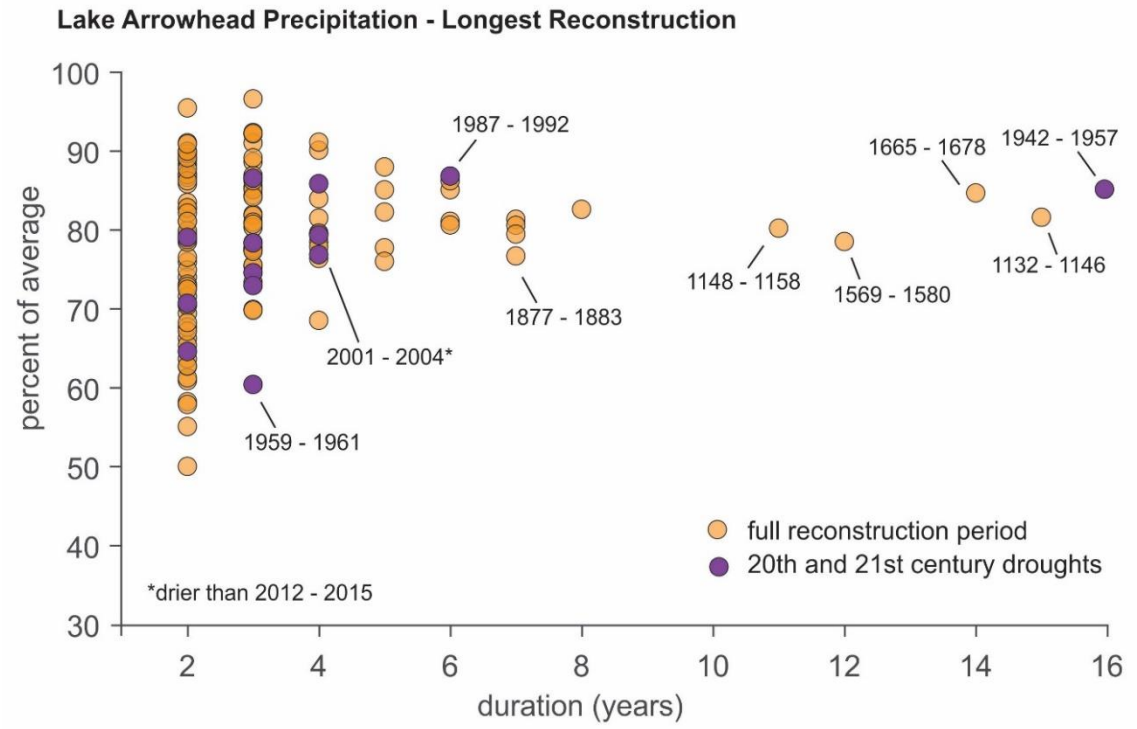
Lake Arrowhead Precipitation - Longest Reconstruction
full reconstruction period
20th and 21st century droughts
*drier than 2012 - 2015
percent of average
duration (years)
1987 - 1992
1665 - 1678
1942 - 1957
1148 - 1158
1569 - 1580
1132 - 1146
1877 - 1883
2001 - 2004*
1959 - 1961

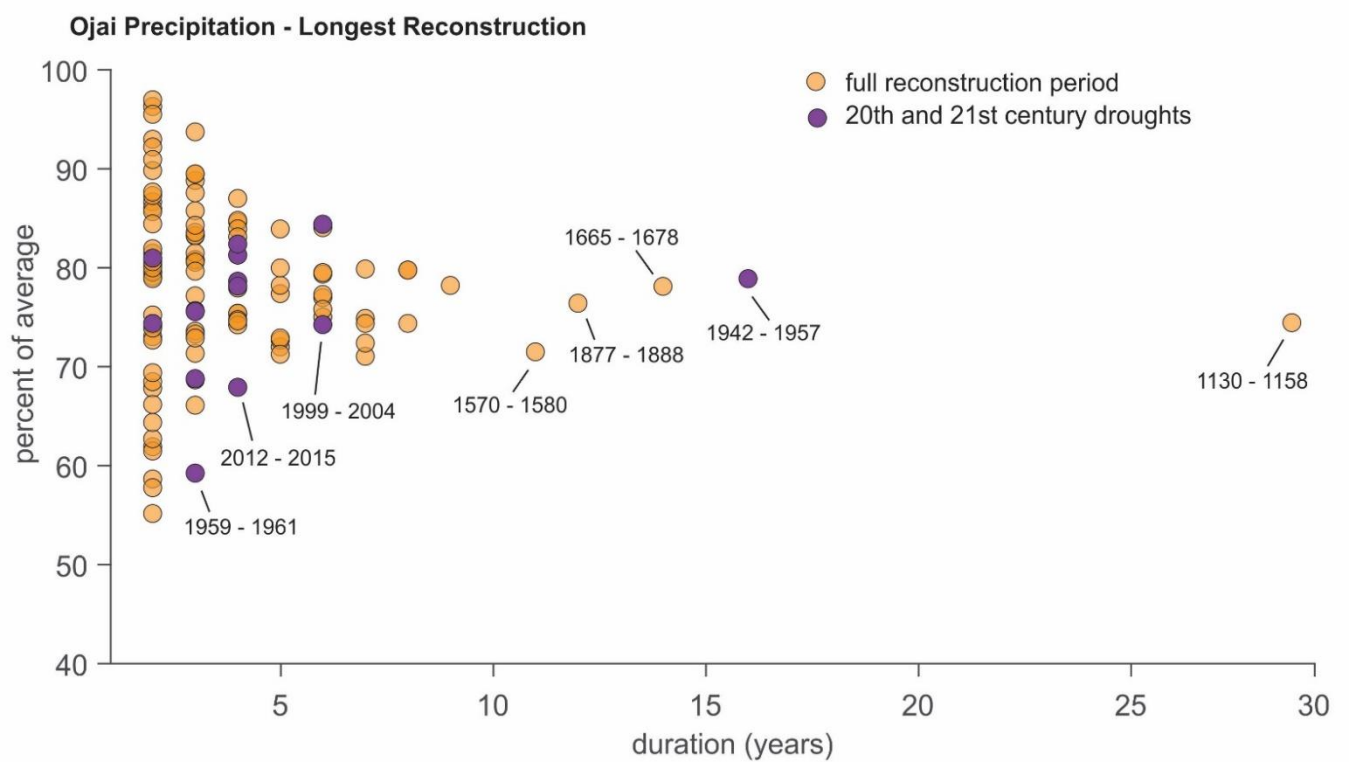
Ojai Precipitation - Longest Reconstruction
full reconstruction period
20th and 21st century droughts
percent of average
duration (years)
100
90
80
70
60
50
40
5
10
15
20
25
30
1665 - 1678
1942 - 1957
1877 - 1888
1130 - 1158
1570 - 1580
1999 - 2004
2012 - 2015
1959 - 1961

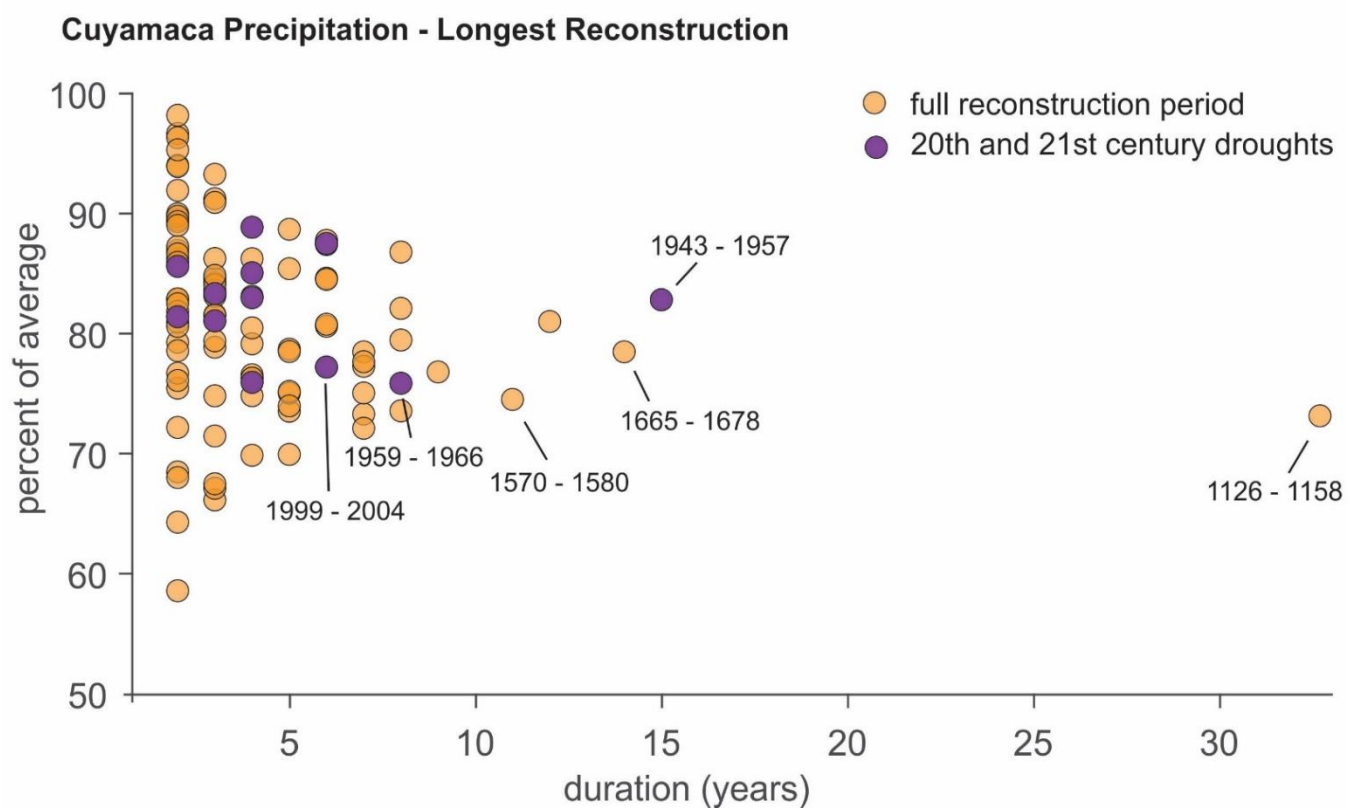
Cuyamaca Precipitation - Longest Reconstruction
full reconstruction period
20th and 21st century droughts
percent of average
duration (years)
100
90
80
70
60
50
5
10
15
20
25
30
1943 - 1957
1665 - 1678
1126 - 1158
1959 - 1966
1570 - 1580
1999 - 2004

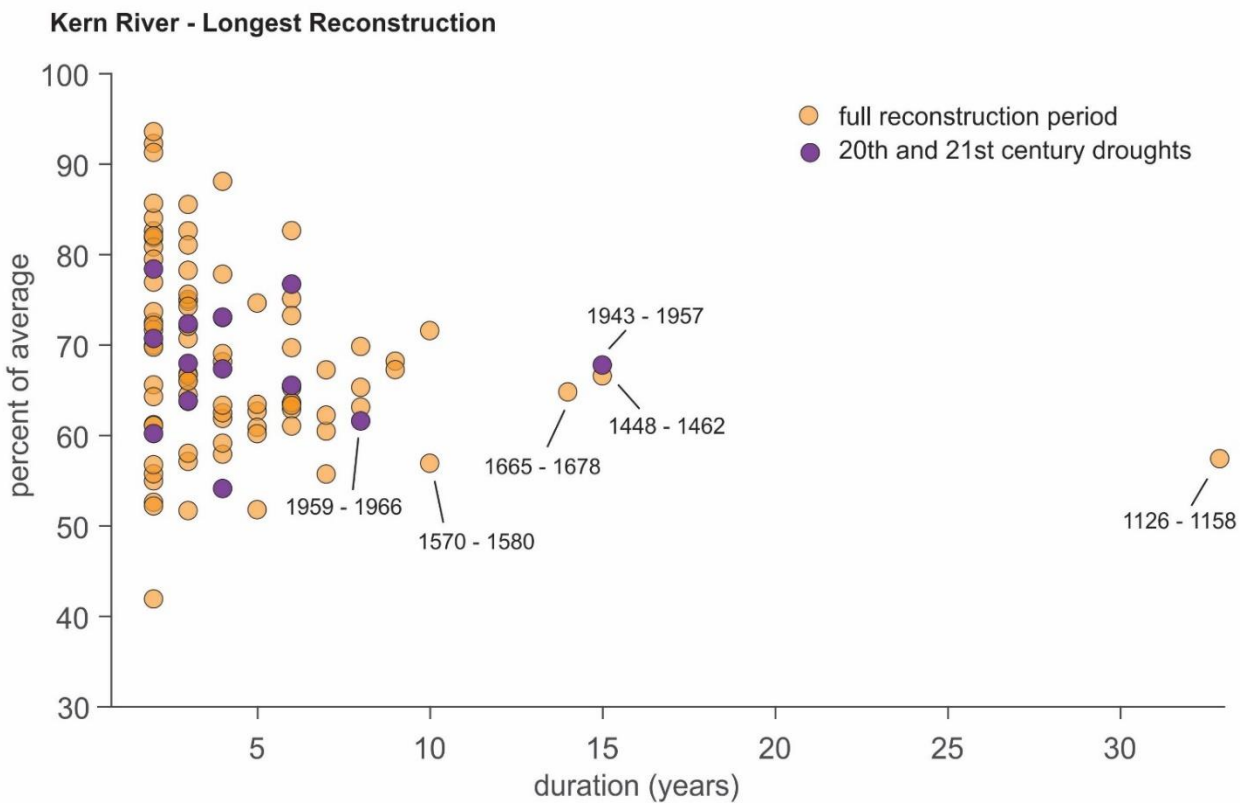
Kern River - Longest Reconstruction
full reconstruction period
20th and 21st century droughts
percent of average
duration (years)
1943 - 1957
1448 - 1462
1665 - 1678
1959 - 1966
1570 - 1580
1126 - 1158

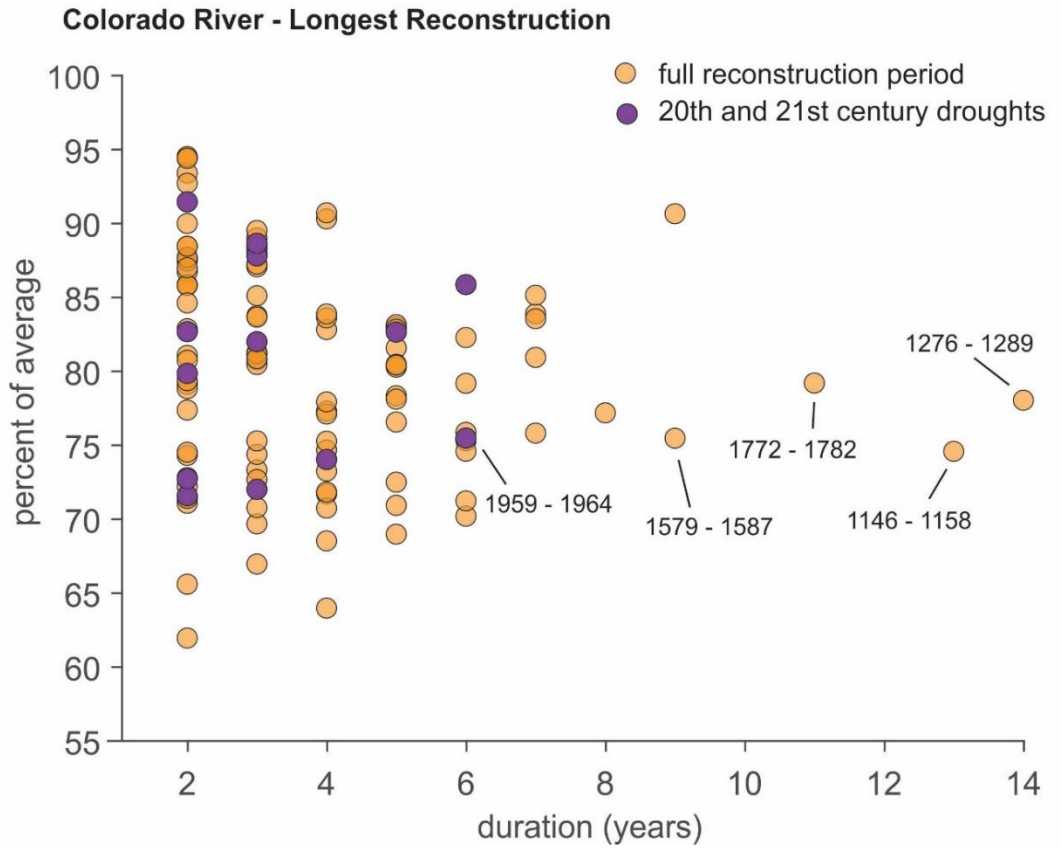
Colorado River - Longest Reconstruction
full reconstruction period
20th and 21st century droughts
percent of average
duration (years)
1276 - 1289
1772 - 1782
1146 - 1158
1579 - 1587
1959 - 1964

Northern California Series:

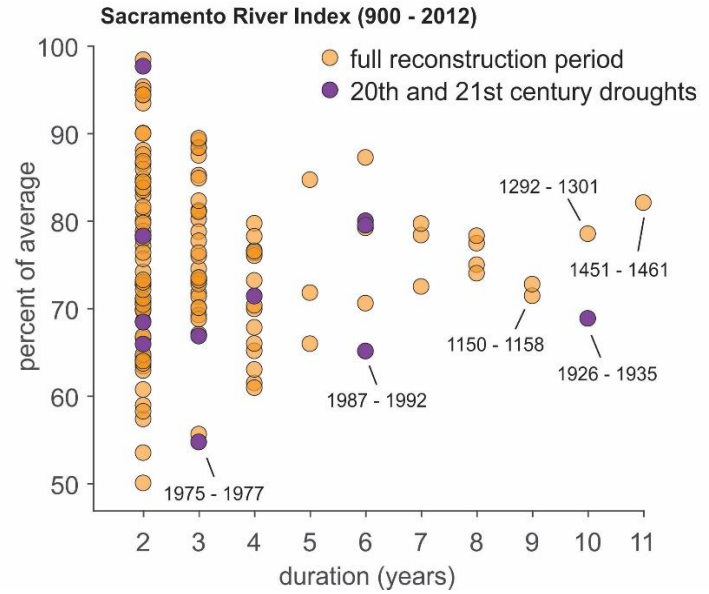

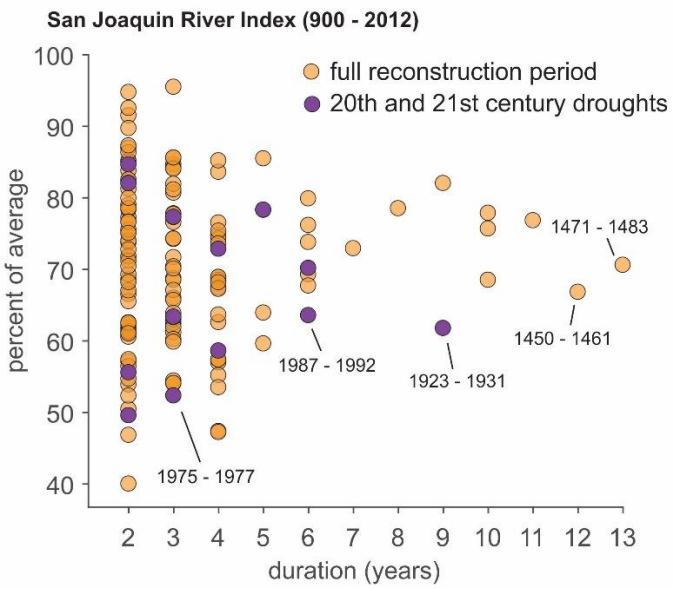

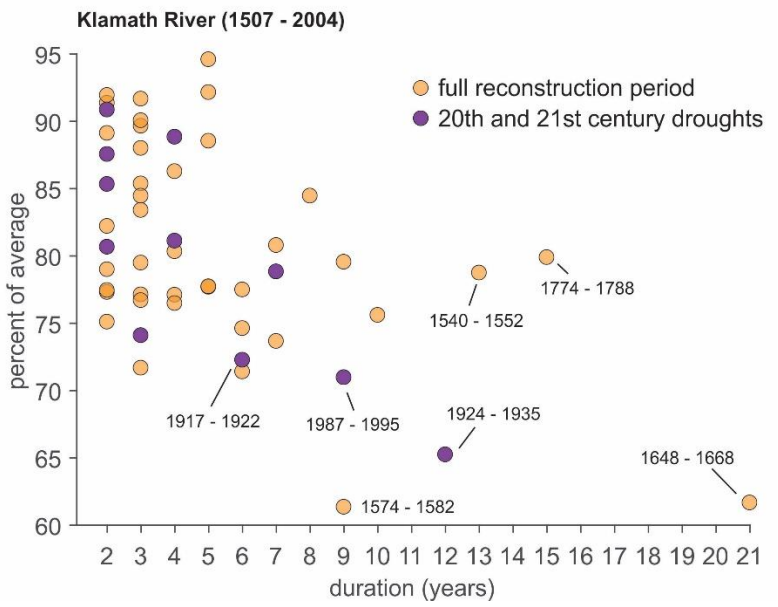

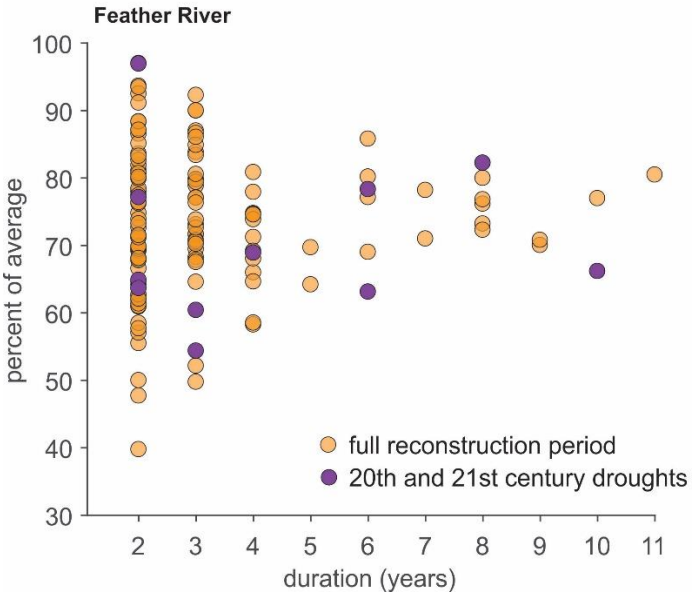
Feather River
percent of average
duration (years)
full reconstruction period
20th and 21st century droughts

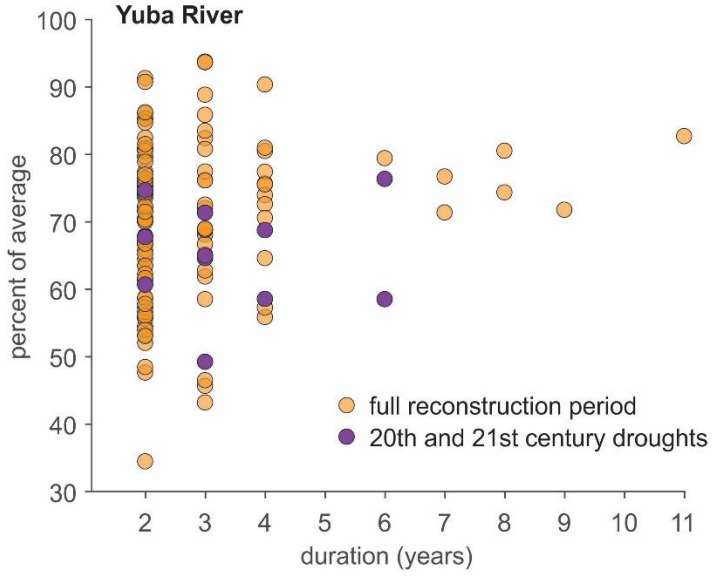
Yuba River
percent of average
duration (years)
full reconstruction period
20th and 21st century droughts

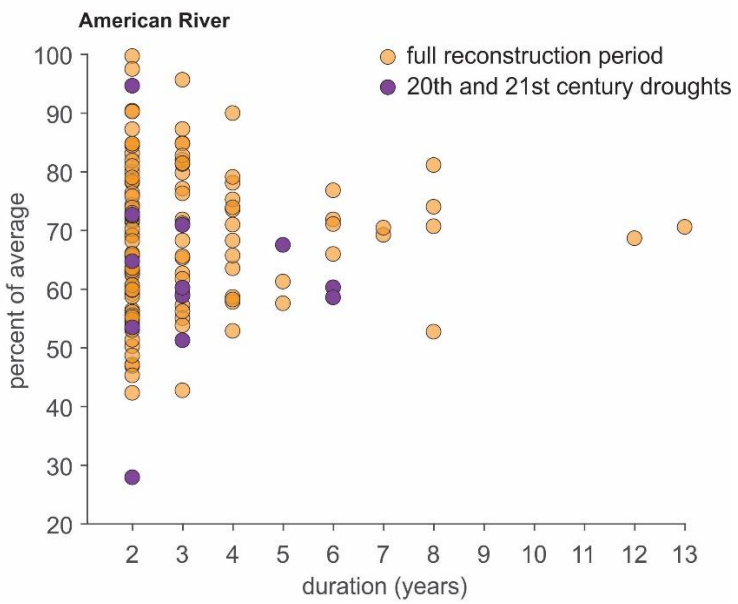
American River
percent of average
duration (years)
full reconstruction period
20th and 21st century droughts

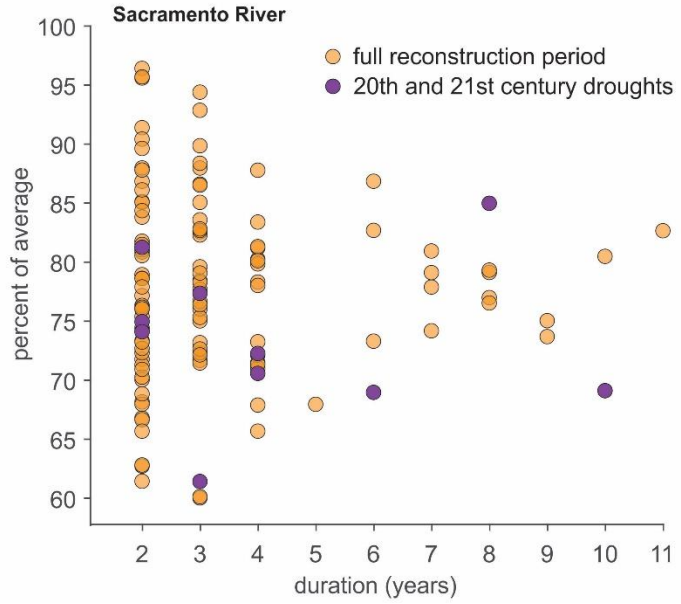
Sacramento River
percent of average
duration (years)
full reconstruction period
20th and 21st century droughts

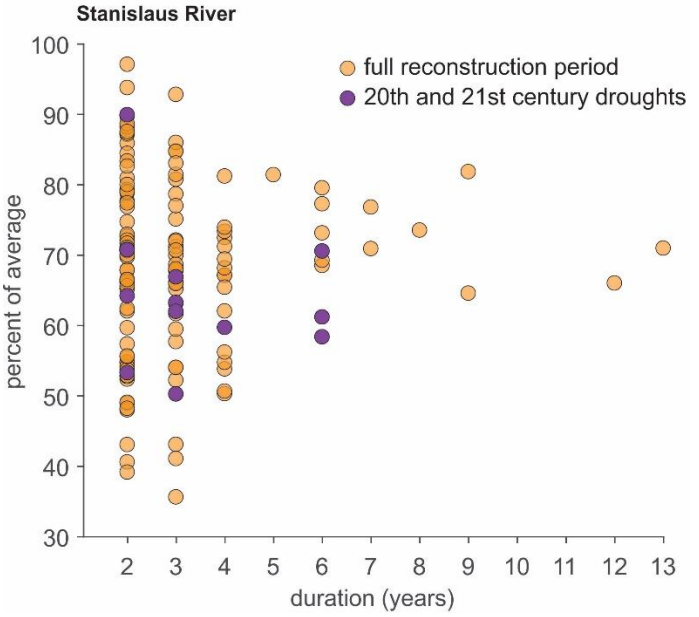
Stanislaus River
full reconstruction period
20th and 21st century droughts
percent of average
duration (years)

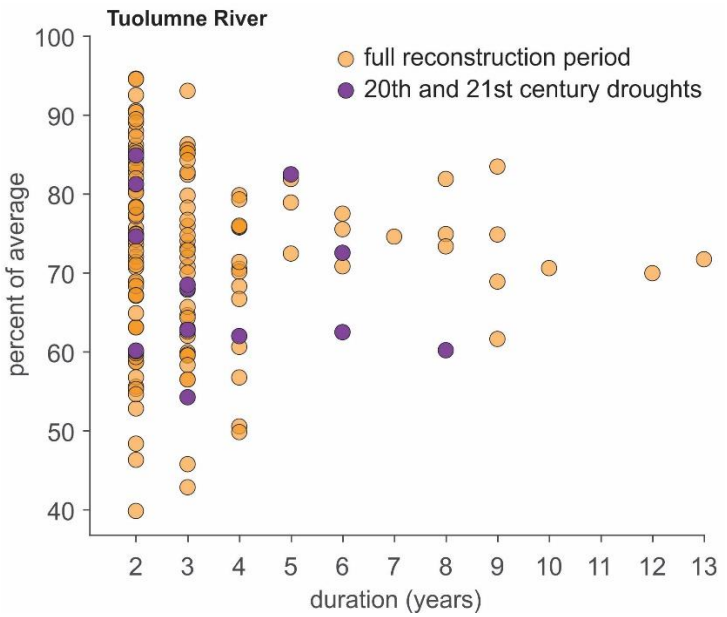
Tuolumne River
full reconstruction period
20th and 21st century droughts
percent of average
duration (years)

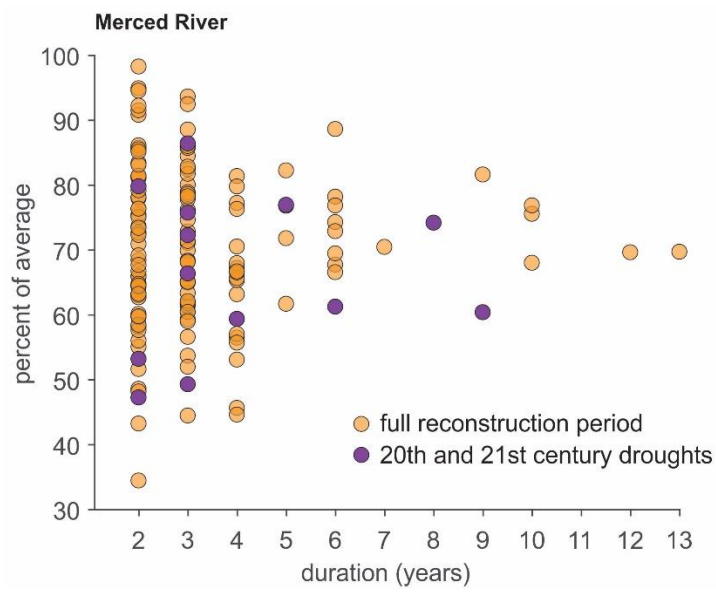
Merced River
full reconstruction period
20th and 21st century droughts
percent of average
duration (years)

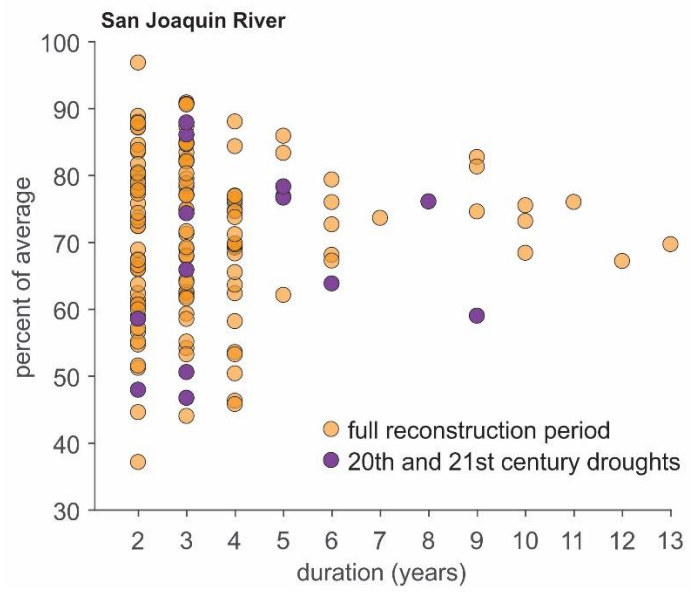
San Joaquin River
full reconstruction period
20th and 21st century droughts
percent of average
duration (years)

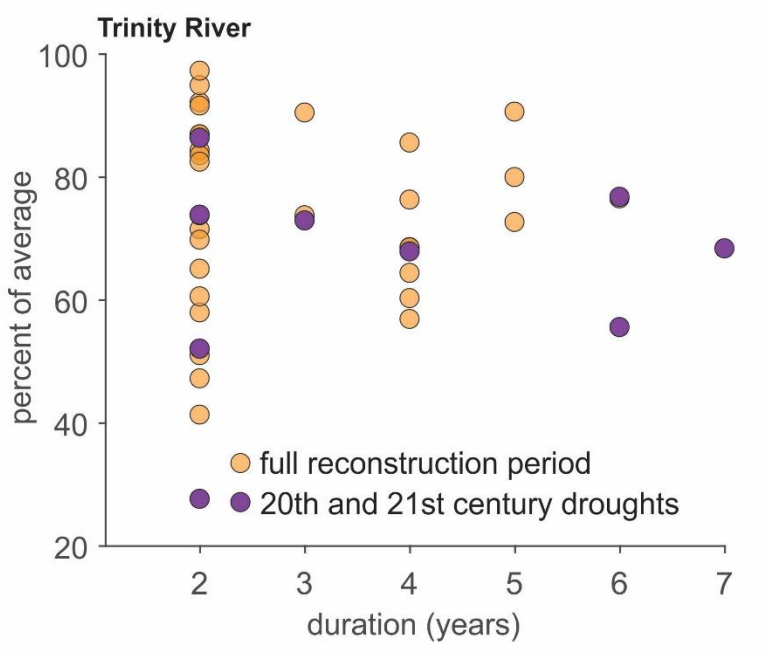
Trinity River
100
80
60
40
20
percent of average
full reconstruction period
20th and 21st century droughts
2
3
4
5
6
7
duration (years)

Appendix G: Moving averages for all Socal gages

Dry periods (MS and longest)
Dry/wet periods (MS)

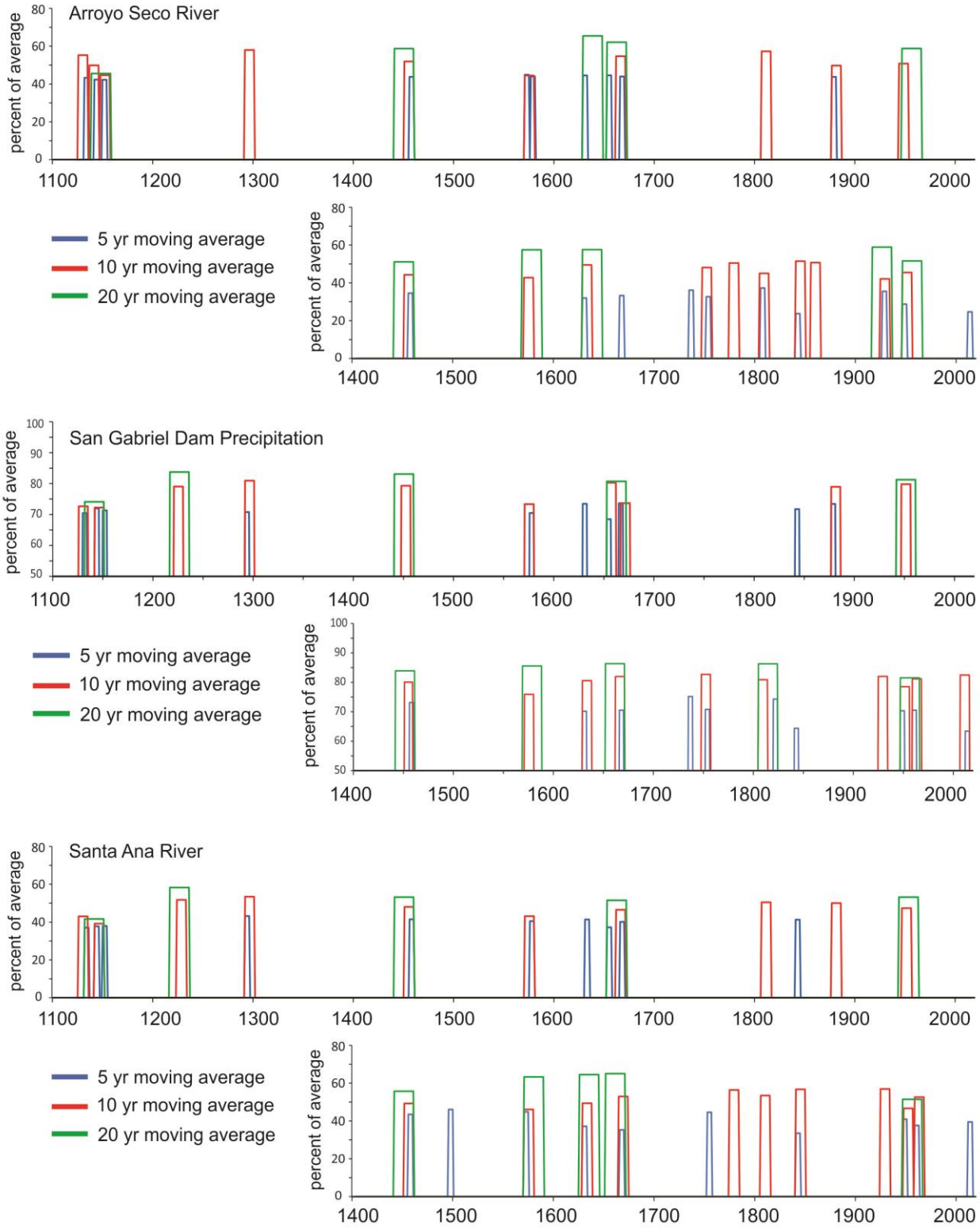

Figure 1 a,b,c. The lowest 5-, 10-, 20-year drought periods based on ranked moving averages for the most skillful and longest reconstructions. The results for the 5- and 10-yr droughts include the lowest 10 rankings, while the 20-yr droughts include the lowest 5 rankings.

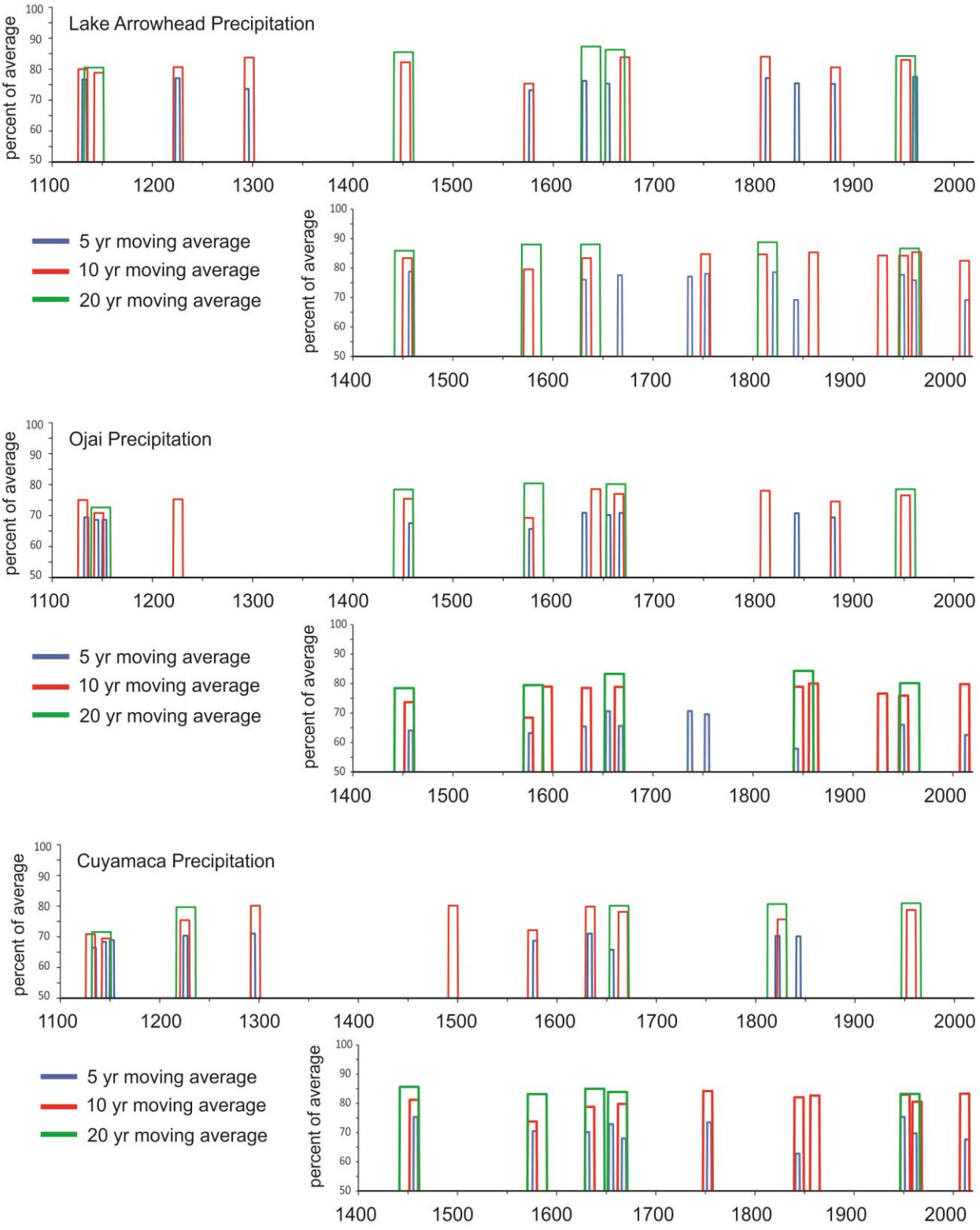

Figure 1 d,e,f. The lowest 5-, 10-, 20-year drought periods based on ranked moving averages for the most skillful and longest reconstructions. The results for the 5- and 10-yr droughts include the lowest 10 rankings, while the 20-yr droughts include the lowest 5 rankings.

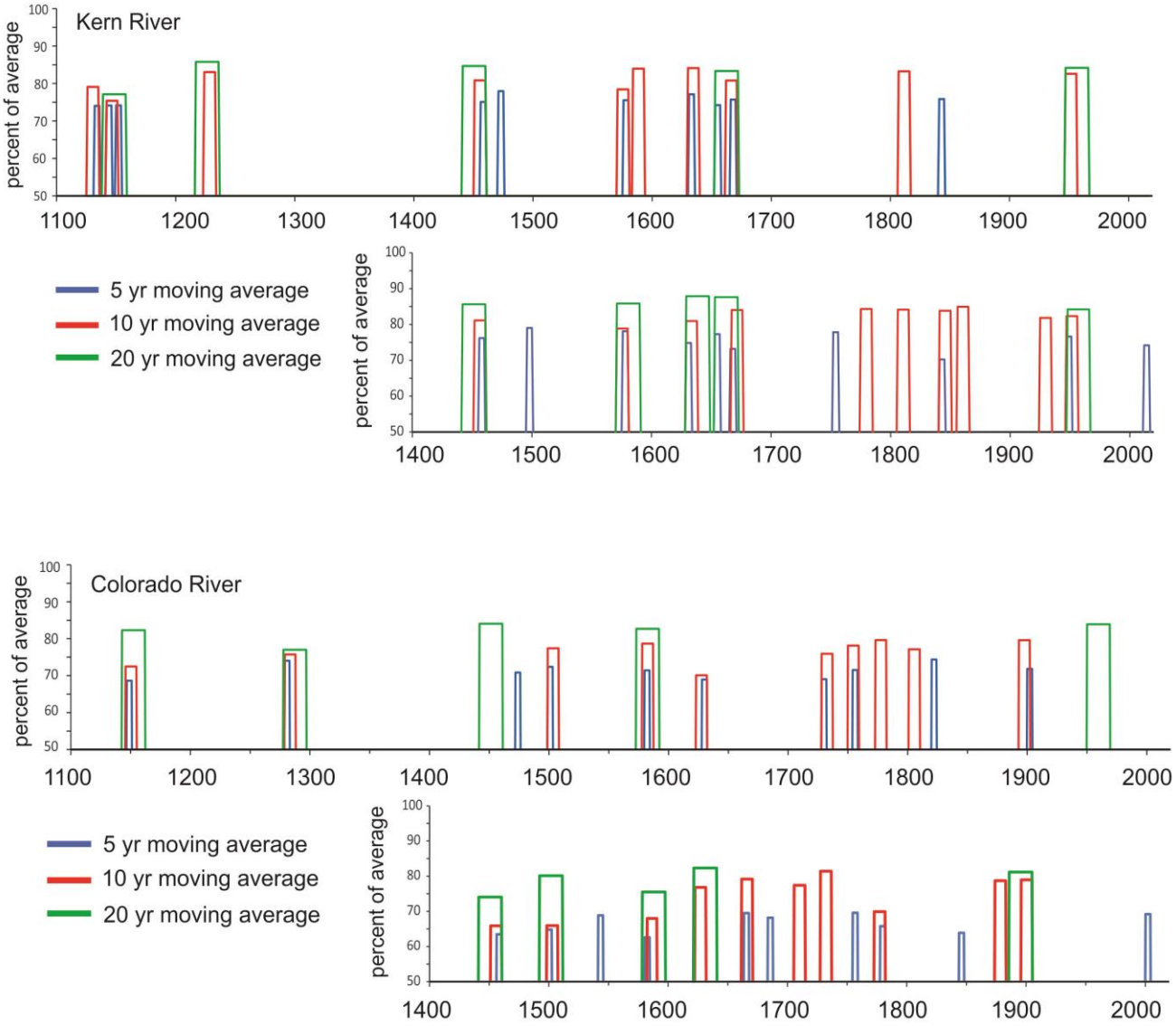

Figure 1 g,h. The lowest 5-, 10-, 20-year drought periods based on ranked moving averages for the most skillful and longest reconstructions. The results for the 5- and 10-yr droughts include the lowest 10 rankings, while the 20-yr droughts include the lowest 5 rankings.

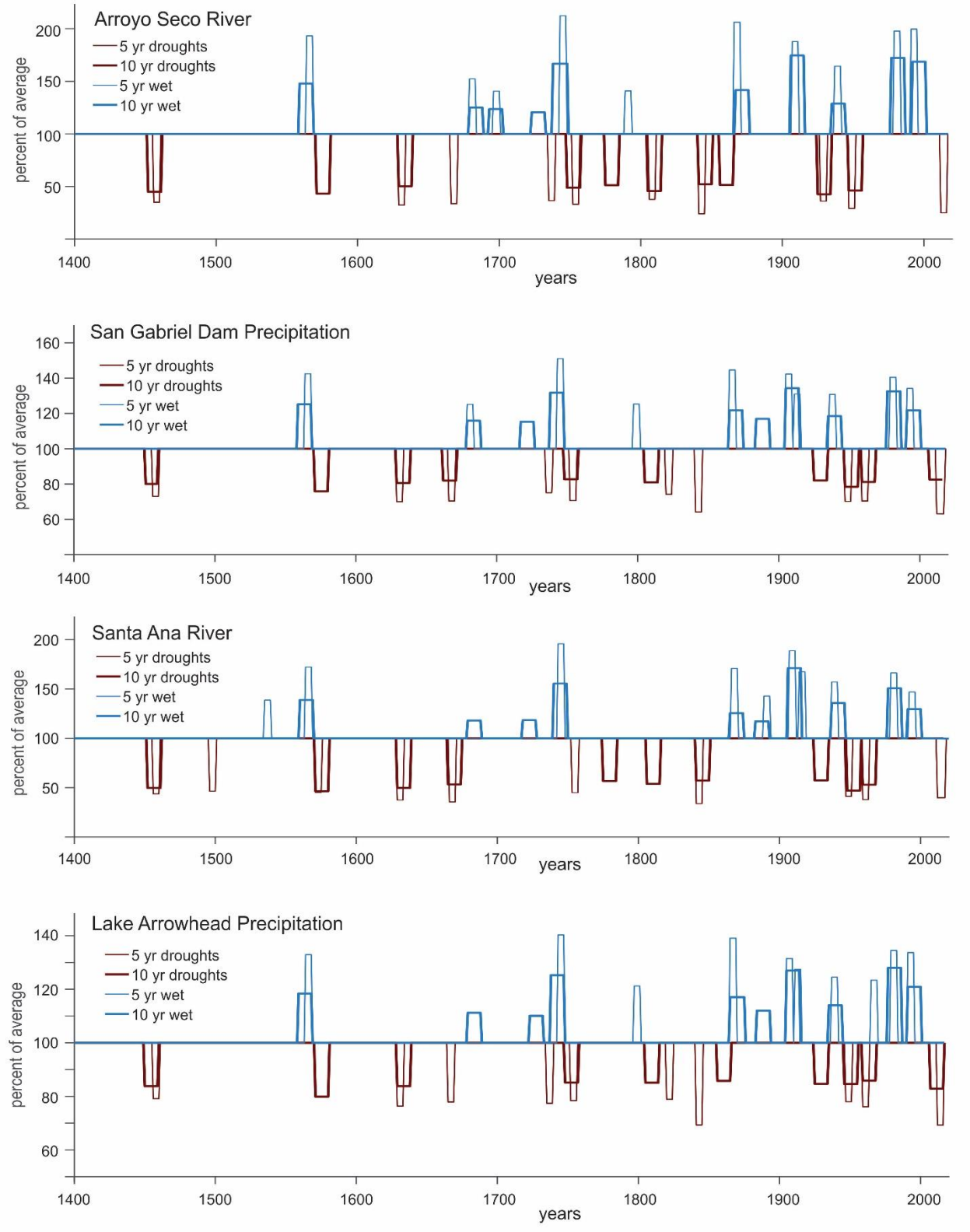

Figure 2a. The 10 lowest 5- and 10-yr droughts and wet periods, based on ranked moving averages.

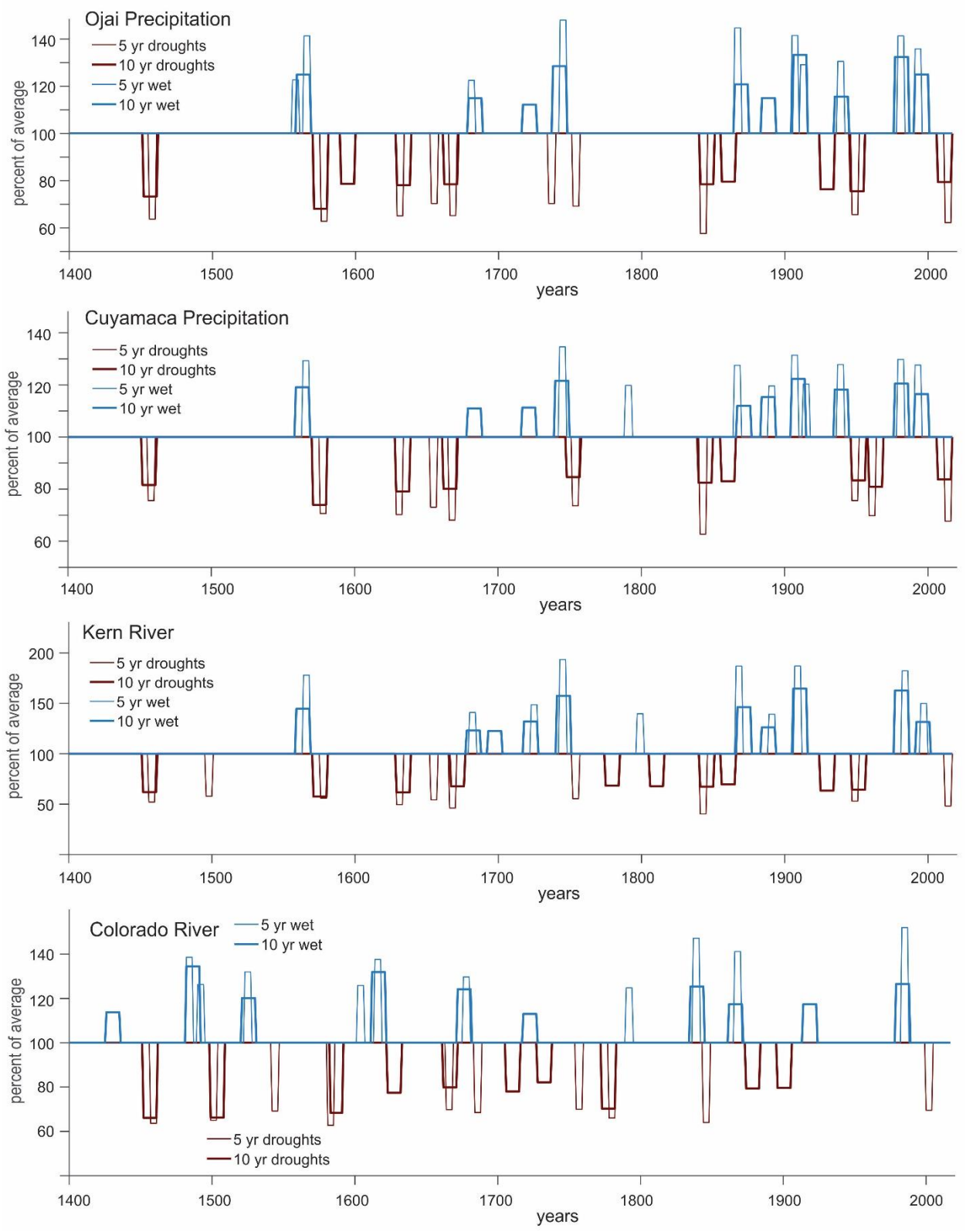

Figure 2b. The 10 lowest 5- and 10-yr droughts and wet periods, based on ranked moving averages.

Appendix H. Spectra and wavelet plots

This appendix contains spectral and wavelet plots for the 8 study basins – Colorado River, Kern River, and 6 basins in Southern California.

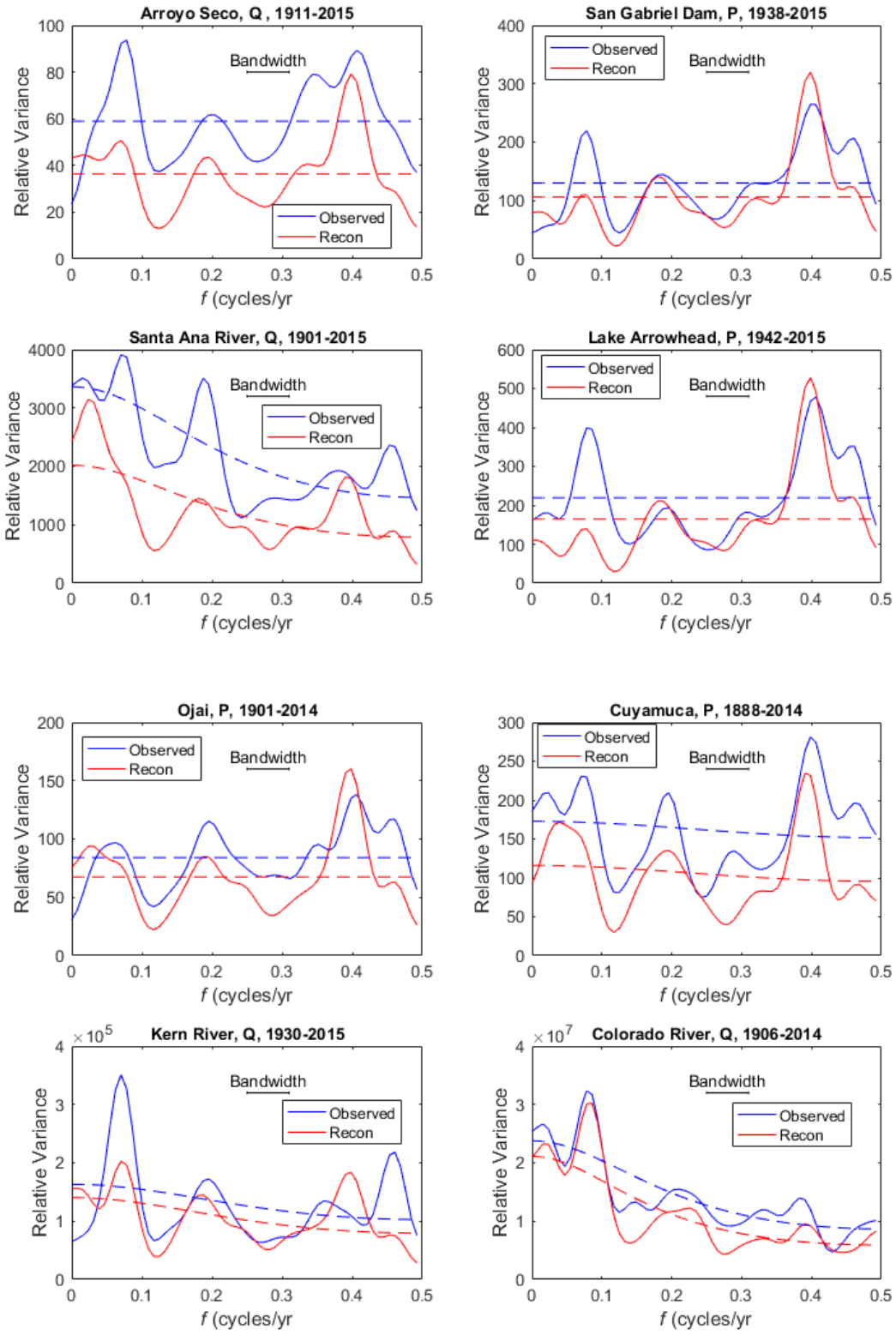

Figure 1a. Comparative spectra of observations and most skillful reconstructions in 8 basins. Series is either flow (Q) or precipitation (P). Series and analysis period identified above each plot. Annotated plot is Figure 9 in main report.

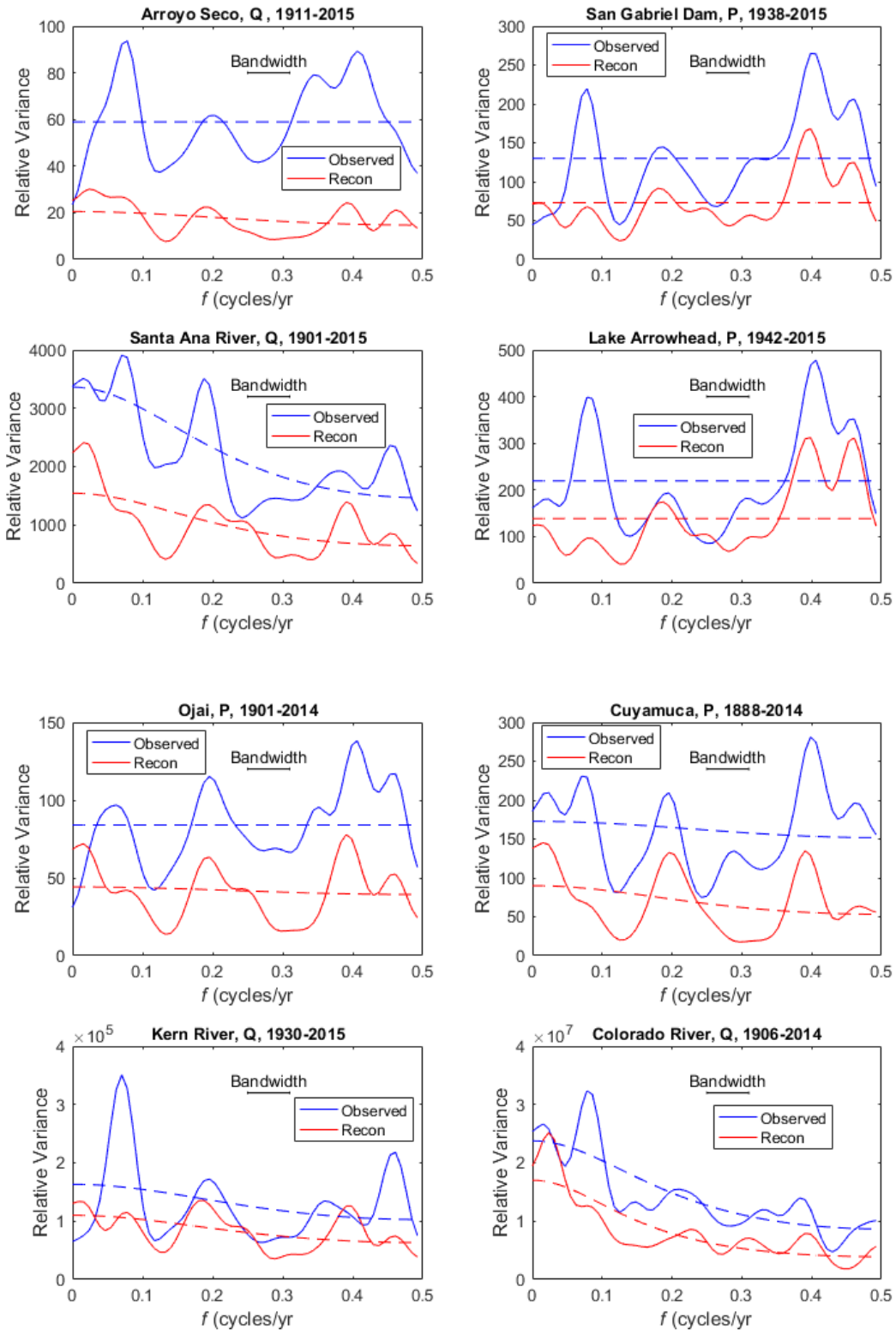

Figure 1b. Comparative spectra of observations and longest reconstructions in 8 basins. Series is either flow (Q) or precipitation (P). Series and analysis period identified above each plot. Prototype is Figure 9 in main report.

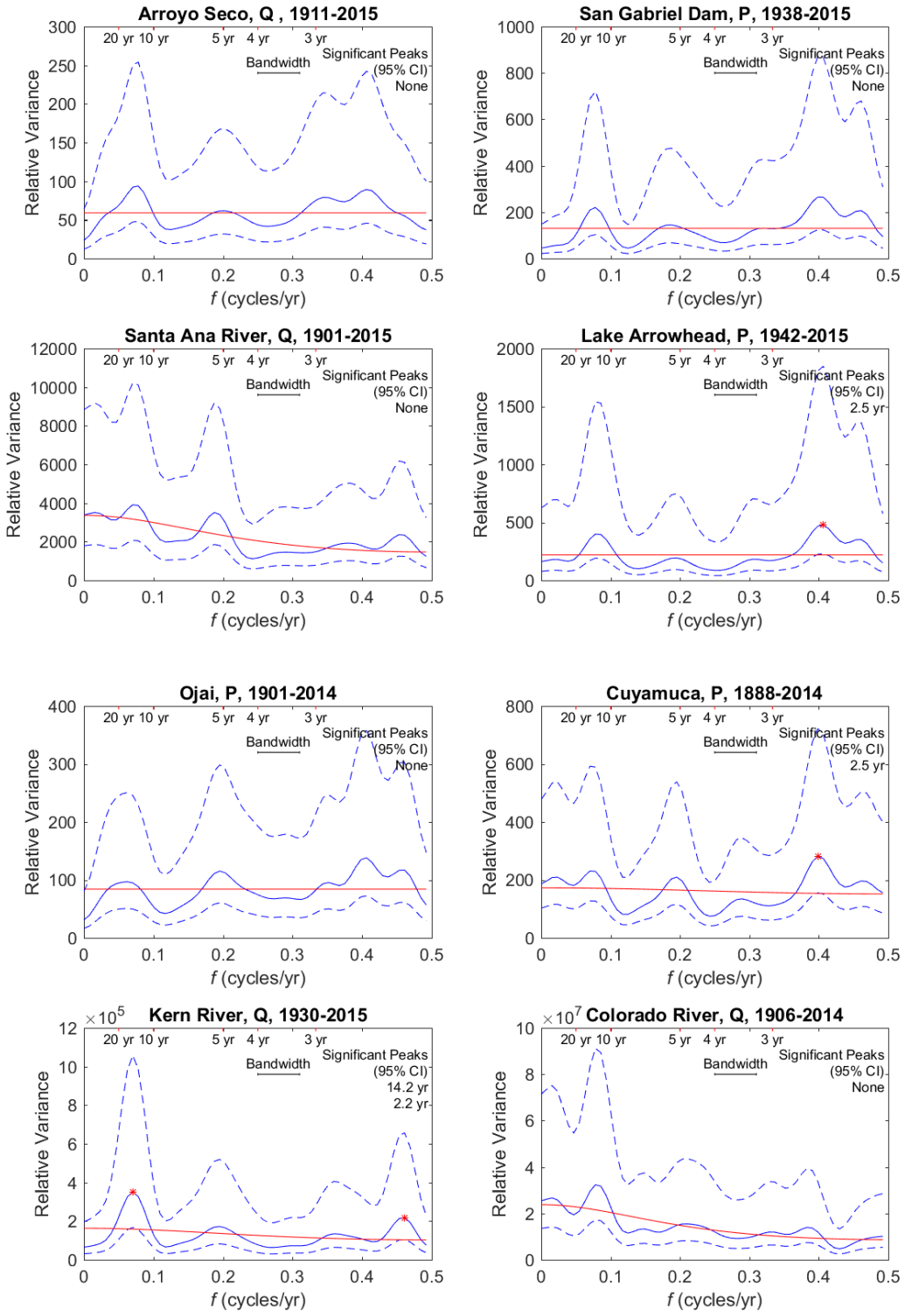

Figure 2. Spectra with confidence bands of observed precipitation or flow in 8 basins. Annotated plot is Figure 10 in main report.

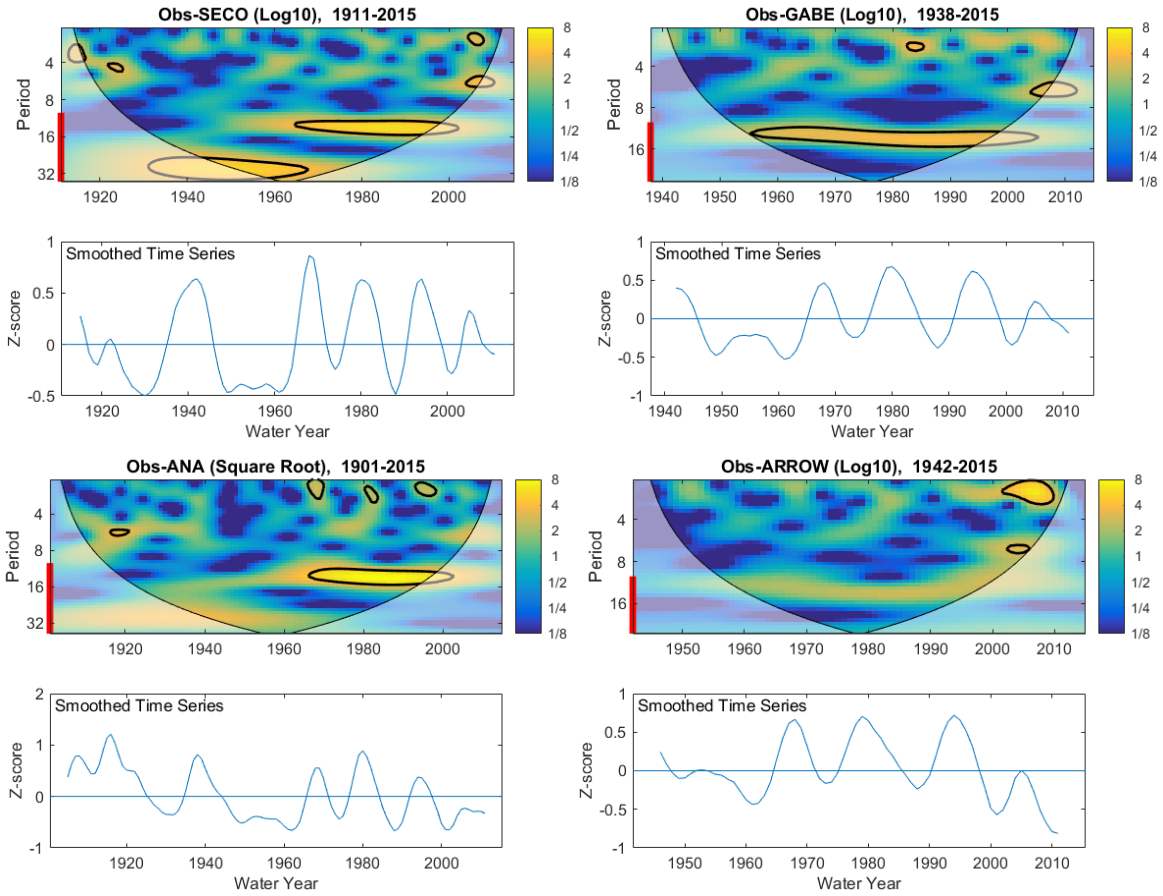

Figure 3a. Continuous wavelet transforms (CWT) of observations for first 4 of 8 study basins. Annotated plot is Figure 11 in main report.

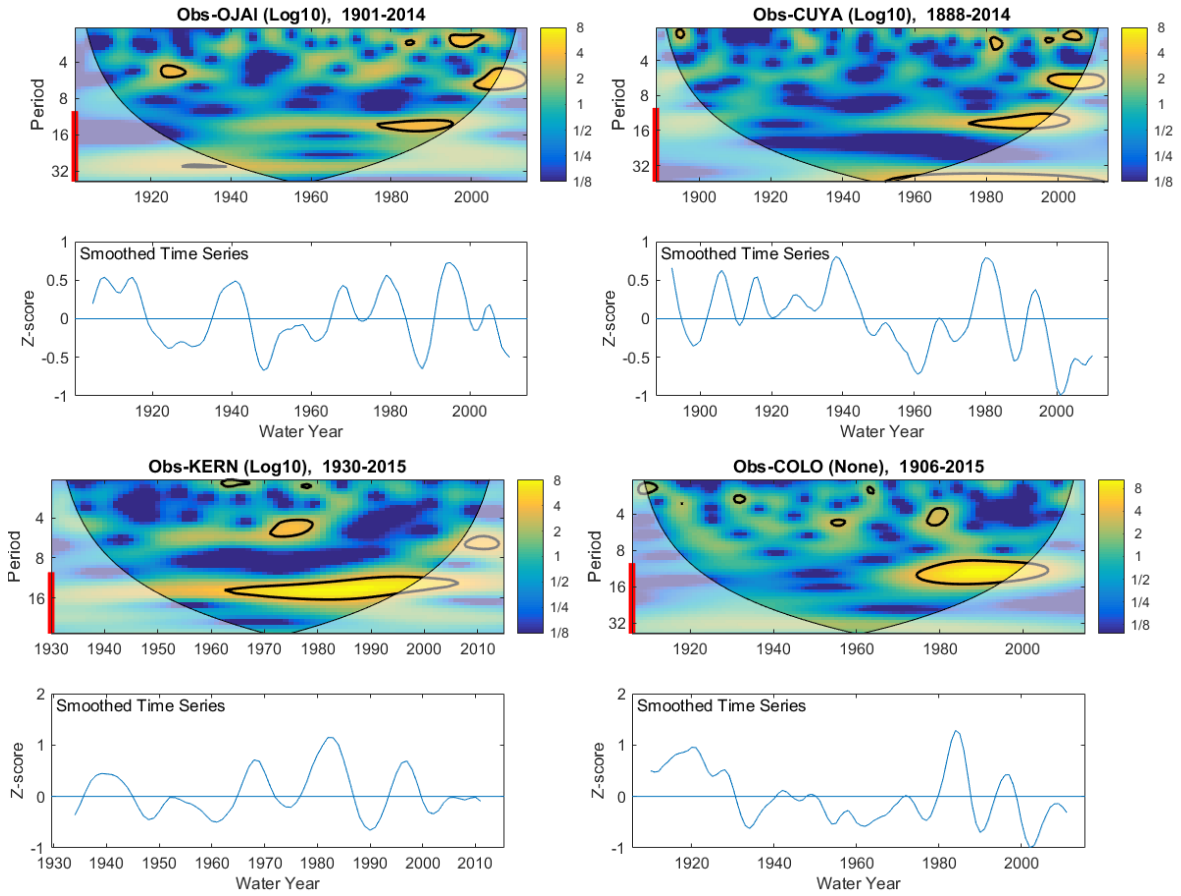

Figure 3b. Continuous wavelet transforms (CWT) of observations for second 4 of 8 study basins. Annotated plot is Figure 11 in main report.

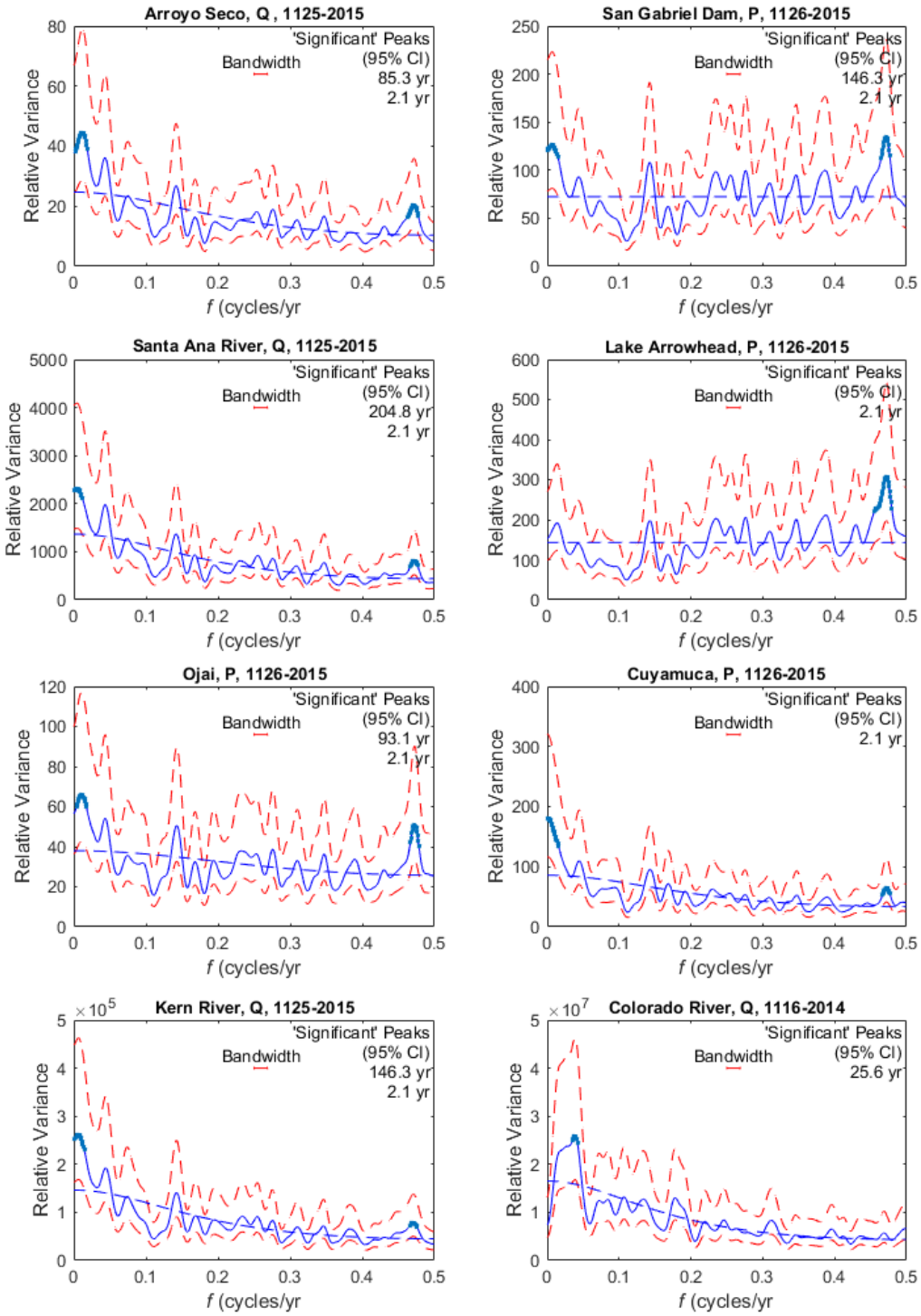

Figure 4. Spectra with confidence bands of longest reconstructions in 8 basins. Corresponding plots for most skillful reconstruction are in Figure 12 in main report.

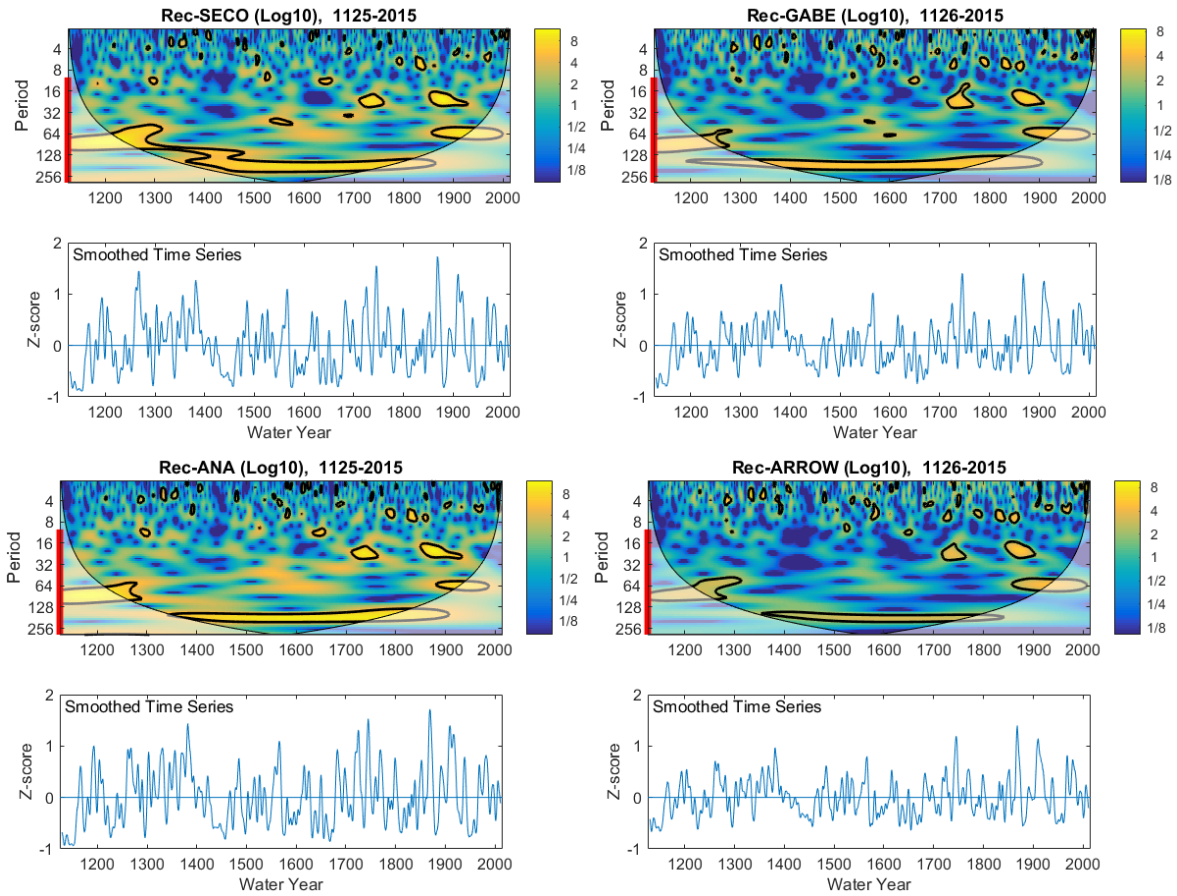

Figure 5a. Continuous wavelet transforms (CWT) and smoothed time plots of longest reconstructions of precipitation or flow for the first 4 of 8 basins. Corresponding plots for most skillful reconstruction are in Figure 13a in main report.

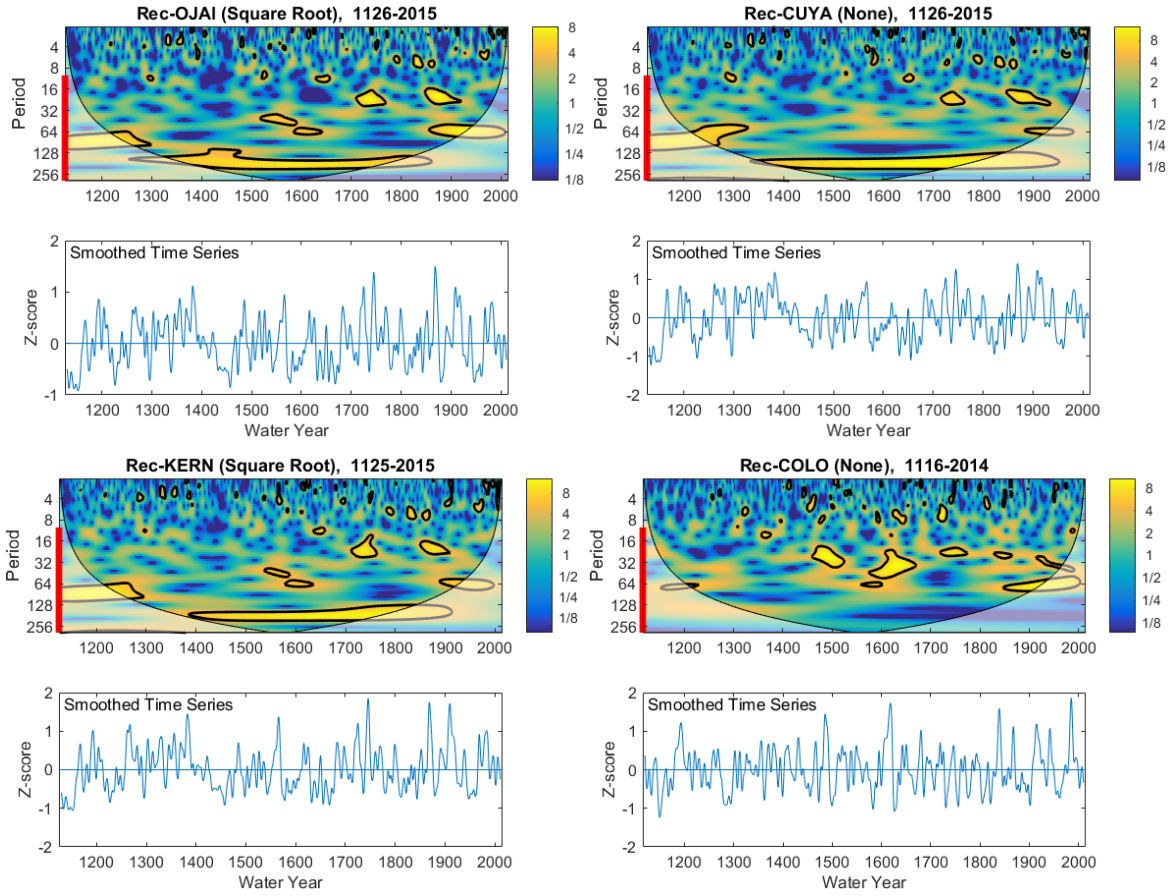

Figure 5b. Continuous wavelet transforms (CWT) and smoothed time plots of longest reconstructions of precipitation or flow for the second 4 of 8 basins. Corresponding plots for most skillful reconstruction are in Figure 13b in main report.

Appendix I: List of digital data products

A zip file, FinalReportFiles_4600011071.zip contains xlsx spreadsheet files with tree-ring chronologies collected and developed under this project, as well as the reconstructions generated. Four files are provided in the zip:

1) **Readme.docx**: A copy of this appendix:
2) **ChronologiesTable1.xlsx**: listing of site chronologies for sites collected under this project. The file has two sheets, one for standard chronologies and one for residual chronologies. Years are listed in the first column, and cover the period 350 – 2016 CE. Each column represents one tree-ring chronology, with a three-letter code as listed in final report Table 1. Columns are ordered from left to right in the same order that sites are listed in Table 1. Therefore, sites on the left of the spreadsheet are from southern California, then the Sierras, followed by sites from Colorado on the right-hand side.
3) **SubperiodReconstructions.xlsx**: individual sub-period model reconstructions, which correspond to reconstructions Rec1, Rec2, Rec3, and Rec4 described in Section 2.3 of the report. After the year column are 5 columns for each reconstruction target basin. First is a column saying which of the 4 sub-period models has priority in supplying values to the blended, or nested, reconstructions listed in NestedReconstructions.xlsx. Next are the time series of Rec1, Rec2, Rec4 and Rec4 sub-period reconstructions, labeled 1, 2, 3, 4 in a header row. Model 1, or Rec1, is the early model for each basin, and is highlighted in yellow. This highlighted yellow time series is by definition the "longest" version of reconstruction described in the report. Units of data in the spreadsheet are inches or thousands of acre-ft (kaf), depending on if the reconstruction is precipitation or full natural flow of a river (see Table 2 in report).
4) **NestedReconstructions.xlsx:** nested reconstructions based on splicing of the sub-period reconstructions from SubperiodReconstructions.xlsx. The time series block build from spliced Rec2 and Rec3 (with additional last year provided by Rec4) is identically the "most skillful" reconstruction as defined in the report. This block defining the most skillful reconstruction is highlighted in yellow. Each gage, identified in the first row, has three columns, identified by the second row. First is the reconstructed value. Second (Low50%) is the lower 50% confidence band as defined by the method of upper and lower smooths described in the report. Third (Up50%) is the upper 50% confidence band. The interval from Low50% to Up50% is the 50% confidence interval for the reconstructed value. Units of data in the spreadsheet are inches or thousands of acre-ft (kaf), depending on if the reconstruction is precipitation or full natural flow of a river (see Table 2 in report).